

Investigation and Suppression of Harmonics and Interharmonics in High-Power PWM Current-
Source Drive Systems

by

Ye Zhang

A thesis submitted in partial fulfillment of the requirements for the degree of

Doctor of Philosophy

in

Energy Systems

Department of Electrical and Computer Engineering
University of Alberta

© Ye Zhang, 2015

Abstract

Among the medium-voltage (MV) high-power industrial drive applications, the PWM current-source drive systems are increasingly used in recent years, due to the simple structure, motor friendly waveforms and fuseless short-circuit protection. A typical challenge being faced by the high-power PWM current-source drives is the problem of harmonics and interharmonics. The harmonics and interharmonics from utility, load, power converters and harmonics interaction between rectifier and inverter may cause a host of impacts on the drive system, such as the deterioration of line power quality, load torsional vibration, LC resonance occurrence, etc.

To solve this problem, this thesis conducts an in-depth study on the harmonics and interharmonics in high-power PWM current-source drive systems, including the mechanism of generation, the impacts on the system, and the active attenuation through the high-power converters. On the one hand, with respect to the generation of harmonics and interharmonics, a systematically investigation of the harmonics interaction phenomenon in high-power PWM current-source drives with thyristor front end (TFE) and active front end (AFE) is carried out respectively. The harmonics interaction is a main source of interharmonics in high-power current-source drive systems and has not been well considered in previous works. For the high-power PWM current-source drives with AFE, where the harmonics interaction phenomenon is more complex due to the PWM converters and LC circuit contained in each ac side, a frequency iteration method is proposed to analyze the produced interharmonics with possible frequencies. In addition, the impacts of the harmonics and interharmonics on the drive systems are carefully studied with respect to three main cases, line-side communication interference, load torsional vibration, and LC resonance excitation. The mechanism and cause factors of impacts' occurrence are analyzed in details, and the frequencies of the harmonics and interharmonics that results in the impacts at certain motor operating frequencies are accurately estimated under each case. On the other hand, to attenuate the harmonics and interhar-

monics without involving additional costs and losses, at first, the active interharmonic compensation capability of high-power PWM current-source converters, which are commonly modulated by the selective harmonic elimination (SHE) scheme, is enabled by a proposed SHE phase jittering method. Such active compensation method can be easily designed and implemented. Based on a dc-link virtual impedance concept, it is applied to actively attenuate the interharmonics caused by the harmonics interaction in high-power PWM current-source drives in this thesis. Besides, the proposed SHE phase jittering method is also developed to actively compensate the system background harmonics from the utility and the load. Compared with the active harmonic compensation strategies of SHE-modulated high-power PWM converters in previous works, the SHE-phase-jittering-based active compensation not only saves the effort on off-line calculations, but also realizes the on-line real-time harmonic compensation without any delay introduced.

Acknowledgement

I would like to express my deepest gratitude and sincere appreciation to my supervisor, Dr. Yunwei (Ryan) Li, for his insightful guidance, constant support, and excellent supervision throughout the whole research work.

I am also thankful to Dr. Navid R. Zargari and Dr. Zhongyuan (George) Cheng from Rockwell Automation Canada. They provided insightful suggestions and valuable feedback to my research work.

Thanks also go to all the colleagues in Dr. Li's research group, especially Jinwei He, Ruoshui (Raison) Ni, Jian Shang, Yuru Zhang, Yujuan (Jane) Lian, Hao Tian, and Zhongyi (Alex) Quan. Their kind support, inspiring advices, and disinterested assistance contributed a lot to my four-year research work in the university.

Besides, I am immensely indebted to my dear wife, Zhaorui (Rachel) Liu, and my parents for their great support and encouragement all the way through.

Finally, the financial support from Alberta Innovates Graduate Student Scholarship and Len Bolger Memorial Scholarship for Energy Research Excellence are also very much appreciated.

List of Abbreviations

AFE	Active Front End
AMR	Automatic Meter Reading
CCV	Cycloconverter
CHB	Cascaded H Bridge
CSI	Current-Source Inverter
CSR	Current-Source Rectifier
DFE	Diode Front End
EMF	Electromotive Force
FOC	Field-Oriented Control
GCT	Gate-Commutated Thyristor
GTO	Gate Turn Off
HV	High Voltage
IEGT	Injection-Enhanced Gate Transistor
IGBT	Insulated-Gate Bipolar Transistor
LCI	Load-Commutated Inverter
LV	Low Voltage
MV	Medium Voltage
PCC	Point of Common Coupling
PLC	Power Line Communication
PLL	Phase-Locked Loop
SCR	Silicon Controlled Rectifier
SHC	Selective Harmonics Compensation
SHE	Selective Harmonics Elimination
SPWM	Sinusoidal PWM
SVM	Space Vector Modulation
TFE	Thyristor Front End
TPWM	Trapezoidal PWM
VSI	Voltage-Source Inverter

Contents

Chapter 1 Introduction.....	1
1.1 Review of medium-voltage industrial drives.....	1
1.1.1 Technical requirements of MV drives.....	2
1.1.2 Configurations of MV industrial drive systems.....	3
1.2 Challenges faced by high-power PWM current-source drives.....	5
1.2.1 Potential <i>LC</i> resonance of PWM current-source converter systems.....	6
1.2.2 Modulation schemes with low device switching frequency.....	8
1.2.3 Interharmonic issues caused by small dc choke.....	11
1.2.4 Attenuation of harmonics and interharmonics.....	13
1.3 Research objectives and thesis layout.....	14
Chapter 2 Investigation of Interharmonics in High-Power PWM Current-Source Drives with Thyristor Front End.....	18
2.1 Analysis of dominant interharmonics in ac sides.....	18
2.1.1 Modulation function of current-source converter.....	19
2.1.2 Distortion of dc-link current.....	20
2.1.3 Frequencies of dominant interharmonics at ac sides.....	23
2.2 Analysis of interharmonics' impacts.....	24
2.2.1 Communication interfered by line-side interharmonics.....	25
2.2.2 Torsional vibration excited by motor-side interharmonics.....	28
2.3 Reduction of interharmonics' impacts through PWM pattern design.....	33
2.4 Verification results.....	37
2.4.1 Verification of interharmonics' frequency analysis and estimation of impacts' occurrence.....	38
2.4.2 Verification of redesigned PWM pattern aiming to reduce line-side communication interference.....	40
2.5 Summary and discussion.....	41
Chapter 3 Investigation of Interharmonics in High-Power PWM Current-Source Drives with Active Front End.....	43

3.1 Investigation of harmonics interaction.....	44
3.1.1 Generalized frequency and sequence relationship between ac side and dc link.....	45
3.1.2 Iteration concept based frequency analysis.....	48
3.2 Analysis of <i>LC</i> resonance occurrence.....	51
3.3 Verification results.....	55
3.3.1 Simulation results.....	55
3.3.2 Experimental results.....	59
3.4 Summary and discussion.....	64
Chapter 4 Active Attenuation of Interharmonics in High-Power PWM Current-Source Drives.....	66
4.1 Active interharmonic compensation based on SHE phase jittering method...	67
4.2 DC-link virtual impedance based active attenuation of harmonics interaction.....	74
4.3 Detailed analysis on the design of dc-link virtual impedance.....	79
4.3.1 Relationship between K_v and Z_v under different resonance conditions...	80
4.3.2 Selection of K_v to Z_v 's enable attenuation effect.....	83
4.4 Verification results.....	87
4.4.1 Simulation results.....	87
4.4.2 Experimental results.....	89
4.5 Summary and discussion.....	92
Chapter 5 Active Compensation of System Background Harmonics in High-Power PWM Current-Source Drives.....	94
5.1 Review of SHC-scheme-based active harmonic compensation.....	96
5.2 Active harmonic compensation based on SHE phase jittering method.....	98
5.2.1 Real-time active harmonic compensation through SHE phase jittering method.....	99
5.2.2 Influence of harmonics in SHE pattern on SHE-phase-jittering-based active harmonic compensation.....	102
5.2.3 Coefficient design in the implementation of SHE-phase-jittering-based active harmonic compensation.....	106

5.3 Compensation of two harmonics based on the combination of SHE phase jittering method and SHC scheme.....	110
5.4 Verification results.....	115
5.4.1 Experimental results of the attenuation on 5th line current harmonic through the SHE phase jittering method.....	115
5.4.2 Experimental results of the attenuation on 5th and 7th line current harmonics based on the combination approach.....	119
5.5 Summary and discussion.....	121
Chapter 6 Conclusions and Future Work.....	125
6.1 Conclusions.....	125
6.2 Thesis contributions.....	127
6.3 Future work.....	130
References.....	132

List of Figures

Fig. 1. 1. Major configurations of MV drive systems.	4
Fig. 1. 2. Typical 6.6kV PWM current-source drive with 18-pulse SCR rectifier. 6	
Fig. 1. 3. Typical 6.6kV PWM current-source drive with PWM CSR.	7
Fig. 1. 4. Modulation schemes for PWM current-source converter: (a) SVM, (b) TPWM, (c) SHE.	9
Fig. 1. 5. FFT analysis of PWM pattern (540Hz switching frequency, 60Hz fundamental frequency) (a) SVM, (b) TPWM, (c) SHE.	10
Fig. 1. 6. Control diagram of a real high-power PWM current-source industrial drive application (with AFE).	11
Fig. 1. 7. Modulation schemes for PWM CSI in Fig. 1. 6.	12
Fig. 2. 1. Schematic diagram of three-phase current-source converter.	19
Fig. 2. 2. Simplified configuration of high-power PWM current-source drive with 18-pulse SCRs TFE.	21
Fig. 2. 3. Mechanism of AMR system interfered by line-side interharmonics produced by drive systems.	25
Fig. 2. 4. Estimation of the occurrence of AMR system interfered by the line-side interharmonics.	27
Fig. 2. 5. Frequencies of line-side current interharmonics related to the interference with AMR system.	28
Fig. 2. 6. PWM pattern of SHE-modulated PWM CSI in a high-power PWM current-source drive application.	29
Fig. 2. 7. Schematic diagram of two-mass system.	30
Fig. 2. 8. Block diagram of two-mass system.	30
Fig. 2. 9. Estimation of the occurrence of torsional vibration due to motor-side interharmonics.	32
Fig. 2. 10. Generation of $ \omega_i \pm 12\omega_i $ -frequency interharmonics in line current. ...	35

Fig. 2. 11. Redesigned SHE patterns of PWM CSI to minimize line-side interference with AMR system.	37
Fig. 2. 12. Simulation results of line current interharmonics with frequencies from 540Hz to 600Hz at different motor operating frequencies.	39
Fig. 2. 13. Simulation results of motor electromagnetic torque interharmonics with frequencies from 1Hz to 100Hz at different motor operating frequencies.	40
Fig. 2. 14. Simulation results of line current interharmonics with frequencies from 540Hz to 600Hz at different motor operating frequencies after adopting the redesigned SHE PWM patterns.	41
Fig. 3. 1. Frequency and sequence relationship between the dc-link current and the ac-side current through the PWM current-source converter.	47
Fig. 3. 2. Frequency and sequence relationship between the ac-side voltage and the dc-link voltage through the PWM current-source converter.	48
Fig. 3. 3. Simplified configuration of high-power PWM current-source drives with PWM CSR.	49
Fig. 3. 4. Flow chart of one iteration.	50
Fig. 3. 5. Frequency analysis during the first iteration.	50
Fig. 3. 6. Equivalent per phase harmonic circuit: (a) line side, (b) motor side. ...	52
Fig. 3. 7. <i>LC</i> resonance occurs in the first iteration.	53
Fig. 3. 8. <i>LC</i> resonance occurs in the second iteration.	54
Fig. 3. 9. Bode plot of transfer function $\bar{V}_c(s) / \bar{I}_w(s)$ shown in (3-12).	56
Fig. 3. 10. Harmonic content in the modulation function of a 9-pulse SHE PWM pattern.	57
Fig. 3. 11. Frequency plot of (3-18) for simulation system.	58
Fig. 3. 12. Steady-state dc-link current harmonics versus motor operating frequency (ω_i).	58
Fig. 3. 13. Line current harmonics vs. motor operating frequency (ω_i).	59
Fig. 3. 14. Motor stator current harmonics vs. motor operating frequency (ω_i)...	59
Fig. 3. 15. Setup of 10kVA/208V PWM current-source drive (with AFE) prototype.....	60

Fig. 3. 16. Frequency plot of (3-18) for experimental system.	61
Fig. 3. 17. Waveforms of line current, dc-link current, and motor stator current at 42Hz motor operating frequency ($\omega_i=42\text{Hz}$) (10A/div., 20ms/div.).	62
Fig. 3. 18. FFT analysis of Fig. 3. 17.	62
Fig. 3. 19. Waveforms of line current, dc-link current, and motor stator current at 53Hz motor operating frequency ($\omega_i=53\text{Hz}$) (10A/div., 20ms/div.).	63
Fig. 3. 20. FFT analysis of Fig. 3. 19.	63
Fig. 4. 1. Diagram of SHE-modulated PWM current-source converter.	68
Fig. 4. 2. Diagram of SHE phase jittering method.	69
Fig. 4. 3. Diagram of \bar{S}_{wh} and \bar{S}_w^{SHEh}	70
Fig. 4. 4. Illustration of the basic operating principle of the SHE phase jittering method.	71
Fig. 4. 5. Properties of Bessel functions: (a) $J_0(M_{comp})$ vs. M_{comp} ; (b) $J_1(M_{comp})$ vs. M_{comp} ; (c) $J_2(M_{comp})$ vs. M_{comp}	72
Fig. 4. 6. Concept of dc-link virtual impedance.	75
Fig. 4. 7. DC-link virtual impedance realized by the SHE phase jittering method adopted at PWM CSR.	75
Fig. 4. 8. Transfer function model of Fig. 4. 7.	76
Fig. 4. 9. Simplified transfer function model of Fig. 4. 8.	77
Fig. 4. 10. Simplified diagram of dc link at ω_{dcm} frequency.	77
Fig. 4. 11. Illustration of dc-link virtual impedance introduced by the active attenuation method.	79
Fig. 4. 12. Illustration of LC resonance conditions' estimation.	81
Fig. 4. 13. Illustration of $ K_v $'s influence on the virtual impedance.	84
Fig. 4. 14. Illustration of $ K_v $'s influence on the modulation index.	85
Fig. 4. 15. Illustration of $ K_v $'s influence on the interharmonics in line-side PWM current.	86
Fig. 4. 16. Steady-state dc-link current harmonics versus motor operating frequency (ω_i) after using the proposed method.	88

Fig. 4. 17. Line current harmonics vs. motor operating frequency (ω_i) after using the proposed method.	88
Fig. 4. 18. Motor stator current harmonics vs. motor operating frequency (ω_i) after using the proposed method.	89
Fig. 4. 19. Waveforms of line current, dc-link current, and motor stator current at $\omega_i=42\text{Hz}$ after using the proposed method (10A/div., 20ms/div.).	90
Fig. 4. 20. FFT analysis of Fig. 4. 19.	90
Fig. 4. 21. Waveforms of line current, dc-link current, and motor stator current at $\omega_i=53\text{Hz}$ after using the proposed method (10A/div., 20ms/div.).	91
Fig. 4. 22. FFT analysis of Fig. 4. 21.	91
Fig. 5. 1. Diagram of SHC-scheme-based active attenuation on 5th line current harmonic in high-power PWM current-source drive system.	96
Fig. 5. 2. Basic operating principle of SHC-scheme-based active harmonic compensation.	97
Fig. 5. 3. Diagram of SHE-phase-jittering-based active attenuation on 5th line current harmonic in high-power PWM current-source drive system.	101
Fig. 5. 4. Influence of harmonics in SHE PWM pattern on 5th harmonic compensation after introducing θ_{comp}	103
Fig. 5. 5. Magnitude of $\bar{S}_{w(-5)}^{SHE(-11)}$ and $\bar{S}_{w(-5)}^{SHE(-17)}$ versus M_{comp}	104
Fig. 5. 6. Influence of harmonics in SHE PWM pattern on 7th harmonic after introducing θ_{comp}	105
Fig. 5. 7. Magnitude of \bar{S}_{w7}^{SHE13} and \bar{S}_{w7}^{SHE19} versus M_{comp}	105
Fig. 5. 8. Simplified steady-state diagram of Fig. 5. 3 at 5th harmonic.	107
Fig. 5. 9. $J_0(M_{comp})$, $J_1(M_{comp})$, and $J_2(M_{comp})$ versus M_{comp}	108
Fig. 5. 10. Diagram of active attenuation on 5th and 7th line current harmonic based on combination approach in high-power PWM current-source drive.	113
Fig. 5. 11. Function f_{cost} of 11-pulse SHC switching angles' solution under different M_{SHC7}^* and φ_{SHC7}^*	114
Fig. 5. 12. Harmonic content of 9-pulse SHE PWM pattern.	116

Fig. 5. 13. Steady-state compensation performance under 1% 5th grid voltage harmonic (i_s : 5A/div, i_w : 10A/div, i_{dc} : 10A/div, time: 10ms/div.).	116
Fig. 5. 14. Current waveforms before and after using the SHE-phase-jittering-based active harmonic compensation under different 5th (1%) and 7th (1%) grid voltage harmonics' phases.	117
Fig. 5. 15. FFT analysis of line current in Fig. 5. 14.	118
Fig. 5. 16. Transient of applying compensation method.	118
Fig. 5. 17. Transient of 1% step change of 5th grid voltage harmonic.	118
Fig. 5. 18. Current waveforms before and after using the combination approach under different 5th (0.7%) and 7th (0.7%) grid voltage harmonics' phases.	120
Fig. 5. 19. FFT analysis of line current in Fig. 5. 18.	121
Fig. 5. 20. Current waveforms before and after using the combination approach under different 5th (1.1%) and 7th (1.1%) grid voltage harmonics' phases.	122
Fig. 5. 21. FFT analysis of line current in Fig. 5. 20.	123

List of Tables

TABLE. 2. 1. Summary of interference occurrence conditions.	28
TABLE. 2. 2. Summary of torsional vibration occurrence conditions.	33
TABLE. 2. 3. Parameters of a 1MVA/4160V PWM current-source drive applica- tion with TFE (simulation).	38
TABLE. 3. 1. Parameters of a 1MVA/4160V PWM current-source drive applica- tion with AFE (simulation).	56
TABLE. 3. 2. Parameters of 10kVA/208V PWM current-source drive prototype with AFE (experiment).	61
TABLE. 4. 1. Magnitude of harmonics before and after attenuation.	92
TABLE. 5. 1. Experiment parameters.	115
TABLE. 5. 2. Experiment parameters.	119

Chapter 1

Introduction

With the fast development of high-power switching devices such as gate-turn-off (GTO) thyristors, gate-commutated thyristors (GCTs), high-power insulated-gate bipolar transistors (IGBTs), and injection-enhanced gate transistors (IEGTs), the medium-voltage (2.3-13.8kV) high-power (megawatt range) motor drives are widely implemented in industrial areas for high-power fans, pumps, compressors, conveyor, and other equipment [1]-[13]. Among the medium-voltage (MV) drive applications, the use of high-power PWM current-source drive systems is increasing during these years, due to the features of simple structure, motor friendly waveforms and reliable short-circuit protection [1],[3],[14]-[23].

A typical challenge being faced by the high-power PWM current-source drives is the problem of system harmonics and interharmonics. In such drive systems, the harmonics and interharmonics from background system (utility and load), power converters and harmonics interaction between rectifier and inverter may result in the deterioration of line power quality, motor derating, load torsional vibration, electrical resonance and etc. The research reported in this thesis was undertaken to (1) thoroughly investigate the harmonics and interharmonics problem in the high-power PWM current-source drives, and (2) actively attenuate the harmonics and interharmonics through the high-power PWM current-source converters.

The following sections in this chapter elaborate the background information of this work, introduce the objectives of this research project, and outline the structure of this thesis.

1.1 Review of medium-voltage industrial drives

The evolution of semiconductor switching devices toward higher power rating with improved efficiency and reliability leads to the wide applications of high-power converters in industry drives. In recent years, due to the fast development of high-power converters, the MV adjustable speed drive systems have found widespread applications in the basic material industry (e.g. process industry, energy, ship propulsion and traction) for the retrofit of conventional mechanically-adjusted systems with fixed-speed drives [1]-[13]. In this section, the technical requirements and the configurations of MV drives are reviewed.

1.1.1 Technical requirements of MV drives

The general requirements of the MV drive systems mainly include

- high reliability, efficiency, and availability,
- low manufacturing, operating, and maintenance cost,
- small space requirement,
- easy installation, integration and maintenance.

Some applications further require the MV drives to be capable of regenerative braking capability and four-quadrant operation.

Besides, the requirements of line power quality and the challenges related to motor operation also need to be considered for the MV drive applications.

For the line-side power quality, certain guidelines for harmonic regulation (e.g. IEEE Standard 519-2014 and IEC 61000-3-6) limit the distortion of the line current drawn by the users [24]-[28]. The MV drives should comply with these guidelines to avoid affecting utility and other users or electrical loads connected at the same point of common coupling (PCC). In addition, most of the electric utility companies have instituted penalties for the users with a low power factor, which is also an important requirement for MV drives due its high power rating. Moreover, for the MV drive systems using line-side capacitors to reduce current distortion and/or improve power factor, the potential resonance problem needs to be considered and addressed during implementation.

For the motor side, the insulation failure of motor windings and the electromagnetic interference associated with high dv/dt and wave reflections should be avoided in MV drive applications. On the other hand, low common-mode voltage stress is expected on the motor in MV drives in order to prevent from being damaged by the failure of winding insulation. Furthermore, as well as the line side, the harmonics produced at the motor side also challenges the MV drive systems, which may also cause numerous problems, such as excessive power losses in motor winding and magnetic core, torsional vibrations of mechanical load, and electrical resonance in the drives with filter capacitors.

1.1.2 Configurations of MV industrial drive systems

To meet the requirements of the MV drive systems, many drive configurations have been developed for different applications, among them, the most commercialized products are classified according to the converter topologies and summarized as shown in Fig. 1. 1 [1]-[3],[29]-[49]. At first, they are simply divided into two groups, direct topologies and indirect topologies, based on the stages of power transfer from the source to the load. The direct topologies directly connect the motor to the power supply through the power converter (ac to ac), while the power is transferred through two stages, rectification (ac to dc) and inversion (dc to ac), in the indirect topologies. In addition, the indirect topologies can be further classified into voltage-source topologies and current-source topologies, depending on the types of energy storage at dc link. The different inverter topologies of MV drives are listed in these two subcategories of indirect topologies. For the rectifier, the multi-pulse diode front end (DFE) with phase-shifting transformer and the PWM active front end (AFE) with isolation transformer are commonly used in voltage-source MV drives, and the multi-pulse thyristor front end (TFE) with phase-shifting transformer and the PWM AFE with isolation transformer are mainly adopted in the current-source drives. The phase-shifting transformer can contribute to the reduction of common-mode voltage stress on the motor so as to avoid the premature failure of motor winding insulation. However, the use of transformer brings a few drawbacks, such as high manufacturing cost (accounts for approximate 20%-25%

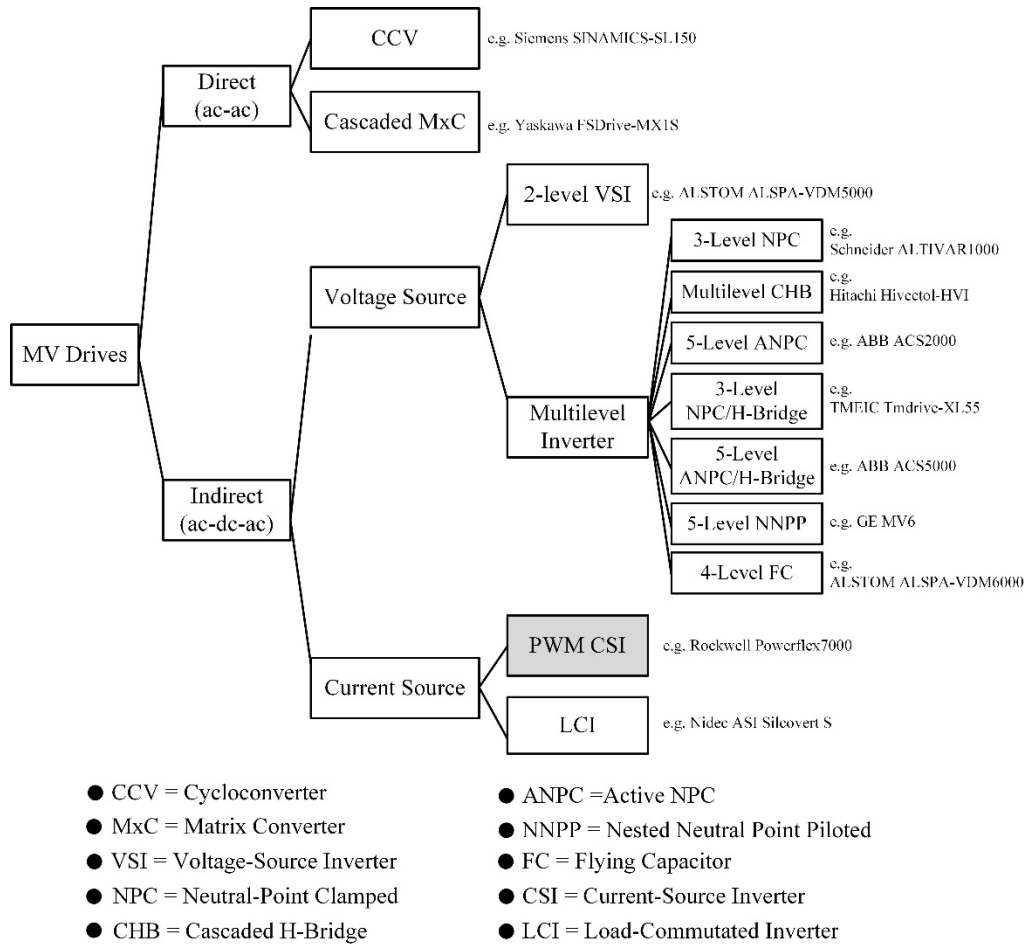


Fig. 1. 1. Major configurations of MV drive systems.

of overall cost [1]), high operating cost due to transformer power losses, and aggravated size and weight. To solve such problems, the transformerless configurations become popular in recent years. Since the common-mode inductance can be easily integrated into the dc choke in current-source drives, which leads to the elimination of the isolation transformer, the transformerless current-source drive technology has wide applications in the industry.

With respect to the power switching devices adopted in recent MV drives, the IGBTs, GCTs and IEGTs are commonly used in PWM voltage-source converter applications, and the symmetrical GCTs (SGCTs) are mainly used in the PWM current-source converter systems. In addition, the low-voltage (LV)-IGBTs (1.2kV

and 1.7kV) are usually applied in the cascaded multi-cell topologies, such as cascaded H-bridge (CHB), while the high-voltage (HV)-IGBTs (3.3kV, 4.5kV, 6.5kV), GCTs (4.5kV, 5.5kV, 6.5kV) and IEGTs (3.3kV, 4.5kV) are widely used in other applications. The silicon controlled rectifier (SCR) devices are adopted in the cycloconverter (CCV) drives, load-commutated inverter (LCI)-fed drives and TFE for higher power rating (tens of megawatts) applications with low manufacturing cost and high energy efficiency. Besides, switching devices are often connected in series in the MV drives to achieve higher voltage capacity.

1.2 Challenges faced by high-power PWM current-source drives

Among the configurations of MV drives, current-source drive technology has been widely accepted in the industry. In general, the current-source converter topologies feature a simple converter structure, motor friendly waveforms (low switching dv/dt), and reliable short-circuit protection. As shown in Fig. 1. 1, two main current-source drive configurations are the LCI-fed drives and the PWM CSI-fed drives (with TFE or AFE). For the SCR-based LCI-fed drives, due to the low manufacturing cost and high efficiency and power rating of SCR devices, it is suitable for very large drives with power rating from tens of megawatts to one hundred megawatt. As the SCR device is naturally commutated by load voltage due to the self-extinguishing incapability, the loads of LCI-fed drives are commonly synchronous motors operating at a leading power factor. In addition, multi-pulse SCR bridges, and harmonic filter and power factor correction are equipped in practical applications to reduce line current distortion; multi-phase synchronous motors are preferred for the reduction of torque pulsations and mechanical stress on the motor shaft [3],[50]-[56]. In comparison with LCI-fed drives, the PWM CSI-fed drives can easily fulfill lower motor torque ripples and higher line power quality (with AFE), and are suitable for both MV induction motors and synchronous motors under various operation conditions, due to the PWM operation. As a result, it is a preferred choice for most MV drive applications in the range of 1-10 megawatt

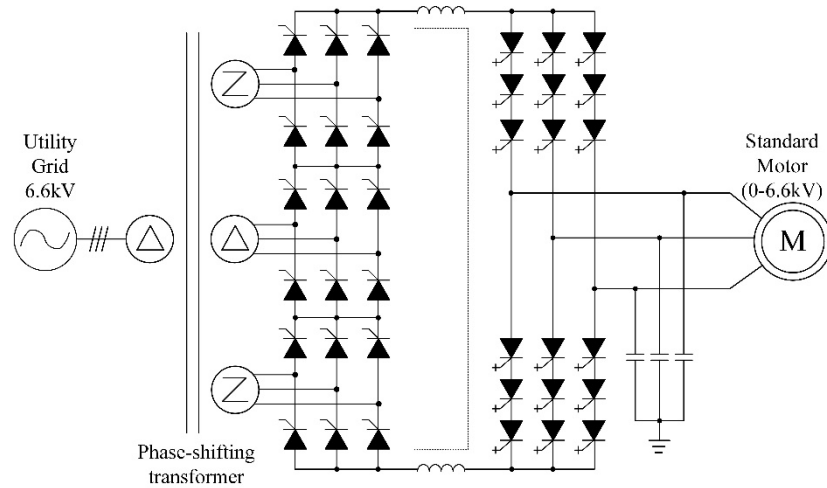


Fig. 1. 2. Typical 6.6kV PWM current-source drive with 18-pulse SCR rectifier.

[1],[14]-[23]. In this section, the challenges faced by the high-power PWM current-source drive systems are elaborated.

1.2.1 Potential *LC* resonance of PWM current-source converter systems

Three typical configurations of high-power PWM current-source industrial drives for 6.6kV applications are shown in Figs. 1. 2 and 1. 3. To meet the harmonic guidelines set by most standards, an 18-pulse SCR bridges or a single-phase PWM current-source rectifier (CSR) is commonly used as front end. The phase-shifting transformer in Fig. 1. 2 and the isolation transformer in Fig. 1. 3(a) can reduce the common-mode voltage stress on the motor as discussed earlier. The common-mode voltage stress can also be relieved by the integrated dc choke that provides both differential and common-mode inductances as shown in Fig. 1. 3(b). The use of the integrated dc choke leads to the elimination of the transformer, which significantly lower the manufacturing and operating costs. Such transformerless configuration is widely applied in real applications.

As shown in Figs. 1. 2 and 1. 3, the PWM current-source converter requires a three-phase capacitor at ac side to assist the commutation of the switching devices. The capacitor provides a current path for ac-side inductances (e.g. line inductance,

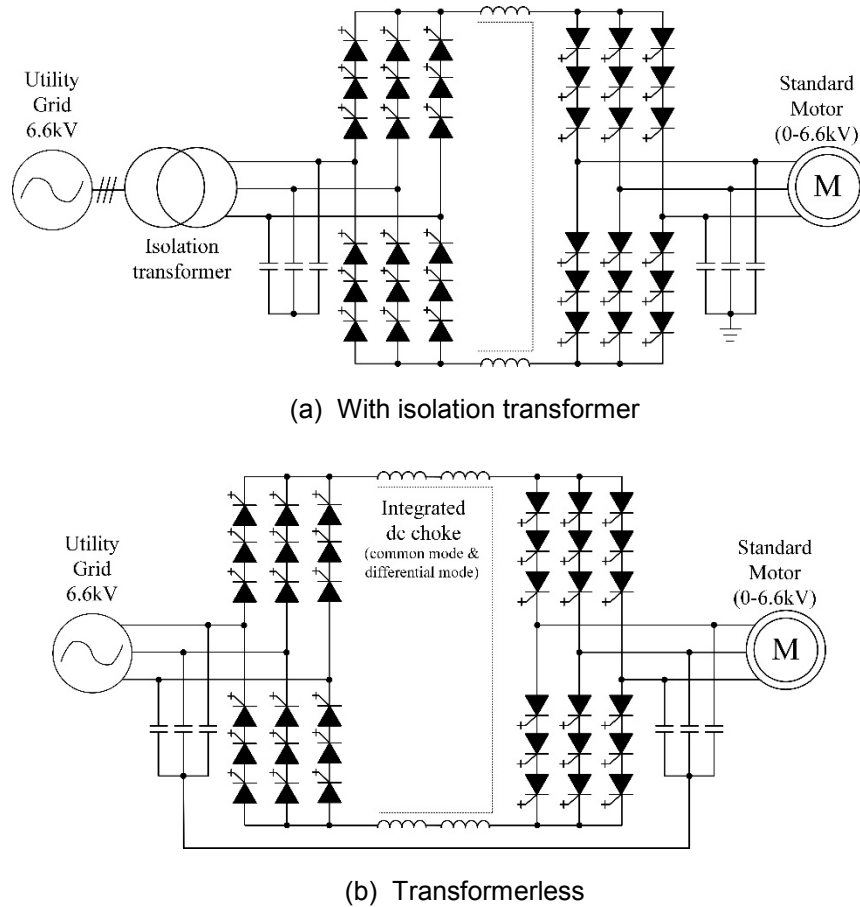


Fig. 1. 3. Typical 6.6kV PWM current-source drive with PWM CSR.

motor inductance) to reduce di/dt at the instant of switching (the rising and falling edge of PWM current). Otherwise, a high voltage spike would be caused that results in the damages of switching devices. The capacitor also acts as a harmonic filter to reduce the distortion of ac-side waveforms. However, it forms an LC circuit with the ac-side inductance so that the potential LC resonance problem exists in the PWM current-source drives. As the MV-level utility supply and motor normally have a very low impedance, the lightly-damped LC resonance may cause significant current distortion, excessive power loss, and even overvoltage that could destroy the devices in the high-power PWM current-source drive systems.

Considering the low switching frequency of high-power PWM converters (will be explained later), the capacitor is commonly sized between 0.3pu to 0.5pu [1],[57]. With respect to the drive system with a PWM CSR, the capacitors at the

line side (input of CSR) and the motor side (output of CSI) are preferred to have a similar size to approach unity power factor at rated condition [58]. In addition, to reduce the line current distortion, a three-phase reactor are inserted at the line side of PWM CSR. Such line reactor also lowers the impact of supply inductance variation on the value of total inductance between the utility supply and the rectifier. In the following analysis, the line inductance of the PWM current-source drives with AFE is considered to include equivalent inductance of the supply, leakage inductance of transformer (if any), and the inductance of line reactor. The value of the line inductance is normally in the range of 0.1pu to 0.15pu. As a result, the line-side LC resonant frequency will be within 3.6pu to 5.8pu (216Hz to 348Hz at 60Hz fundamental frequency). For the motor side, the resultant LC resonant frequency is in the similar range as the line side by taking the normal leakage inductance of high-power motors into account [14].

1.2.2 Modulation schemes with low device switching frequency

For the MV drives with PWM converters, the device switching loss makes up a significant proportion of the total power loss. The minimization of switching loss not only lowers the operating cost of the drive system, but also leads to the reduction of system cooling requirements so as to reduce physical size and manufacturing cost. To minimize the switching loss, the device switching frequency is normally limited to a few hundred hertz [1],[14]. Due to the reduction of switching frequency, the high-power PWM converter is prone to produce low-frequency harmonics, such as 5th-order and 7th-order harmonics (300Hz and 420Hz at 60Hz fundamental frequency). According to the analysis in previous section, such low-frequency harmonics may cause significant distortion waveforms at the line and/or motor side due to the LC resonance mode.

To reduce the waveform distortion, the modulation schemes of high-power PWM converters are expected to have a superior harmonic performance with limited switching frequency. With respect to the modulation of PWM current-source converters, three schemes are most studied and employed, space vector modulation

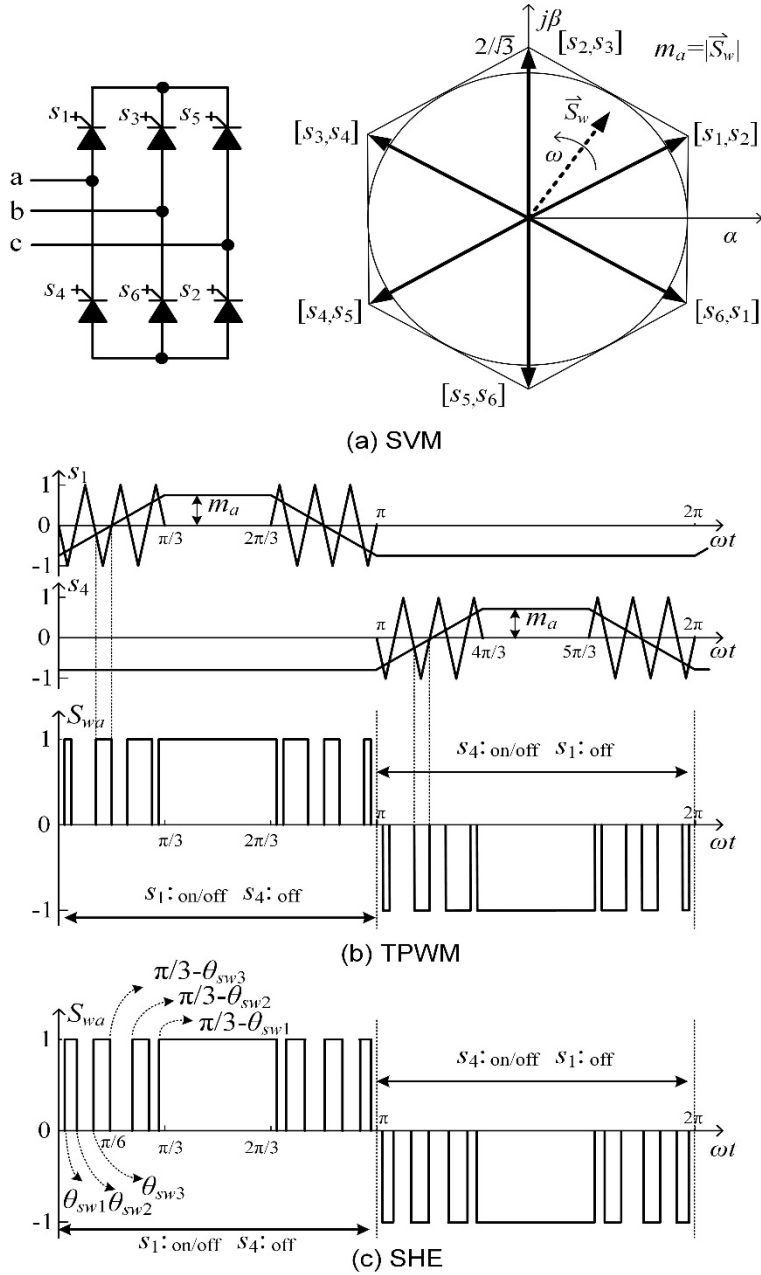


Fig. 1. 4. Modulation schemes for PWM current-source converter: (a) SVM, (b) TPWM, (c) SHE.

(SVM), trapezoidal PWM (TPWM), and selective harmonic elimination (SHE) [59]-[65]. The basic principle of such three schemes can be illustrated as shown in Fig. 1. 4. For the SVM scheme, the three-phase PWM pattern vector \vec{S}_w is synthesized by three nearby stationary vectors, based on which the state of each switch in the converter can be determined. The TPWM is similar to the carrier-based PWM

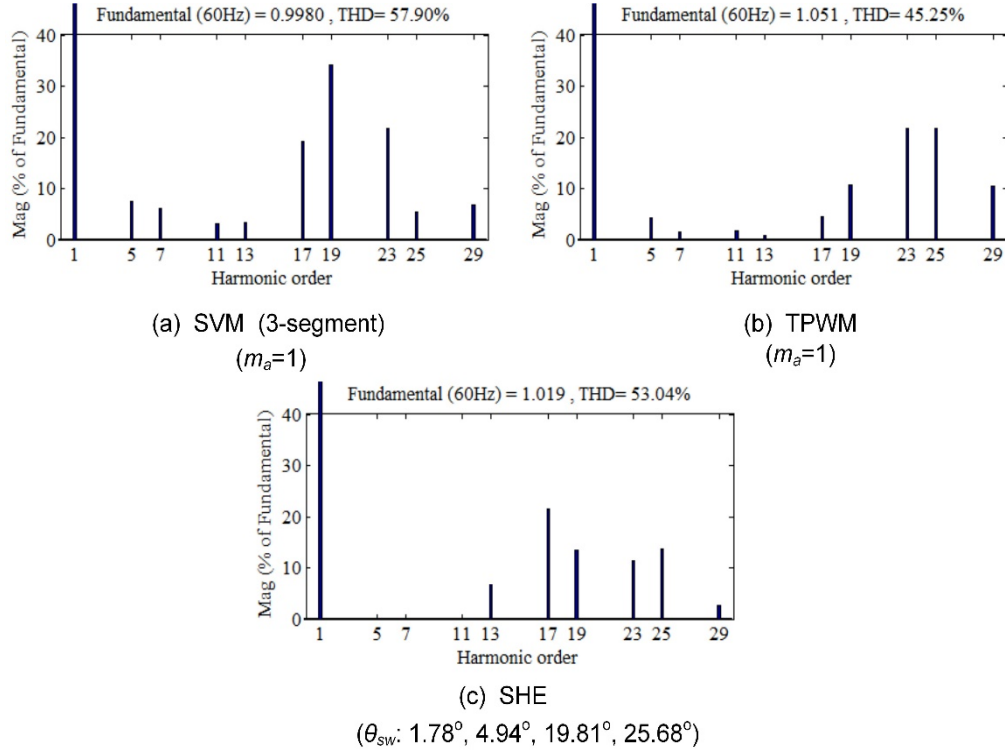


Fig. 1. 5. FFT analysis of PWM pattern (540Hz switching frequency, 60Hz fundamental frequency) (a) SVM, (b) TPWM, (c) SHE.

schemes for voltage-source converters, where the PWM pattern per phase (the state of switches in one leg) is determined by comparing the trapezoidal modulation wave with the carrier wave. With respect to the SHE scheme, the switching angles θ_{sw} are off-line calculated to eliminate a number of unwanted harmonics in the PWM pattern by solving a nonlinear trigonometry equation set. For instance, a 7-pulse (half cycle) SHE scheme as shown in Fig. 1. 4(c) has three independent switching angles θ_{sw1} , θ_{sw2} , and θ_{sw3} that can be calculated to eliminate maximum three harmonics in PWM pattern. To illustrate the harmonic performance under the conditions of low switching frequency, a FFT analysis of the PWM pattern produced by the three modulation schemes is shown in Fig. 1. 5. It can be observed that significant low-order harmonics (e.g. 5th, 7th and 11th) are produced by the SVM scheme and the TPWM scheme. Note that the problem of low-order harmonics is still severe at other modulation index (m_a) value in this two schemes [62]. Compared with the SVM and the TPWM scheme, the SHE scheme has a superior harmonic performance with low switching frequency. Therefore, it is normally

adopted to modulate PWM CSR (60Hz line frequency) and PWM CSI at high motor operating frequency (fundamental frequency) in the high-power PWM current-source drive systems [1],[15]-[17],[19],[20],[22]. In addition, since the switching frequency is the product of the pulse number of SHE scheme and the fundamental frequency, the pulse number of SHE scheme at PWM CSI can be increased to eliminate more low-order harmonics as the decrease of motor operating frequency while guarantees the switching frequency within the limit. However, as the number of unwanted harmonics increases, the complexity of SHE switching angles' calculation will be significantly increased. As a result, at very low motor operating frequency, the TPWM or the SVM is normally utilized to modulate the PWM CSI [16],[17],[22]. The control diagram of a real high-power PWM current-source industrial drive application (with AFE) is shown in Fig. 1. 6, and the detailed modulation scheme of PWM CSI is illustrated in Fig. 1. 7 (switching frequency is confined within 420Hz). To minimize the dc-link current so as to reduce power losses, the modulation index of PWM CSI is maintained at the maximum (around 1) and the dc-link current is controlled through the delay angle α of PWM CSR. Note that the modulation index of SHE-modulated PWM CSR is also fixed at the maximum.

1.2.3 Interharmonic issues caused by small dc choke

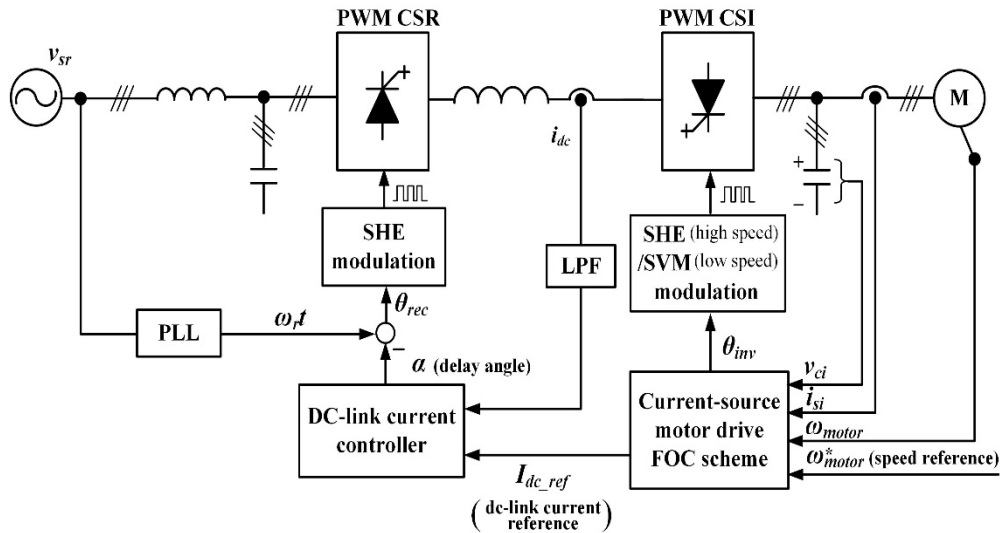


Fig. 1. 6. Control diagram of a real high-power PWM current-source industrial drive application (with AFE).

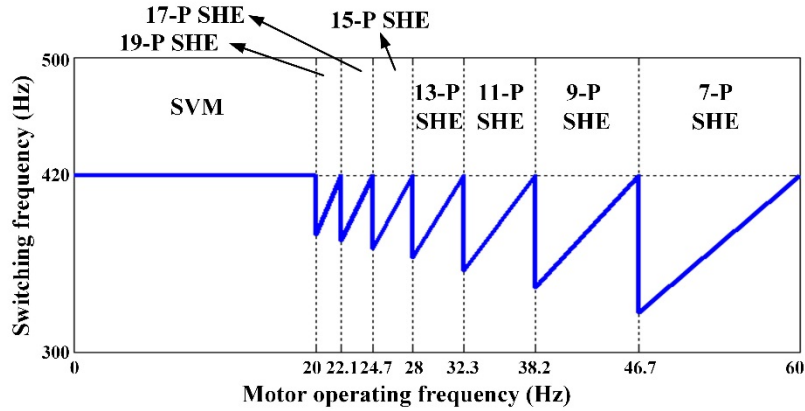


Fig. 1. 7. Modulation schemes for PWM CSI in Fig. 1. 6.

For current-source systems, a dc choke is required to provide constant current for the load. In the practice for common-mode voltage reduction, it is preferred to have a magnetic core with two coils connected in the positive and negative dc bus respectively as shown in Fig. 1. 3(b) [66],[67]. With respect to the high-power current-source drives, in order to reduce the physical size, the inductance of dc choke is normally confined within a reasonably low value ($<0.8\text{pu}$) [1]. As discussed earlier, the SHE-modulated PWM CSR (as AFE) and the 18-pulse SCR rectifier with phase-shifting transformer (as TFE) are able to effectively reduce the low-order harmonics in line-side current so as to meet the harmonic requirements of MV drives. Nevertheless, the harmonics produced by such two types of rectifier at dc link (e.g. 18th harmonic of TFE, 18th and 24th harmonics of AFE) cannot sufficiently attenuated by the small dc choke inductance, which results in a non-negligible distortion of dc-link current. In the same manner, the dc-link harmonics produced by the PWM CSI may also distort the dc-link current. Through the rectifier and the inverter, the distorted dc-link current will introduce harmonics and interharmonics in both the line side and the motor side. Due to the ac-side LC circuit, the newly-introduced harmonics and interharmonics may be amplified and further aggravate the distortion of dc-link current through the converters. Following this procedure of harmonics interaction between the rectifier and the inverter through the dc link, the interharmonics with many possible frequencies may be generated in the entire drive system.

The interharmonics produced by the drive system may give rise to a host of problematic cases. For the utility supply, the interharmonic current drawn by the users will result in a variety of system impacts, such as heating effects, flicker, overload of conventional series tuned filters, current transformer saturation and communications interference [68]-[72]. For the motor, the torque pulsation due to the interharmonic current may cause speed jitter, intolerable acoustic noise and additional copper losses in the stator and the rotor [69],[73]. Moreover, the frequencies of the interharmonics will be varied at different motor speeds. In high-power PWM current-source drives, when the motor operates at certain speeds, the interharmonic frequencies can be very close to the LC resonant frequency. It will excite the electrical resonance that may result in further deterioration of line power quality and significant motor torque ripples. Besides, for the applications with high torque and large inertia load, a potential resonance normally exists in mechanical system. The low-frequency torque pulsation due to the interharmonic current at motor side may also give rise to the mechanical resonance problems, always referring as “torsional vibration problem”. Consequently, the system immediate failure or cumulative damage that may go unnoticed catastrophic failure will occur [74]-[77].

1.2.4 Attenuation of harmonics and interharmonics

Although the aforementioned adoption of modulation schemes can effectively reduce the current/voltage distortion caused by the low-order PWM harmonics of high-power converters, the problem of harmonics and interharmonics remains in the high-power PWM current-source drives that should be addressed. On the one hand, the interharmonic problem due to the small dc choke may have strong impacts on the drive systems as mentioned above. On the other hand, the low-order harmonics (e.g. 5th and 7th) from utility supply can result in significant current distortion due to the LC resonance mode when the PWM CSR is adopted as AFE. Similarly, due to the imperfect winding distributions, the motor back electromotive force (EMF) may contain low-order harmonics even with sinusoidal excitation current, which can severely distort the stator current due to the motor-side LC resonance as

well [78]. Consequently, the attenuation of harmonics and interharmonics is a critical issue in high-power PWM current-source drives.

To reduce the harmonics and interharmonics, the mostly used method in industry is through passive damping and passive filter. However, all of them are not practical under the MV high-power condition, since considerable power losses and additional costs are involved. Therefore, the active attenuation of harmonics and interharmonics is preferred in high-power PWM current-source drives. Nonetheless, as an off-line modulation scheme, the SHE scheme, that is mostly adopted to modulate the high-power PWM converters, lacks the capability to realize the active compensation of harmonics and interharmonics [57]. On the one hand, with the fixed modulation index (m_a) in a fundamental cycle of SHE PWM pattern, the proposed m_a -based active compensation methods [21],[57],[79]-[87] cannot be applied on such off-line technique. On the other hand, the constraint of quarter-wave symmetry in SHE scheme confines all the harmonics in PWM pattern to be either in phase or anti-phase with the fundamental [88]-[90], which means that the phase of each harmonic is uncontrollable. In order to attenuate the harmonics and interharmonics without additional costs and losses involved, the active compensation ability of SHE-modulated PWM converters is expected to be enabled in the high-power drive systems.

1.3 Research objectives and thesis layout

Aiming to solve the problem of harmonics and interharmonics faced by the high-power PWM current-source drives, a thorough investigation of harmonics interaction phenomenon and a comprehensive study of active compensation strategies based on the SHE scheme are conducted in this thesis.

Regarding the related analysis of interharmonics in high-power drive systems, many studies have been carried out with focuses on the two-level PWM VSI-fed drives and the LCI-fed drives. In the PWM voltage-source drives, since the dc link is usually equipped with a large capacitor, the harmonics interaction problem is not

significant [91]. In the LCI-fed drives, the harmonics interaction appears stronger [92], and several models have been proposed for the frequencies analysis of interharmonics. Unlike the thyristor-based converters in LCI-fed drives, the SHE-modulated PWM current-source converters are flexible in eliminating harmonics during the modulation, so that the frequencies of the produced interharmonics are not easily determined as they are in LCI-fed drives. Besides, the inherent LC resonance problem could make the analysis of harmonics interaction more complex in PWM current-source drives due to its amplification of low-order harmonics. In this thesis, the generation of interharmonics due to the harmonics interaction is thoroughly investigated in the high-power PWM current-source drives with TFE and AFE respectively. In addition, the impacts of the interharmonics are studied with respect to three specific cases: communication interference, mechanical torsional vibration and electrical LC resonance.

With respect to the SHE-scheme-based active compensation, only a quasi-online selective harmonics compensation (SHC) scheme has been proposed [93]. Although it enables the high-power PWM current-source converters to actively compensate the utility harmonics, several disadvantages still exist, such as incapability of interharmonic compensation, considerable off-line calculation and difficulty in multiple harmonic compensation. To overcome these limitations, a real-time SHE-based active compensation strategy is proposed in this work. It not only saves the efforts on off-line calculation and realize the real-time compensation, but also enable the interharmonics and multi-harmonics compensation capability of SHE-modulated PWM current-source converters. The utilization of the proposed method to actively compensate the interharmonics and the utility harmonics in high-power PWM current-source drive system are also developed respectively in this work.

A summary of the research objectives addressed in each chapter is listed here.

Chapter 2

The interharmonics caused by the harmonics interaction in high-power PWM current-source drives with TFE is investigated in this chapter. The following research tasks are carried out.

- The dominant interharmonics produced in ac sides due to the weak dc link is investigated.
- The impacts of interharmonics is analyzed based on two main cases: line-side communication interference and motor-side torsional vibration problem.
- An estimation of the conditions that the impacts of interharmonics occur during the drive operation is conducted.
- A simple solution to reduce the impacts of interharmonics through the design of SHE PWM pattern is proposed.

Chapter 3

For the high-power PWM current-source drives with AFE, due to the SHE scheme adopted at both the PWM CSR and CSI and potential LC resonance exists in each ac side, the harmonics interaction phenomenon is more complex, and its impact related to the LC resonance will be more serious. Considering this issue, three research objectives are addressed in this chapter.

- The generalized frequency relationship between the ac-side components and dc-link components is derived.
- A frequency iteration concept is proposed to investigate the interharmonics with possible frequencies in entire system resulted from the harmonics interaction.
- An estimation method is developed to predict the conditions that the LC resonance is excited by the produced interharmonics and predetermine the frequencies of the significant interharmonics caused by the LC resonance.

Chapter 4

To actively attenuate the interharmonics in high-power PWM current-source drive systems so as to reduce its impacts without additional costs and losses, the following research objectives are addressed in Chapter 4.

- An SHE phase jittering method is proposed to enable the active interharmonic capability of SHE-modulated high-power PWM converters.
- A dc-link virtual impedance strategy is developed to actively attenuate the interharmonics in high-power PWM current-source drive systems based on the proposed SHE phase jittering method.
- Detailed discussions on the design and implementation of dc-link virtual impedance strategy are presented.

Chapter 5

The proposed SHE phase jittering method can also be developed to actively compensate the system background harmonics (from utility and load) through the PWM converter in high-power PWM current-source drives. It offers some advantages over the SHC-scheme-based active harmonic compensation proposed in previous works. In Chapter 5, the following research objectives are realized.

- A brief review of the SHC-scheme-based active harmonic compensation is conducted, and its drawbacks are discussed in details.
- The SHE-phase-jittering-based active harmonic compensation is developed to overcome the disadvantages of SHC scheme. Discussions on the design and implementation are provided with respect to its application on high-power PWM current-source drive system.
- Combined with the SHC scheme, the SHE phase jittering method is also developed to overcome the limitations of the previous works on the compensation of multiple harmonics.

Chapter 6

The conclusions of the research are presented in this chapter and a future research work is suggested.

Chapter 2

Investigation of Interharmonics in High-Power PWM Current-Source Drives with Thyristor Front End

Double conversion systems, where two ac systems with different frequencies are connected through a dc link, is one of the main interharmonic sources. A typical example of this class of sources is adjustable speed drives. Regarding the analysis of interharmonics in the adjustable speed drives, many studies have been carried out with focuses on the 2-level PWM voltage-source inverter (VSI)-fed drives with diode front end (DFE) [73],[94]-[97] and the load-commutated inverter (LCI)-fed drives [92],[94],[98],[99]. Several models have been developed to analyze the frequencies of the interharmonics produced in ac side. Based on the related studies, in this chapter, a frequency analysis of the dominant interharmonics is conducted with respect to the high-power PWM current-source drives with 18-pulse SCRs-based rectifier (commonly adopted as thyristor front end (TFE) in real application as discussed in Chapter 1) and PWM current-source inverter (CSI). Then, regarding two main impacts of the interharmonics in the system, line-side communication interference and motor-side torsional vibration problem, the mechanisms and conditions of their occurrence are thoroughly studied. Based on the analysis, a solution through the PWM pattern design is proposed to minimize the detrimental influence of the interharmonics. Finally, simulation results on a high-power PWM current-source drive application are provided to verify the analysis in this section.

2.1 Analysis of dominant interharmonics in ac sides

Most important impacts of the interharmonics, such as communication interference and resonance excitation, occur when their frequencies fall within a certain range. In addition, the frequencies of the interharmonics produced in drive systems will vary with the motor operating frequency. As a result, to investigate and minimize the impacts of the interharmonics in drives, their frequencies at different motor operating frequencies are required to be analyzed at first. In this section, such analysis is conducted with respect to the high-power PWM current-source drive system with TFE.

2.1.1 Modulation function of current-source converter

For the three-phase current-source converter sketched as shown in Fig. 2. 1, the relationship between the ac-side components and the dc-link components can be developed based on the modulation function of current-source converter defined as shown in (2-1). It is applicable for both the SCRs-based current-source converter and the PWM current-source converter.

$$S_{wk(k=a,b,c)} = \begin{cases} 1 & \text{the upper arm in leg } k \text{ is on} \\ -1 & \text{the lower arm in leg } k \text{ is on} \\ 0 & \text{both arms in leg } k \text{ is on or off} \end{cases} \quad (2-1)$$

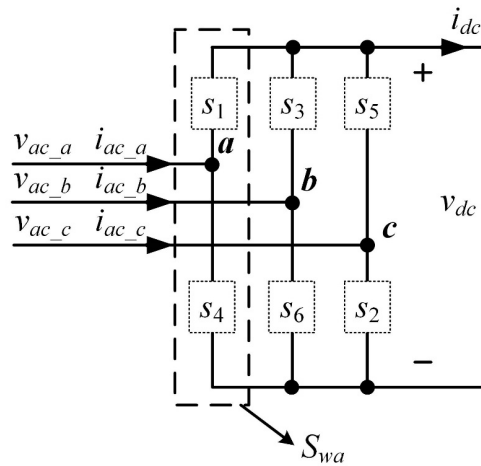


Fig. 2. 1. Schematic diagram of three-phase current-source converter.

Based on the modulation function theory [100],[101], (2-2) and (2-3) can be obtained for current-source converter system as

$$\vec{I}_{ac} = i_{dc} \vec{S}_w = [i_{ac_a}, i_{ac_b}, i_{ac_c}] = [i_{dc} S_{wa}, i_{dc} S_{wb}, i_{dc} S_{wc}], \quad (2-2)$$

$$v_{dc} = \vec{V}_{ac} \bullet \vec{S}_w = v_{ac_a} S_{wa} + v_{ac_b} S_{wb} + v_{ac_c} S_{wc}, \quad (2-3)$$

where \vec{I}_{ac} is the space phasor of three-phase ac-side current ($i_{ac_a}, i_{ac_b}, i_{ac_c}$); \vec{V}_{ac} is the space phasor of three-phase ac-side voltage ($v_{ac_a}, v_{ac_b}, v_{ac_c}$); i_{dc} is the dc-link current; v_{dc} is the dc-link voltage; \vec{S}_w is the space phasor of three-phase modulation function. Note that, if the commutation overlap effect for the SCR bridges and the dead zone effect for the PWM converter are considered, (2-2) and (2-3) may no longer be valid. However, since such effects only have slight influence on the magnitude of system components but not the frequencies [102]-[105], they are neglected during the analysis in this section.

At steady state, the modulation function \vec{S}_w can be represented by a summation of a characteristic positive-sequence Fourier series set ($h=1, 7, 13, \dots$) and a characteristic negative-sequence Fourier series set ($h=5, 11, 17, \dots$) as shown in (2-4). In (2-4), ω is the fundamental frequency of ac side; M_{sh} and φ_{sh} are the magnitude and initial phase angle of h th harmonic component in \vec{S}_w respectively.

$$\vec{S}_w = \sum_{h=1,7,13,\dots} -jM_{sh} e^{j(h\omega t + \varphi_{sh})} + \sum_{h=5,11,\dots} jM_{sh} e^{-j(h\omega t + \varphi_{sh})} \quad (2-4)$$

2.1.2 Distortion of dc-link current

The simplified configuration of high-power PWM current-source drive system with TFE can be drawn as shown in Fig. 2. 2. Since the non- $(18n \pm 1)$ th harmonics ($n=1, 2, \dots$) in ac-side current are fully canceled by the 18-pulse SCRs rectifier with phase-shifting transformer, the modulation function of rectifier can be obtained as

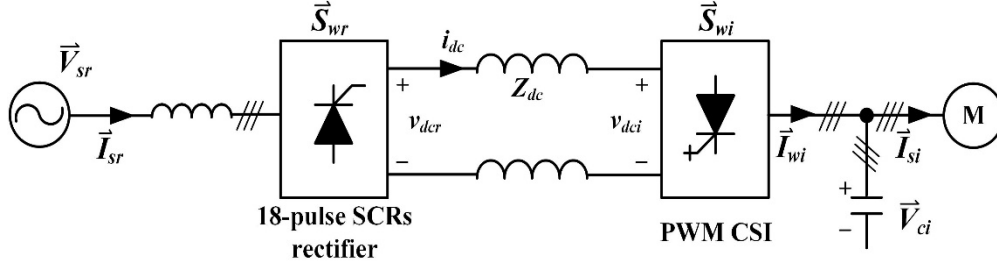


Fig. 2. 2. Simplified configuration of high-power PWM current-source drive with 18-pulse SCRs TFE.

$$\vec{S}_{wr} = \sum_{\substack{h=18n+1 \\ n=0,1,2,\dots}} -jM_{srh}e^{j(h\omega_r t + \varphi_{srh})} + \sum_{\substack{h=18n-1 \\ n=1,2,\dots}} jM_{srh}e^{-j(h\omega_r t + \varphi_{srh})}, \quad (2-5)$$

where ω_r is the line-side fundamental frequency; M_{srh} and φ_{srh} are the magnitude and initial phase angle of h th harmonic component in \vec{S}_{wr} respectively. Without considering the commutation overlap effect, M_{srh} is equal to $2\sqrt{3}/h\pi$ [102]-[105]. Accordingly, the 17th and 19th harmonics have the most significant magnitude (M_{sr17} and M_{sr19} respectively) that are dominant among the harmonic components in (2-5). Assume that the utility supply is harmonicless, defined as $\vec{V}_{sr} = -jV_{sr}e^{j\omega_r t}$ (V_{sr} is the magnitude of grid phase voltage), and line current is sinusoidal. Based on (2-3) ($\vec{V}_{ac} = \vec{V}_{sr}$), the dc-link voltage generated by the 18-pulse SCRs rectifier can be obtained as (2-6). It can be observed that the harmonics contained in v_{dcr} are of $18n\omega_r$ frequencies ($n=1,2,\dots$). Since M_{sr17} and M_{sr19} are significant, the $18\omega_r$ -frequency component will be the dominant harmonics in (2-6).

$$v_{dcr} = \frac{3}{2}V_{sr}M_{sr1} \cos(\varphi_{sr1}) + \frac{3}{2}V_{sr} \sum_{n=1,2,\dots} \left(\pm M_{sr(18n\pm 1)} \cos(18n\omega_r t + \varphi_{sr(18n\pm 1)}) \right) \quad (2-6)$$

Similarly, the modulation function of PWM CSI can be defined as \vec{S}_{wi} shown in (2-7), where ω_i is the motor-side fundamental frequency (also the motor operating frequency); M_{sih} and φ_{sih} are the magnitude and initial phase angle of h th harmonic component in \vec{S}_{wi} respectively. By assuming that the voltage on the inverter-side capacitor is harmonicless, defined as $\vec{V}_{ci} = -jV_{ci}e^{j\omega_i t}$ (V_{ci} is the magnitude of phase

voltage), the dc-link voltage produced by the CSI can be obtained as shown in (2-8), which contains the harmonics of $6n\omega_i$ frequencies. Note that, for the selective harmonic elimination (SHE)-modulated PWM CSI, certain order harmonics can be fully eliminated in PWM pattern as discussed earlier. If both the two adjacent harmonics, $(6n-1)$ th and $(6n+1)$ th, are removed in PWM pattern, the corresponding $6n\omega_i$ -frequency harmonics will disappear in v_{dci} shown in (2-8). For instance, v_{dci} will not contain $6\omega_i$ -frequency harmonic if both the 5th and 7th harmonics are eliminated in SHE PWM pattern.

$$\bar{S}_{wi} = \sum_{\substack{h=6n+1 \\ n=0,1,2,\dots}} -jM_{sih} e^{j(h\omega_i t + \varphi_{sih})} + \sum_{\substack{h=6n-1 \\ n=1,2,\dots}} jM_{sih} e^{-j(h\omega_i t + \varphi_{sih})} \quad (2-7)$$

$$v_{dci} = \frac{3}{2}V_{ci}M_{si1} \cos(\varphi_{si1}) + \frac{3}{2}V_{ci} \sum_{n=1,2,\dots} \left(\pm M_{si(6n\pm 1)} \cos(6n\omega_i t + \varphi_{si(6n\pm 1)}) \right) \quad (2-8)$$

According to Fig. 2. 2, the dc-link current i_{dc} is equal to the difference between v_{dcr} and v_{dci} divided by dc-link impedance Z_{dc} as

$$i_{dc} = \frac{v_{dcr} - v_{dci}}{Z_{dc}}. \quad (2-9)$$

Then, based on (2-6) and (2-8), we can obtain that the dc-link current contains $18n\omega_r$ -frequency harmonics from the rectifier and $6n\omega_i$ -frequency harmonics from the inverter. Since the inductance of dc choke is commonly small in high-power current-source drives as mentioned in Section 1. 2. 3, the distortion of dc-link current caused by those harmonics cannot be ignored, especially for the components with low frequencies (n is small). In addition, among the $18n\omega_r$ -frequency dc-link current harmonics generated from the rectifier side, since the $18\omega_r$ -frequency harmonic is dominant in (2-6) and dc choke has least attenuation effect on such harmonic frequency, the $18\omega_r$ -frequency component will be far more significant than the other harmonics. In the following analysis, we can only consider such dc-link current harmonic generated from the rectifier. For the $6n\omega_i$ -frequency dc-link current harmonics resulted from the inverter, since their frequencies and magnitude

are highly related to the CSI PWM pattern, the dominant components need to be analyzed case-by-case. For the further analysis, the dc-link current is defined as (2-10), where I_{DC} is the dc component in dc-link current; I_{dcr_18} , φ_{Idcr_18} , I_{dci_6n} and φ_{Idci_6n} represent the magnitude and phase angle of $18\omega_r$ -frequency harmonic and $6n\omega_i$ -frequency harmonics in dc-link current respectively.

$$\begin{cases} i_{dc} = I_{DC} + i_{dcr} + i_{dci} \\ i_{dcr} \triangleq I_{dcr_18} \cos(18\omega_r t + \varphi_{Idcr_18}) \\ i_{dci} \triangleq \sum_{n=1,2,\dots} I_{dci_6n} \cos(6n\omega_i t + \varphi_{Idci_6n}) \end{cases} \quad (2-10)$$

2.1.3 Frequencies of dominant interharmonics at ac sides

Through the modulation of the rectifier and the inverter, the distorted dc-link current shown in (2-10) will introduce interharmonics in both the line side and the motor side. Based on (2-2), (2-5), and (2-10), we can obtain that, the $6n\omega_i$ -frequency dc-link current harmonics generated from the inverter (i_{dci} defined in (2-10)) modulated by the modulation function of rectifier (\bar{S}_{wr}) will produce interharmonics in line-side current \bar{I}_{sr} . Since the fundamental component in \bar{S}_{wr} , defined as \bar{S}_{wr1} , is much more significant than the harmonic components ($M_{sr1} \gg M_{sr(18n\pm1)} \quad n > 0$), the dominant interharmonics in line side can be obtained as shown in (2-11), the frequencies of which are $(\omega_r \pm 6n\omega_i)$ as ω_{line_inter} defined in (2-12).

$$i_{dci} \bar{S}_{wr1} = -j \frac{1}{2} M_{sr1} \sum_{n=1,2,\dots} \left(I_{dci_6n} \left(e^{j(\omega_r t + 6n\omega_i t + \varphi_{sr1} + \varphi_{Idci_6n})} + e^{j(\omega_r t - 6n\omega_i t + \varphi_{sr1} - \varphi_{Idci_6n})} \right) \right) \quad (2-11)$$

$$\omega_{line_inter} = |\omega_r \pm 6n\omega_i| \quad n \in \mathbb{N}^* \quad (2-12)$$

In the same manner, the dominant $18\omega_r$ -frequency dc-link current harmonics generated from the rectifier (i_{dcr}) modulated by the inverter's modulation function (\bar{S}_{wi}) will introduce current interharmonics in inverter-side PWM current \bar{I}_{wi} with frequencies shown in (2-13). Note that, due to the existence of LC circuit in inverter

side, certain interharmonics in \bar{I}_{wi} may be amplified on the motor stator current \bar{I}_{si} . As a result, we cannot simply consider the fundamental component in the modulation function of CSI to analyze the dominant interharmonics in motor side as we did for the line side.

$$\omega_{motor_inter} = |(6n \pm 1)\omega_i \pm 18\omega_r| \quad n \in \mathbb{N}^0 \quad (2-13)$$

According to (2-12) and (2-13), since the line-side fundamental frequency (ω_r) is fixed, the frequencies of the ac-side current interharmonics are the functions of the motor operating frequency (ω_i) and the CSI PWM pattern (n). On the one hand, if the modulation schemes of PWM CSI have been predesigned, the frequencies of the ac-side current interharmonics can be determined at any motor operating frequencies. As a result, we can off-line estimate the motor operating frequencies, at which the produced interharmonics may harm the system, such as communication interference, torsional vibration and *LC* resonance. On the other hand, it is possible to avoid the produced interharmonics affecting the system at certain motor operating frequencies through altering the CSI PWM pattern.

2.2 Analysis of interharmonics' impacts

As discussed earlier, the interharmonics produced in the drive systems may result in detrimental influence at both the line side and the motor side, such as communication interference, torsional vibration and *LC* resonance. With respect to the high-power PWM current-source drives with TFE, the occurrence of two main impacts, the line-side communication interference and the motor-side torsional vibration problem, caused by the ac-side dominant interharmonics is thoroughly studied in this section. Since the potential *LC* resonance exists at both the line side and the motor side in high-power PWM current-source drives with active front end (AFE), the impact of interharmonics on the excitation of *LC* resonance is more serious and required to be carefully considered in such system. As a result, the *LC* resonance problem will be mainly focused and analyzed in next chapter regarding the high-power current-source drives with AFE.

2.2.1 Communication interfered by line-side interharmonics

Power-line communication (PLC) techniques have long been a favorite to many utility companies for telecommunication, tele-protection, and tele-monitoring between the electrical substations and the users, which are basically operated by coupling high-frequency signals into the power lines. The interharmonics produced by the drive systems at line side may interfere with the PLC, when the interharmonic frequencies are close to the communication frequencies. In this section, with respect to a specific application of PLC technologies in utility companies, automatic meter reading (AMR), the interference resulted from the interharmonics produced by the high-power PWM current-source drives is analyzed in details.

A. Mechanism of PLC-based AMR interfered by line-side interharmonics

PLC technology is utilized by some utility companies for automatic meter reading (AMR), which can automatically collect information, such as power consumption, diagnostic data, and status, from energy metering devices for billing, troubleshooting and analysis. The diagram of a typical AMR system can be sketched as shown in Fig. 2. 3. Two current signals at 555Hz and 585Hz are injected into the power lines through a transformer coupling unit at substations and transferred to

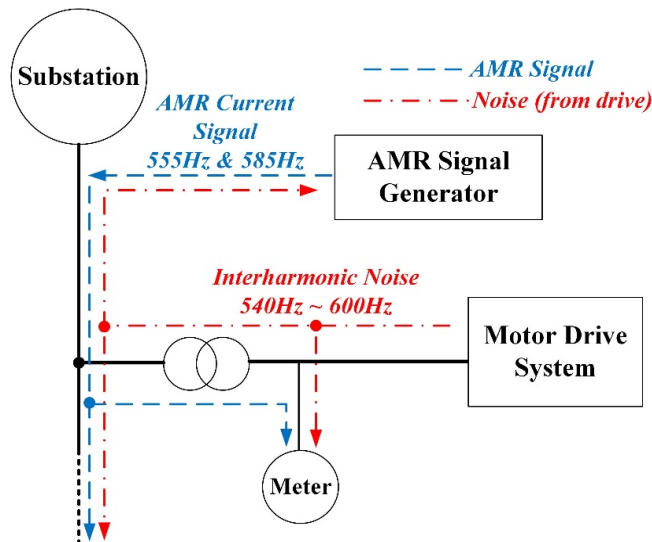


Fig. 2. 3. Mechanism of AMR system interfered by line-side interharmonics produced by drive systems.

downstream. The injected current signals will interact with the downstream impedance to create the corresponding voltage signals, and such voltage signals can be decoded by the meters at the endpoints for metering purpose.

The performance of AMR system may be affected by the unexpected interharmonic noise at the downstream. With respect to the AMR system shown in Fig. 2. 3, the interharmonics with frequencies in the range of 540Hz to 600Hz may disable the metering function of the endpoints if their magnitude is higher than a certain level [106][107]. As analyzed above, the high-power PWM current-source drives may introduce the current interharmonics at line side and their frequencies will vary with the motor operating frequency. At certain motor operating frequencies, the frequencies of the produced line-side current interharmonics may fall within the AMR interference range (540Hz-600Hz), and if the magnitude of the induced voltage interharmonics on upstream impedance is high enough, the metering function of AMR system will be disabled.

B. Estimation of interference occurrence

According to the previous analysis, if the frequencies of the dominant interharmonics produced at line side, ω_{line_inter} , fall within the range of 540Hz to 600Hz as shown in (2-14), the AMR system may be interfered. Since the line-side fundamental frequency ω_r is 60Hz, (2-14) can be rewritten as (2-15). It means that, if the non-negative integer n satisfies either of two inequalities shown in (2-15), the interference occurs.

$$540 \leq \omega_{line_inter} = |\omega_r \pm 6n\omega_i| \leq 600 \quad n \in \mathbb{N}^* \quad (2-14)$$

$$\frac{80}{\omega_i} \leq n \leq \frac{90}{\omega_i} \quad or \quad \frac{100}{\omega_i} \leq n \leq \frac{110}{\omega_i} \quad n \in \mathbb{N}^* \quad (2-15)$$

As mentioned in Section 1. 2. 2, different modulation schemes are adopted for PWM CSI at different regions of motor operating frequencies to achieve a good harmonic performance with limited switching frequency as shown in Fig. 1. 7. To

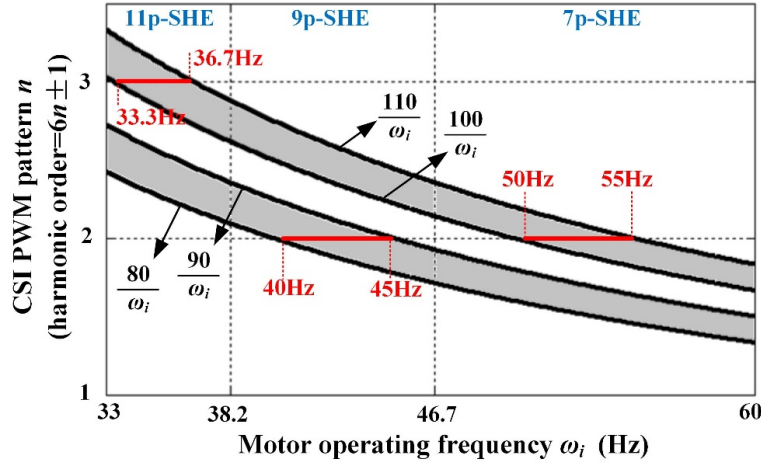


Fig. 2. 4. Estimation of the occurrence of AMR system interfered by the line-side interharmonics.

simplify the following analysis, we consider a certain range of motor operating frequencies, 33Hz to 60Hz, to estimate the occurrence of interference (the same approach can be used for the estimation at other motor operating frequencies). For a high-power PWM current-source drive application, within such range of motor operating frequencies, 11-pulse SHE, 9-pulse SHE, and 7-pulse SHE can be used to modulate PWM CSI in [33Hz, 38.2Hz], (38.2Hz, 46.7Hz], and (46.7Hz, 60Hz] respectively to limit the switching frequency within 420Hz (as shown in Fig. 1. 7). The occurrence of interference within 33Hz to 60Hz motor operating frequency can be estimated based on Fig. 2. 4. In Fig. 2. 4, the two shaded areas formed by the reciprocal function curves represents the interference occurrence conditions derived as shown in (2-15). Since n is a non-negative integer, if horizontal lines at integers (e.g. $n=1$, $n=2$) fall within the shaded areas, the interference will occur at corresponding motor operating frequencies. Also, as n is related to the CSI PWM pattern ($(6n\pm 1)$ th harmonics), the orders of PWM harmonics which cause the interference can be known correspondingly. For example, as shown in Fig. 2. 4, $n=3$ falls within the shaded area when motor operates in the range of 33.3Hz to 36.7Hz. It means that, when motor operates within such region, 17th and/or 19th ($6n\pm 1$, $n=3$) harmonics in CSI PWM pattern will cause the interharmonics with frequencies between 540Hz and 600Hz contained in the line current so that interferes with the

TABLE. 2. 1. SUMMARY OF INTERFERENCE OCCURRENCE CONDITIONS

CSI modulation scheme	CSI PWM harmonics ($6n\pm 1$)th-order	Motor operating frequency (ω_i)
11-pulse SHE	17th, 19th ($n=3$)	33.3Hz ~ 36.7Hz
9-pulse SHE	11th, 13th ($n=2$)	40Hz ~ 45Hz
7-pulse SHE	11th, 13th ($n=2$)	50Hz ~ 55Hz

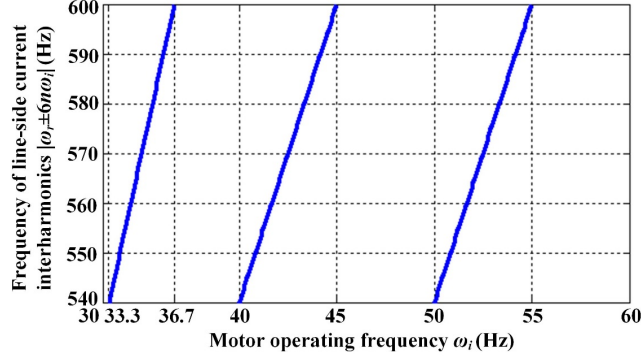


Fig. 2. 5. Frequencies of line-side current interharmonics related to the interference with AMR system.

AMR system. The conditions of interference occurrence are summarized in TABLE. 2. 1 according to Fig. 2. 4. Moreover, based on (2-12), we can figure out the frequencies of such line current interharmonics (ω_{line_inter}) as plotted in Fig. 2. 5.

Fig. 2. 6 shows the PWM pattern of 11-pulse SHE, 9-pulse SHE and 7-pulse SHE designed for the PWM CSI in a real application with the consideration of reducing motor-side current distortion. The concerned harmonics in CSI PWM pattern, which are related to the interference with AMR system as listed in TABLE. 2. 1, are circled in Fig. 2. 6. It can be observed that the circled PWM harmonics are not negligible in the adopted modulation schemes. As a result, the interference may occur during the implementation of high-power PWM current-source drives.

2.2.2 Torsional vibration excited by motor-side interharmonics

Regarding the interharmonics produced at the motor side, one of the main impacts is the load torsional vibration. Generally, the electrical drive system with only

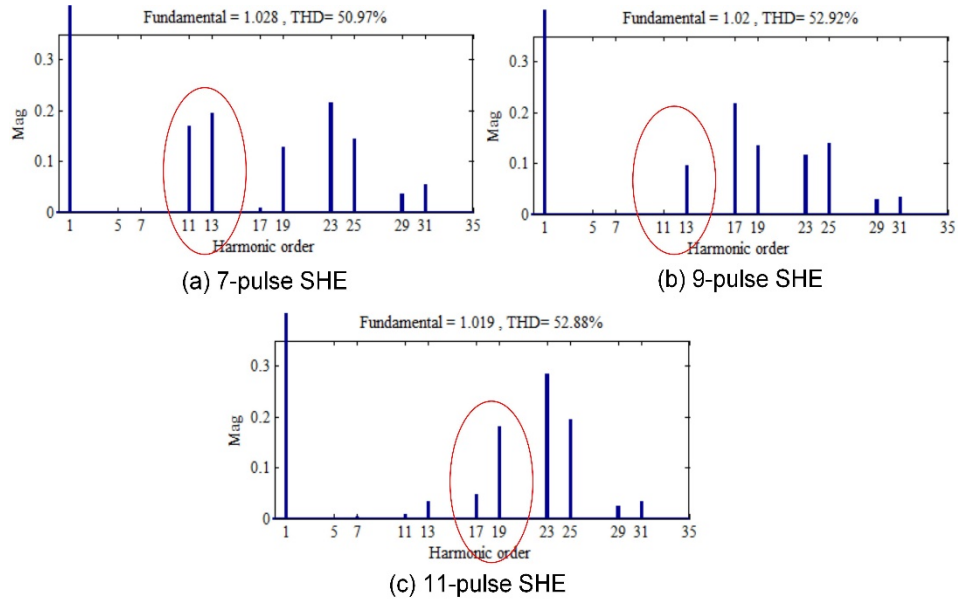


Fig. 2. 6. PWM pattern of SHE-modulated PWM CSI in a high-power PWM current-source drive application.

inertia load is considered as a one-mass system by ignoring the stiffness of the shaft connecting between the motor and the load [75]. Therefore, the entire mechanical system can be simplified as a first-order element without any resonant characteristics. However, there are many types of industrial applications, especially with high torque conditions (e.g. rolling mill), which do not admit such simplification. Unlike one-mass system, a potential mechanical resonance problem, also referring as “torsional vibration problem”, exists in this class of drive applications and may be excited by the interharmonics in motor-side current. Since a large portion of medium-voltage (MV) drives are implemented under such high torque conditions, the torsional vibration problem caused by the motor-side interharmonics needs to be carefully addressed in real applications. In this section, with respect to the high-power PWM current-source drives, the impact of the motor-side interharmonics on the load torsional vibration will be investigated. Note that the significant motor torque ripples caused by the motor-side LC electrical resonance in such a drive system is not considered in this section. Also, in this research, only the harmonics and interharmonics caused by the drive system at steady state are focused on. For high-power PWM current-source drives, the dynamic performance is usually not a prime

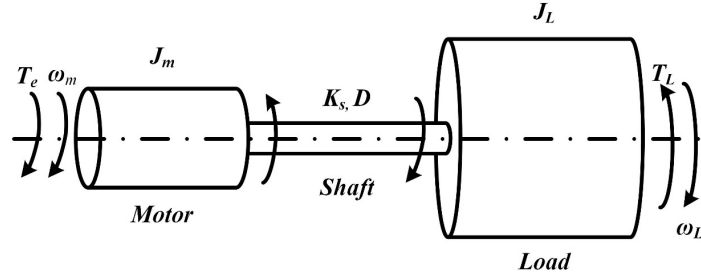


Fig. 2. 7. Schematic diagram of two-mass system.

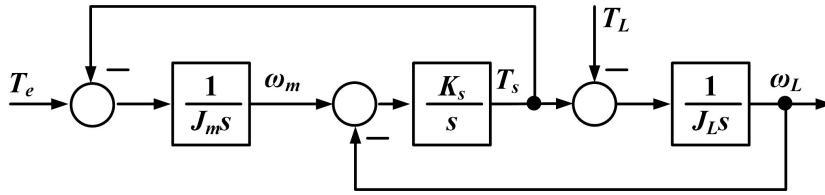


Fig. 2. 8. Block diagram of two-mass system.

importance due to the use of a dc choke that limits the changing rate of dc current [1]. As a result, the control bandwidth of drive system is normally designed to be low, and the impacts caused by the transient of motor operation is not a main issue.

A. Mechanism of torsional vibration caused by motor-side interharmonics

In the drive systems with high torque conditions, there is an evident difference between the motor speed and the load speed during the transients, which means that the motor shaft is undertaking a great torsional torque that affects it negatively. To take this phenomenon into account, a two-mass model is normally adopted in the researches of such drive systems [99],[108]-[110]. The first mass and second mass refer to the inertia of motor and the inertia of load respectively, and the connecting shaft is treated as inertia free [111]. A schematic diagram of the two-mass motor load system is shown in Fig. 2. 7 without the consideration of friction, where T_m and T_L are the electromagnetic torque and the load torque respectively; J_m and J_L are the inertia of motor and load respectively; K_s and D are the stiffness coefficient and inertia damping coefficient of the connecting shaft respectively; ω_m and ω_L represent the motor speed and the load speed respectively. Since the connecting

shafts are commonly made from steel [76], the internal damping coefficient D normally has a negligible value. The block diagram of such two-mass system can be obtained as shown in Fig. 2. 8. Based on Fig. 2. 8, we can derive the transfer function between motor speed ω_m and electromagnetic torque T_e , and transfer function between load speed ω_L and electromagnetic torque T_e as shown in (2-16).

$$\left\{ \begin{array}{l} \frac{\omega_m(s)}{T_e(s)} = \frac{1}{J_m s} \frac{s^2 + \omega_{mech_antires}^2}{s^2 + \omega_{mech_res}^2} \\ \frac{\omega_L(s)}{T_e(s)} = \frac{1}{J_m s} \frac{\omega_{mech_antires}^2}{s^2 + \omega_{mech_res}^2} \end{array} \right. , \text{ where } \left\{ \begin{array}{l} \omega_{mech_antires} = \sqrt{\frac{K_s}{J_L}} \\ \omega_{mech_res} = \sqrt{\frac{K_s}{J_L} + \frac{K_s}{J_m}} \end{array} \right. \quad (2-16)$$

According to (2-16), we can observe that there is a two-order resonant element contained in the two-mass system, which has no damping effect. Even if considering the friction in real applications, the mechanical damping effect is still small. Therefore, if the electromagnetic torque T_e contains the component with frequency ω_{mech_res} , the torsional vibration problem will occur. As shown in (2-16), the resonant frequency ω_{mech_res} has an inverse relationship with the motor and load inertia (J_m and J_L). Thus, large load inertia in MV drive applications generally results in a low-frequency mechanical resonance mode, which is below 100Hz in most conditions [111]. Since the electromagnetic torque T_e is induced by the motor-side current, the low-frequency current interharmonics produced at the motor side may give rise to the load torsional vibration if the frequency of the induced torque is coincident with the ω_{mech_res} .

B. Estimation of torsional vibration occurrence

As analyzed in Section 2. 1. 3, the dominant interharmonics contained in CSI output PWM current \bar{I}_{wi} are of frequencies $\omega_{motor_inter} = |(6n \pm 1)\omega_i \pm 18\omega_r|$ as shown in (2-13). According to Fig. 2. 2, since the motor-side capacitor only bypasses the high-frequency interharmonics in \bar{I}_{wi} , with respect to the low-frequency region of mechanical resonance problem, the motor stator current \bar{I}_{si} will contain the dominant interharmonics with ω_{motor_inter} as well. The relationship between the motor

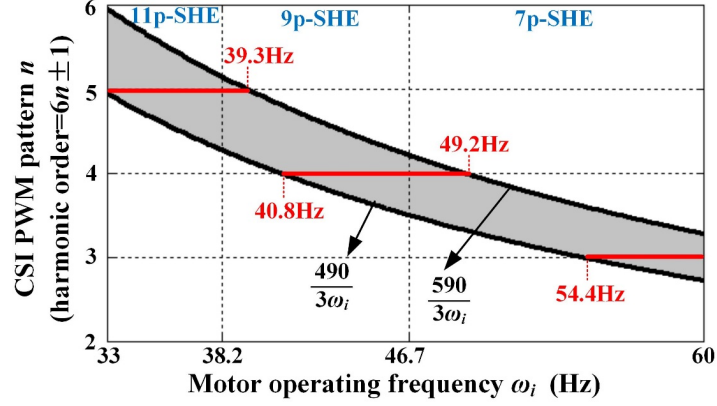


Fig. 2. 9. Estimation of the occurrence of torsional vibration due to motor-side interharmonics.

stator current \bar{I}_{si} and the electromagnetic torque T_e can be obtained as shown in (2-17), where P is motor pole pairs; $\bar{\lambda}_s$ is motor stator flux. By considering $\bar{\lambda}_s = -j\lambda_s e^{j(\omega_s t + \varphi_{\lambda_s})}$ (λ_s and φ_{λ_s} are the magnitude and initial phase of $\bar{\lambda}_s$ respectively), based on (2-2), (2-7), (2-10) and (2-17), we can obtain that the induced dominant interharmonics in electromagnetic torque are of frequencies ω_{Te_inter} as shown in (2-18).

$$T_e = \frac{3P}{2} \text{Re}(j\bar{\lambda}_s \bar{I}_{si}^*) \quad (2-17)$$

$$\omega_{Te_inter} = |6n\omega_i \pm 18\omega_r| \quad (2-18)$$

If taking the general range of mechanical resonant frequency in MV drive applications (below 100Hz as mentioned above) into consideration, the torsional vibration will occur when the inequality shown in (2-19) is satisfied. (2-19) can be further simplified as (2-20).

$$\omega_{Te} = |6n\omega_i \pm 18\omega_r| \leq 100 \quad (2-19)$$

$$\frac{490}{3\omega_i} \leq n \leq \frac{590}{3\omega_i} \quad (2-20)$$

TABLE. 2. 2. SUMMARY OF TORSIONAL VIBRATION OCCURRENCE CONDITIONS

CSI modulation scheme	CSI PWM harmonics ($6n\pm 1$)th-order	Motor operating frequency (ω_i)
11-pulse SHE	29th, 31st ($n=5$)	33Hz ~ 39.3Hz
9-pulse SHE	23rd, 25th ($n=4$)	40.8Hz ~ 46.7Hz
7-pulse SHE	17th, 19th ($n=3$)	54.4Hz ~ 60Hz

Following the same procedure as the analysis of line-side communication interference in previous section, at first, Fig. 2. 9 is plotted under the adoption of the same PWM CSI modulation schemes shown in Fig. 2. 6. Then, based on Fig. 2. 9, the regions of motor operating frequencies that certain harmonics in CSI PWM pattern may give rise to the torsional vibration problem are summarized in TABLE. 2. 2.

2.3 Reduction of interharmonics' impacts through PWM pattern design

With respect to the high-power PWM current-source drives with TFE, the impacts of the interharmonics produced in the system are investigated based on two specific cases, line-side interference with AMR system and motor-side torsional vibration problem. According to the two studies, we can observe in evidence that the PWM pattern of CSI plays an important role in the occurrence of the impacts. During the implementation of high-power PWM current-source drives, certain order harmonics in CSI PWM pattern may introduce the unexpected interharmonics at certain motor operating frequencies. For the SHE scheme that commonly adopted to modulate the high-power PWM converters, it offers some degrees of freedom in designing the PWM pattern. If we could reduce those impacts-related harmonics in the practically-used SHE PWM patterns without affecting other harmonics too much (especially the low-order harmonics), not only could the interharmonics' impacts be weakened, but also there would be negligible influence on system perfor-

mance. In this section, with respect to the previously-studied interharmonics' interference with AMR system, a solution through redesigning the CSI PWM pattern is proposed to address this problem.

As mentioned in section 1. 2. 2, the modulation index of SHE scheme is normally uncontrolled in the high-power PWM current-source drive applications. As a result, the 7-pulse SHE, 9-pulse SHE and 11-pulse SHE that have three, four and five free switching angles can fully eliminate maximum three, four and five harmonics in PWM pattern respectively. According to the analysis in Section 2. 2. 1, the CSI PWM harmonics related to the interference with AMR system are 11th and 13th ($6n\pm 1, n=2$) in 7-pulse SHE, 11th and 13th ($6n\pm 1, n=2$) in 9-pulse SHE, and 17th and 19th ($6n\pm 1, n=3$) in 11-pulse SHE. The simplest method to weaken such interference is to minimize the magnitude of those harmonics in SHE PWM pattern. Besides, to avoid exciting the motor-side LC resonance, the elimination of the low-order harmonics in PWM pattern, such as 5th and 7th, are not expected to be affected. With four free switching angles, the 9-pulse SHE scheme can effectively attenuate the 11th and 13th PWM harmonics which are related to the interference, while fully eliminate the 5th and 7th harmonics in PWM pattern. However, for the 7-pulse SHE and 11-pulse SHE, due to the limitation of design freedom, it is difficult to reduce the interference-related PWM harmonics on the premise of an effective attenuation on low-order harmonics. Especially for the 7-pulse SHE scheme, minimizing both the 11th and 13th harmonics while attenuating the 5th and 7th harmonics effectively is less likely to be achieved with only three free switching angles. Therefore, alternatives need to be considered for the two SHE schemes.

Regarding the design of SHE PWM pattern, the optimization algorithms have been adopted to find the optimum solution of the switching angles to minimize the quadratic cost function as shown in (2-21) [89],[112],[113]

$$f_{\text{cost}} = \sum_h W_h (M_{sh})^2 \quad W_h > 0 \quad , \quad (2-21)$$

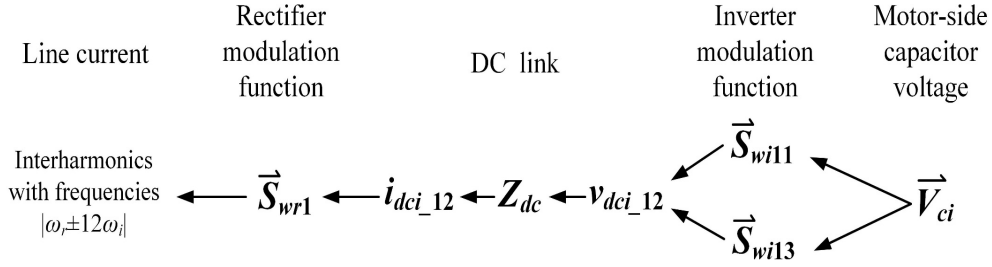


Fig. 2. 10. Generation of $|\omega_r \pm 12\omega_i|$ -frequency interharmonics in line current.

where W_h is the weighing coefficient of h th-order harmonic's magnitude. If the SHE scheme has sufficient degrees of freedom, the weighing coefficient can be selected as 1 for each unwanted harmonics in PWM pattern, which is equivalent to conventional SHE design method (solving nonlinear equation set). Regarding the 7-pulse SHE scheme that has limited degrees of freedom, to solve the interference problem while guarantee a great attenuation on 5th and 7th harmonics in PWM pattern, a smaller weighing coefficient can be placed on the magnitude of 11th and 13th harmonics respectively in the cost function than on the magnitude of 5th and 7th harmonics as shown in (2-22). The same strategy can also be used in the design of 11-pulse SHE scheme to solve the interference problem, with a comparatively low weighing coefficient on 17th and 19th harmonics while higher weighing coefficients on 5th, 7th, 11th and 13th harmonics.

$$f_{\text{cost_7pSHE}} = (M_{si5})^2 + (M_{si7})^2 + K(M_{si11})^2 + K(M_{si13})^2 \quad K < 1 \quad (2-22)$$

Moreover, to further reduce the interference with AMR system under the adoptions of 7-pulse SHE scheme and 11-pulse SHE scheme, we can reinvestigate the generation of the line-side interharmonics. Taking the 7-pulse SHE scheme for instance again, as shown in Fig. 2. 4, when motor operates between 50Hz and 55Hz, the line-side interharmonics that interferes with the AMR system are of frequencies $|\omega_r \pm 12\omega_i|$ ($n=2$ in (2-12)), and the generation of such interharmonics can be illustrated as shown in Fig. 2. 10 based on previous analysis. At first, the motor-side capacitor voltage \vec{V}_{ci} modulated by the 11th and/or 13th harmonics in PWM CSI

modulation function \bar{S}_{wi} produces the $12\omega_i$ -frequency dc-link voltage harmonics, defined as v_{dci_12} . Then, v_{dci_12} introduces the dc-link current harmonics with same frequency, which further generates the line-side interharmonics with $|\omega_r \pm 12\omega_i|$ frequency through the fundamental component (\bar{S}_{wr1}) in SCRs rectifier modulation function \bar{S}_{wr} . According to (2-8), the dc-link voltage harmonics v_{dci_12} can be obtained as

$$v_{dci_12} = \frac{3}{2} V_{ci} \left(-M_{si11} \cos(12\omega_i t + \varphi_{si11}) + M_{si13} \cos(12\omega_i t + \varphi_{si13}) \right) \quad (2-23)$$

We can observe that, if the 11th and 13th harmonics in CSI PWM pattern could be designed to have a similar magnitude and phase angle, as $M_{si11} \approx M_{si13}$ and $\varphi_{si11} \approx \varphi_{si13}$, the v_{dci_12} would be close to zero. Correspondingly, the $|\omega_r \pm 12\omega_i|$ -frequency line-side interharmonics could be greatly reduced so that the interference problem would be solved. Note that, the magnitude of 11th and 13th harmonics in CSI PWM pattern, M_{si11} and M_{si13} , are still expected to be small to avoid significant 11th and 13th current harmonics being introduced in motor side. According to [90], the magnitude and phase angle of h th harmonic in 7-pulse SHE PWM pattern can be obtained as

$$\begin{cases} M_{sih} = \sqrt{A_{sih}^2 + B_{sih}^2} \\ \varphi_{sih} = \arctan\left(\frac{B_{sih}}{A_{sih}}\right) \end{cases} \quad (2-24)$$

where
$$\begin{cases} A_{sih} = \frac{4}{h\pi} \cos\left(\frac{h\pi}{6}\right) \left[(-1)^3 + 2 \sum_{p=1}^3 (-1)^{p+1} \cos\left(h\left(\theta_{swp} - \frac{\pi}{6}\right)\right) \right] \\ B_{sih} = 0 \end{cases}$$

Based on (2-24), to further reduce the line-side interference under the adoption of 7-pulse SHE scheme, (2-22) can be improved as (2-25). The design of 11-pulse SHE scheme can follow the same procedure as well.

$$f_{\text{cost_7pSHE}} = A_{si5}^2 + A_{si7}^2 + K_1 (A_{si11}^2 + A_{si13}^2) + K_2 (A_{si11} - A_{si13})^2 \quad K_1, K_2 < 1 \quad (2-25)$$

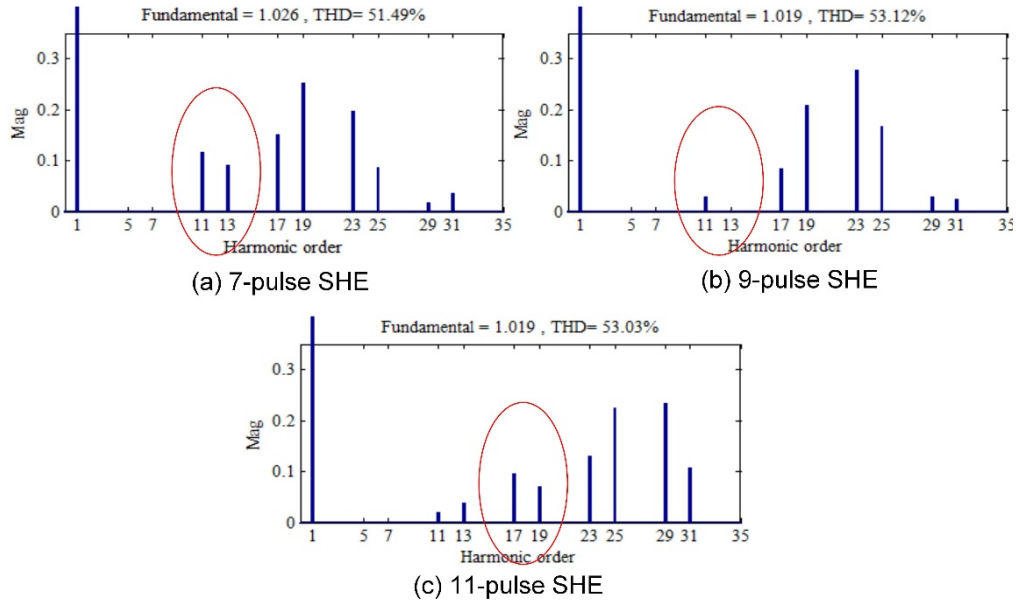


Fig. 2. 11. Redesigned SHE patterns of PWM CSI to minimize line-side interference with AMR system.

On the basis of the analysis in this section, a new set of CSI PWM patterns is designed as shown in Fig. 2. 11, and the harmonics in PWM pattern that may cause the interference with AMR system are circled in Fig. 2. 11 as well.

2.4 Verification results

To verify the analysis of the dominant ac-side interharmonics and their impacts on the line-side communication and the motor-side torsional vibration problem, plenty of simulations are conducted on a 1MVA/4160V/60Hz high-power PWM current-source drive application with an 18-pulse SCRs rectifier at different motor operating frequencies. In addition, simulation results are also provided to demonstrate the effectiveness of the redesigned PWM pattern on the reduction of the interharmonic interference with AMR system. In the simulations, the detailed model of power converters and the full-order model of induction motor are adopted. Note that, the simulations conducted in this section are mainly aiming to prove the previous frequency analysis of the system dominant interharmonics, and to demonstrate that the interharmonics, generated at the estimated motor operating frequencies, will have the frequencies that may result in the detrimental influence. Thus,

TABLE. 2. 3. PARAMETERS OF A 1MVA/4160V PWM CURRENT-SOURCE DRIVE APPLICATION WITH TFE (SIMULATION)

Nominal power	1MVA		
Nominal grid voltage (line-to-line)	4160V		
Frequency	60Hz		
Motor rated voltage (line-to-line)	4000V		
Motor rated power	1100hp		
Motor rated speed	1190rpm		
	Line-side	DC-link	Motor-side
Voltage base value	2401.8V	5094.9V	2309.4V
Current base value	140A	198A	145.6A
Impedance base value	17.2Ω	25.7Ω	15.9Ω
Inductance base value	45.5mH	68.3mH	42.1mH
Capacitance base value	154.6μF		167.2μF
	Real value	P.U. value	
Line resistance	0.034Ω	0.002	
Line inductance (supply inductance, transformer leakage inductance, line reactor)	8.93mH	0.20	
DC choke	31.5mH	0.46	
Motor-side filter capacitance	45.98μF	0.27	
Motor stator leakage inductance	5.20mH	0.12	
Motor stator resistance	0.21Ω	0.013	
Motor magnetizing inductance	155mH	3.68	
Motor rotor leakage inductance	5.20mH	0.12	
Motor rotor resistance	0.146Ω	0.01	
Load torque	0.4174*(ω_m) ² (Nm) ($K_{fric}=0.4174$)		

on the one hand, the magnitude threshold of the line-side current interharmonics that interferes with the AMR system is not the focus in this work. On the other hand, the mechanical resonance phenomenon caused by the motor stator current interharmonics is not essential in this section as well. As a result, to simplify the simulations, a one-mass fan-type load model is adopted in this simulation, where the load torque is proportional to the motor speed as $T_L=K_{fric}(\omega_m)^2$ (K_{fric} is a constant coefficient). The parameters of the drive system are listed in TABLE. 2. 3.

2.4.1 Verification of interharmonics' frequency analysis and estimation of impacts' occurrence

Simulations are conducted at each 0.5Hz frequency interval within the range of 33Hz to 60Hz motor operating frequencies as considered in previous analysis. In addition, the practically-used 11-pulse SHE, 9-pulse SHE and 7-pulse SHE scheme

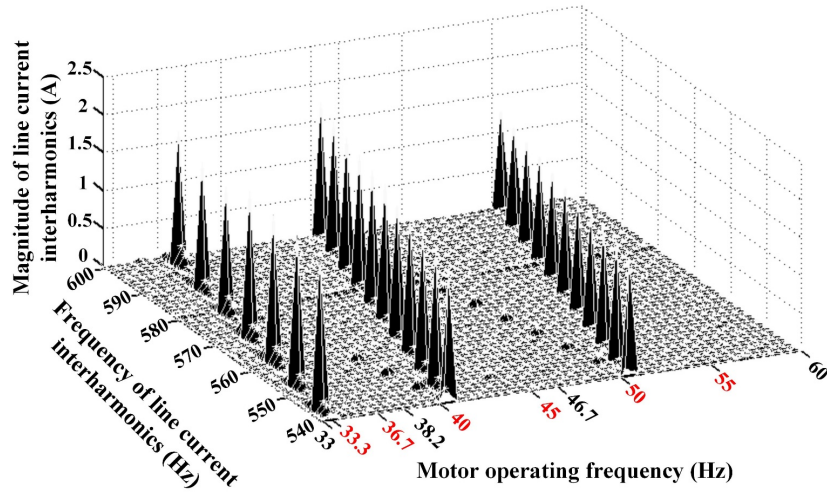


Fig. 2. 12. Simulation results of line current interharmonics with frequencies from 540Hz to 600Hz at different motor operating frequencies.

as shown in Fig. 2. 6 are adopted at different frequency regions as discussed earlier. Fig. 2. 12 shows line current interharmonics with frequencies within 540Hz to 600Hz (frequency range of interference with AMR system) at different motor operating frequencies. According to Fig. 2. 12, we can observe that the ranges of motor operating frequencies, where significant current interharmonics with the frequencies in the AMR interference region are produced in line side, are in accordance with the estimation as shown in TABLE. 2. 1. In addition, the frequencies of such line-side current interharmonics also coincide with the estimated values as shown in Fig. 2. 5. The correctness of the frequency analysis of line-side dominant interharmonics is proved, and the accuracy of the estimation of line-side interference with AMR system is also verified.

Fig. 2. 13 shows the low-frequency (within 100Hz) motor electromagnetic torque interharmonics at different motor operating frequencies. According to TABLE. 2. 2, when motor operates within [54.4Hz, 60Hz], 17th and 19th harmonics in 7-pulse SHE PWM pattern will result in $|18\omega_i \pm 1080|$ Hz ($|6n\omega_i \pm 18\omega_r|$, $n=3$ in (2-12)) low-frequency electromagnetic torque interharmonics; when motor operates within [40.8Hz, 49.2Hz], 23rd and 25th harmonics in 7-pulse SHE scheme and 9-pulse SHE scheme respectively will cause $|24\omega_i \pm 1080|$ Hz ($|6n\omega_i \pm 18\omega_r|$, $n=4$) low-

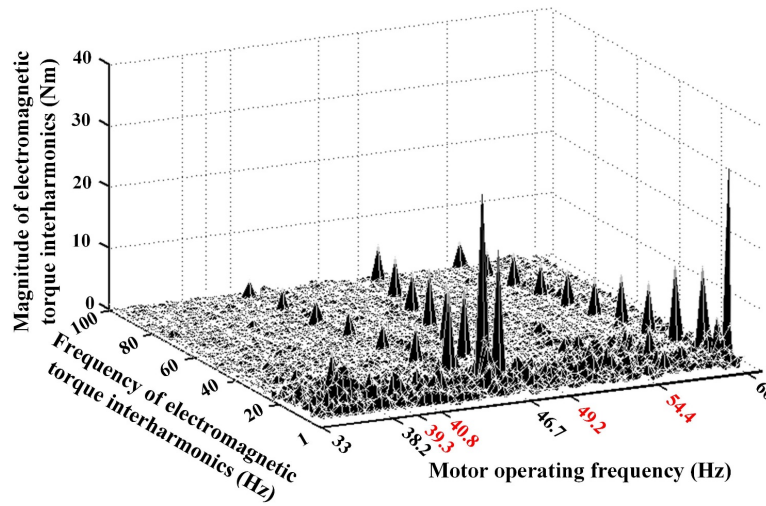


Fig. 2. 13. Simulation results of motor electromagnetic torque interharmonics with frequencies from 1Hz to 100Hz at different motor operating frequencies.

frequency motor torque interharmonics. As shown in Fig. 2. 13, the significant electromagnetic torque interharmonics with such low frequencies can be observed within the estimated regions of the motor operating frequencies. In addition, when motor operates within [33Hz, 39.3Hz], 29th and 31st PWM harmonics in 11-pulse SHE are estimated to produce low-frequency torque interharmonics as shown in TABLE. 2. 2. However, since the 29th and 31st harmonics are not significant in 11-pulse SHE PWM pattern according to Fig. 2. 6(c), the low-frequency motor torque interharmonics are hard to be observed in Fig. 2. 13. The simulation results verified the frequency analysis of motor-side interharmonics and the estimation of the possible occurrence of torsional vibration as well.

2.4.2 Verification of redesigned PWM pattern aiming to reduce line-side communication interference

With the adoption of the redesigned SHE PWM pattern for minimizing line-side interference with AMR system, simulations are conducted under the same conditions as in previous section. Fig. 2. 14 shows the line current interharmonics after using the redesigned SHE PWM pattern. Compared with the Fig. 2. 12, it can be

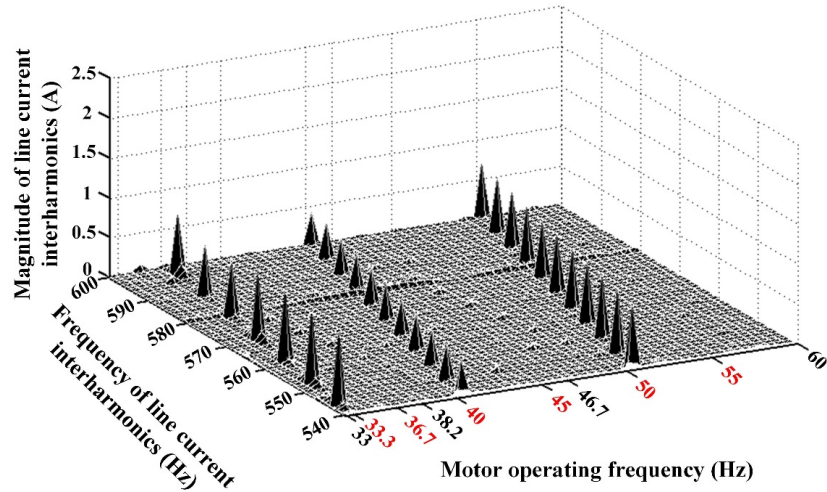


Fig. 2. 14. Simulation results of line current interharmonics with frequencies from 540Hz to 600Hz at different motor operating frequencies after adopting the redesigned SHE PWM patterns.

observed that the magnitude of the current interharmonics is significantly reduced, so that their interference with AMR system could be effectively reduced.

2.5 Summary and discussion

In this chapter, the interharmonic problems in high-power PWM current-source drives with SCRs rectifier as front end are thoroughly investigated. Firstly, the generation of line-side and motor-side interharmonics are analyzed, and the frequencies of the dominant interharmonics at each side are developed. Then, the impacts of the produced interharmonics are studied with respect to two cases, line-side communication interference and motor-side torsional vibration problem. Based on the developed frequencies of the dominant ac-side interharmonics, estimations on the occurrence of impacts are presented in each of the two cases. Note that, the same procedure can also be used to analyze other interharmonics' impacts on the drive system, such as the excitation of motor-side LC resonance. According to the analysis, certain order harmonics in CSI PWM pattern introduces the interharmonics that cause the impacts at certain motor operating frequencies. In light of this conclusion, regarding the case of line-side communication interference, the practically-

used SHE PWM patterns are redesigned to properly reduce the harmonics related to the generation of the line-side interharmonics that result in the interference. The analysis conducted in this chapter and the effectiveness of the redesigned SHE schemes to solve the line-side communication interference problem are verified through simulations at last.

Although the SHE PWM patterns can be designed to reduce the production of the interharmonics, in general, it is difficult to minimize two or more interharmonic impacts at the same time. On the one hand, the limited design freedom of SHE schemes, especially with few pulse numbers, constrains the numbers of PWM harmonics that can be adjusted. On the other hand, provided that one harmonic in PWM pattern causes two or more impacts of the interharmonics, compromise has to be made in most cases if the impacts were expected to be solved through the PWM pattern design. As a result, active compensation of the interharmonics is expected to overcome the interharmonic problems. In Chapter 4, an active attenuation strategy through the control of high-power PWM current-source converter will be proposed to reduce the interharmonics.

Chapter 3

Investigation of Interharmonics in High-Power PWM Current-Source Drives with Active Front End

Compared with the high-power PWM current-source drives with thyristor front end (TFE), the interharmonic problems caused by the harmonics interaction between the rectifier and the inverter through the weak dc link are more serious and complex in high-power PWM current-source drive systems with active front end (AFE). On the one hand, with the adoption of the PWM current-source rectifier (CSR) and the PWM current-source inverter (CSI), the PWM current-source drives with AFE contains potential LC resonance in both the line side and the motor side. The LC resonance may amplify the harmonics and interharmonics in ac side produced by the distorted dc-link current (due to the small dc choke) through the PWM converter. Such amplified ac-side harmonics and interharmonics can further distort the dc-link current, and may even introduce harmonics and interharmonics in the other ac side through the PWM process which can be significant due to the LC circuit as well. On the other hand, unlike the thyristor converters that the dominant component in modulation function is the lowest-order harmonic, the dominant harmonics of PWM current-source converters depend on its modulation scheme. Especially for the commonly-adopted selective harmonic elimination (SHE) modulation scheme in the high-power PWM current-source converters, as certain order harmonics can be eliminated in PWM pattern, the dominant components in SHE

Publications out of this chapter:

- (1) Y. Zhang, and Y. W. Li, "Investigation and suppression of harmonics interaction in high-power PWM current-source motor drives," IEEE Transaction on Power Electronics, vol. 30, no. 2, pp. 668-679, Feb. 2015.

modulation function will vary with the design of SHE scheme. Regarding the interharmonics caused by the harmonics interaction, since the SHE scheme is used to modulate both the PWM CSR and the PWM CSI, the frequency analysis of interharmonics will be more complicated in the high-power PWM current-source drive systems with AFE than the TFE-based drives. Therefore, the interharmonic problems, especially the excitation of LC resonance, are expected to be thoroughly studied with respect to the high-power PWM current-source drives with AFE. With such motivation, in this chapter, the harmonics interaction phenomenon in such drive systems is thoroughly investigated and the LC resonance excited by the produced interharmonics is analyzed in details. Both simulation and experimental results are provided to verify the analysis.

3.1 Investigation of harmonics interaction

As mentioned in Chapter 2, the analysis of interharmonics caused by the harmonics interaction phenomenon have been carried out on the PWM voltage-source inverter (VSI) drives and the load-commutated inverter (LCI) drives [73],[91],[92],[94-99]. In the PWM VSI-fed drives, since dc link is usually equipped with sufficiently large capacitor, the harmonics interaction problem is not significant [91]. Most papers only consider the influence of the harmonics generated by one ac-side converter on the interharmonics at the other ac side [94]-[96]. E.g. [73] and [97] analyze the line-side interharmonic current generated by the drive system based on only one direction of the harmonics interaction. With respect to the LCI-fed drives, where harmonics interaction appears stronger, the adoption of thyristor converters enables all possible frequencies of interharmonics in two ac sides and dc link to be obtained through a single round of harmonics interaction (e.g. from dc link to ac sides and then back to dc link). Also, for the high-power PWM current-source drives with TFE studied in Chapter 2, the provided verification results demonstrate that the conducted single round of harmonics interaction is sufficient to cover the dominant ac-side interharmonics produced in the drive system. However, with re-

spect to the high-power PWM current-source drive systems with AFE, not all possible frequencies of the introduced interharmonics are guaranteed to be obtained through a single round of harmonics interaction due to the SHE-modulated PWM current-source converters, which will be explained later. As a result, more iterations may be required to find the interharmonics that may cause impacts on the drive system. In this section, to investigate the harmonics interaction phenomenon in the PWM current-source drives with AFE, a generalized frequency and sequence relationship between the ac-side components and the dc-link components is developed at first. Then, an iteration concept is proposed to analyze the possible frequencies of the produced interharmonics.

3.1.1 Generalized frequency and sequence relationship between ac side and dc link

In Chapter 2, based on the modulation function theory, a simple frequency analysis is conducted for the dominant dc-link harmonics produced by the fundamental ac component and the modulation function of current-source converters and the dominant ac-side interharmonics generated by the dc-link harmonics through the current-source converters respectively. To facilitate the following frequency analysis of the interharmonics in high-power PWM current-source drives with AFE, a generalized frequency and sequence relationship between the components in ac side and the components in dc link through the PWM current-source converter is developed at first in this part. For the convenience of presentation, all the ac components are named as “harmonics”, regardless of the harmonics and the interharmonics in ac sides and dc link.

A. Frequency and sequence relationship between dc-link and ac-side current

Define a certain harmonic in dc-link current (i_{dc}), i_{dcm} , as

$$i_{dcm} = I_{dcm} \sin(\omega_{dcm} t + \varphi_{dcm}), \quad (3-1)$$

where I_{dcm} , ω_{dcm} , and φ_{dcm} are the magnitude, frequency and initial phase of i_{dcm} respectively. Also, define the positive-sequence h th harmonic \bar{S}_{wh}^+ and the negative-sequence h th harmonic \bar{S}_{wh}^- in modulation function \bar{S}_w respectively as

$$\bar{S}_{wh}^+ = -jM_{sh}^+ e^{j(h\omega t + \varphi_{sh}^+)}, \quad (3-2)$$

$$\bar{S}_{wh}^- = jM_{sh}^- e^{-j(h\omega t + \varphi_{sh}^-)}, \quad (3-3)$$

where M_{sh}^+ , φ_{sh}^+ and M_{sh}^- , φ_{sh}^- are the magnitude and initial phase of the positive-sequence and negative-sequence harmonic respectively; ω is the fundamental frequency. Then, based on (2-2), we can obtain that the dc-link current harmonic modulated by the h th harmonic in modulation function will produce the ac-side harmonics as

$$\bar{I}_{acm} = i_{dcm} \bar{S}_{wh}^+ = -\frac{1}{2} I_{dcm} M_{sh}^+ \left(e^{j((\omega_{dcm} + h\omega)t + (\varphi_{dcm} + \varphi_{sh}^+))} - e^{-j((\omega_{dcm} - h\omega)t + (\varphi_{dcm} - \varphi_{sh}^+))} \right), \quad (3-4)$$

$$\bar{I}_{acm} = i_{dcm} \bar{S}_{wh}^- = -\frac{1}{2} I_{dcm} M_{sh}^- \left(e^{-j((\omega_{dcm} + h\omega)t + (\varphi_{dcm} + \varphi_{sh}^-))} - e^{j((\omega_{dcm} - h\omega)t + (\varphi_{dcm} - \varphi_{sh}^-))} \right). \quad (3-5)$$

It can be observed that the ω_{dcm} -frequency harmonic in i_{dc} modulated by the h th-order harmonic component in \bar{S}_w will produce two ac current harmonics with $(\omega_{dcm} + h\omega)$ and $(\omega_{dcm} - h\omega)$ frequency respectively. If \bar{S}_{wh} is of the positive sequence, such two ac current harmonics will be of the positive sequence and the negative sequence respectively according to (3-4); if \bar{S}_{wh} is of the negative sequence, such two ac current harmonics will be of the negative sequence and the positive sequence respectively as shown in (3-5). The frequency and sequence relationship between the dc-link current and the ac-side current through the modulation function is summarized as shown in Fig. 3. 1.

B. Frequency and sequence relationship between ac-side and dc-link voltage

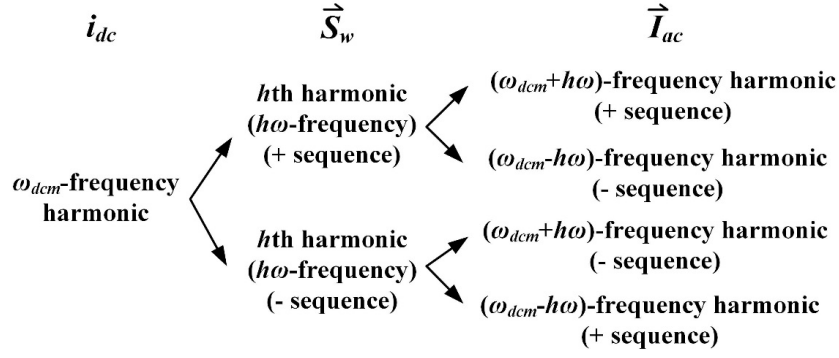


Fig. 3. 1. Frequency and sequence relationship between the dc-link current and the ac-side current through the PWM current-source converter.

Define a certain positive-sequence and negative-sequence ω_{acm} -frequency ac-side voltage harmonic, \bar{V}_{acm}^+ and \bar{V}_{acm}^- , respectively as

$$\bar{V}_{acm}^+ = -jV_{acm}^+ e^{j(\omega_{acm}t + \varphi_{acm}^+)}, \quad (3-6)$$

$$\bar{V}_{acm}^- = jV_{acm}^- e^{-j(\omega_{acm}t + \varphi_{acm}^-)}, \quad (3-7)$$

where V_{acm}^+ , φ_{acm}^+ and V_{acm}^- , φ_{acm}^- are the magnitude and initial phase of the positive-sequence and negative-sequence ac-side voltage harmonic respectively. Based on (2-3), \bar{V}_{acm}^+ and \bar{V}_{acm}^- modulated by \bar{S}_{wh}^+ and \bar{S}_{wh}^- will produce the dc-link voltage harmonics as

$$v_{dcm} = \bar{V}_{acm}^+ \bullet \bar{S}_{wh}^+ = \frac{3}{2} V_{acm}^+ M_{sh}^+ \cos\left((\omega_{acm} - h\omega)t + (\varphi_{acm}^+ - \varphi_{sh}^+)\right), \quad (3-8)$$

$$v_{dcm} = \bar{V}_{acm}^- \bullet \bar{S}_{wh}^- = \frac{3}{2} V_{acm}^- M_{sh}^- \cos\left((\omega_{acm} - h\omega)t + (\varphi_{acm}^- - \varphi_{sh}^-)\right), \quad (3-9)$$

$$v_{dcm} = \bar{V}_{acm}^+ \bullet \bar{S}_{wh}^- = -\frac{3}{2} V_{acm}^+ M_{sh}^- \cos\left((\omega_{acm} + h\omega)t + (\varphi_{acm}^+ + \varphi_{sh}^-)\right), \quad (3-10)$$

$$v_{dcm} = \bar{V}_{acm}^- \bullet \bar{S}_{wh}^+ = -\frac{3}{2} V_{acm}^- M_{sh}^+ \cos\left((\omega_{acm} + h\omega)t + (\varphi_{acm}^- + \varphi_{sh}^+)\right). \quad (3-11)$$

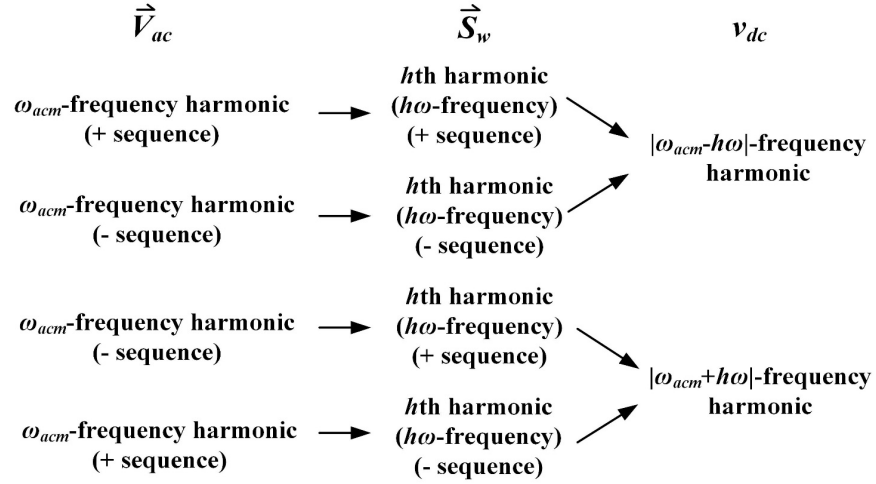


Fig. 3. 2. Frequency and sequence relationship between the ac-side voltage and the dc-link voltage through the PWM current-source converter.

We can observe that, when ω_{acm} -frequency ac voltage harmonic and h th harmonic in modulation function are of the same sequence, only the $|\omega_{acm}-h\omega|$ -frequency harmonic will be generated in dc-link voltage, and when they are of the different sequences, only the $|\omega_{acm}+h\omega|$ -frequency dc-link voltage harmonic will be produced. According to the analysis above, the frequency and sequence relationship between the ac-side voltage and the dc-link voltage through the modulation function can be summarized as shown in Fig. 3. 2.

3.1.2 Iteration concept based frequency analysis

Fig. 3. 3 shows a simplified topology of PWM current-source drive system with AFE. As discussed earlier, the dc choke with limited inductance cannot sufficiently attenuate the PWM harmonics produced by the rectifier and the inverter, so that the distortion of dc-link current i_{dc} cannot be ignored. The distorted dc-link current will generate harmonics in PWM current at the line side (\bar{I}_{wr}) and the motor side (\bar{I}_{wi}) through the PWM CSR and the PWM CSI respectively. The PWM current \bar{I}_{wr} and \bar{I}_{wi} will further produce the harmonics in capacitor voltage \bar{V}_{cr} and \bar{V}_{ci} through the line-side circuit and the motor-side circuit respectively. The produced capacitor voltage harmonics will then generate the harmonics in dc-link voltage v_{dcr} and v_{dci}

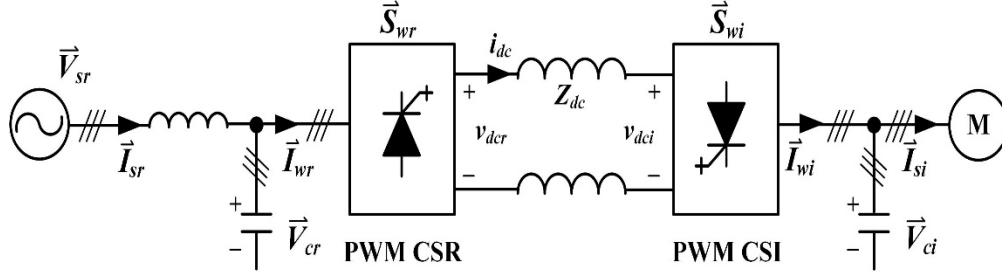


Fig. 3. 3. Simplified configuration of high-power PWM current-source drives with PWM CSR.

through the PWM converters, which produce the newly-generated harmonics in dc-link current i_{dc} . Following this procedure of harmonics interaction, harmonics with many possible frequencies will be introduced in entire system, and their frequencies vary with the motor operating frequencies. To perform the frequency analysis of such harmonics interaction phenomenon, the iteration concept developed as follows can be adopted.

According to the analysis in Section 2. 1. 2, if the modulation function of PWM CSI (\vec{S}_{wi}) contains h_{inv} th harmonics ($h_{inv}=6n_{inv}\pm 1$, $n_{inv}\in\mathbb{N}^0$, $h_{inv}>0$), the dc-link current will contain $6n_{inv}\omega_i$ -frequency harmonics (ω_i is the motor operating frequency, also the motor-side fundamental frequency). Similarly, if the modulation of PWM CSR (\vec{S}_{wr}) contains h_{rec} th harmonics ($h_{rec}=6n_{rec}\pm 1$, $n_{rec}\in\mathbb{N}^0$, $h_{rec}>0$), the dc-link current will contain $6n_{rec}\omega_r$ -frequency harmonics (ω_r is the line-side fundamental frequency). Combining the two parts of harmonics in dc-link current, we can define the initial condition of iteration, and the frequencies of such dc-link current harmonics can be termed as $6n_{rec}^{iter0}\omega_r$ and $6n_{inv}^{iter0}\omega_i$ respectively. Following the procedure of harmonics interaction phenomenon mentioned in last paragraph, we can define one iteration as depicted in Fig. 3. 4. In Fig. 3. 4, the transfer functions, $G_r(s)=\vec{V}_{cr}(s)/\vec{I}_{wr}(s)$ and $G_i(s)=\vec{V}_{ci}(s)/\vec{I}_{wi}(s)$, are adopted to represent the line-side and motor-side circuit respectively. Starting from the initial condition and utilizing the developed frequency relationship, the frequencies of harmonics generated in the first iteration can be obtained as shown in Fig. 3. 5, where the superscripts of n_{rec}

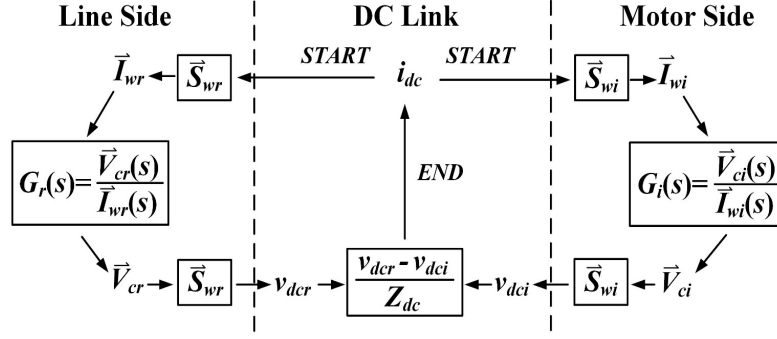


Fig. 3. 4. Flow chart of one iteration.

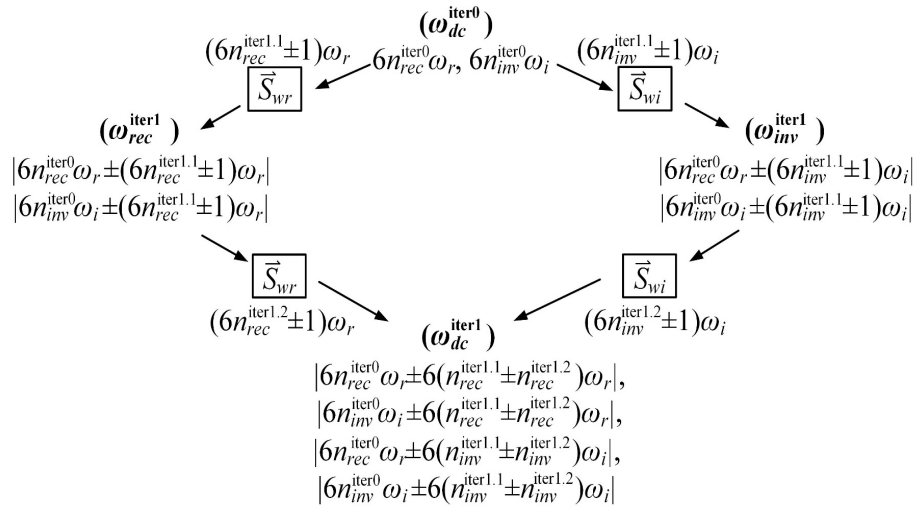


Fig. 3. 5. Frequency analysis during the first iteration.

and n_{inv} , iter1.1 and iter1.2, represent the first and second interaction with the modulation function \bar{S}_w respectively. The ω_{dc}^{iter0} denotes the frequencies of initial harmonics at dc link, and ω_{rec}^{iter1} , ω_{inv}^{iter1} , and ω_{dc}^{iter1} denote the frequencies of the harmonics generated at line side, motor side and dc link during the first iteration respectively. Following the same procedure, we can obtain the frequencies of the produced harmonics after arbitrary rounds of iteration.

For the thyristor converters based LCI-fed drives, it can be proved that single round of iteration defined above can cover all possible frequencies of the produced harmonics. Consider an LCI-fed drive system with 6-pulse SCRs rectifier and 6-pulse SCRs inverter for instance, which means that $n_{rec}, n_{inv} = 0, 1, 2, \dots$. Based on

Fig. 3. 5, after one iteration, we can obtain that the dc link will contain the harmonics with $6p\omega_r$, $6q\omega_i$, and $|6p\omega_r \pm 6q\omega_i|$ frequencies; the line side contains $|(6p \pm 1)\omega_r|$ -frequency and $|6p\omega_r \pm (6q \pm 1)\omega_r|$ -frequency harmonics; the motor side contains $|(6p \pm 1)\omega_i|$ -frequency and $|6p\omega_r \pm (6q \pm 1)\omega_i|$ -frequency harmonics ($p, q=0, 1, 2, \dots$). Since n_{rec} , n_{inv} , p , q represent all non-negative integers, a single round of iteration produces harmonics with all possible frequencies. Similar conclusion can be drawn to the LCI-fed drives with k_r -pulse SCR rectifier and k_i -pulse SCR inverter ($k_r, k_i=6, 12, 18, \dots$). However, for the SHE-modulated PWM current-source converters, n_{rec} and/or n_{inv} are not always equal to all non-negative integers, as certain order harmonics can be eliminated in PWM pattern. As a result, the frequency analysis is more complex for the high-power PWM current-source drives. Especially for the drive systems with AFE, since the PWM current-source converters are adopted at two sides, more iterations are needed to find the harmonics with possible frequencies caused by the harmonics interaction.

3.2 Analysis of LC resonance occurrence

As mentioned earlier, the impact of the interharmonics caused by the harmonics interaction on the LC resonance occurrence is serious in high-power PWM current-source drives with AFE, due to the LC circuit contained in each ac side. With respect to such critical problem, an in-depth analysis is conducted in this section. Based on the investigation in previous section, the motor operating frequencies, where the harmonics interaction excites the LC resonance, are estimated in the following analysis, and the frequencies of the significant harmonics in ac sides and dc link caused by the LC resonance are predetermined. Note that, the same analysis procedure can also be used to study other interharmonics' impacts, such as the communication interference and the torsional vibration problem. As have been focused in Chapter 2, they are not discussed in this Chapter to avoid redundancy.

According to the above analysis, if only the fundamental component \bar{S}_{w1} in modulation function \bar{S}_w is used (which means that $h_{rec}, h_{inv}=1$), $n_{rec}^{iterk.1}$, $n_{rec}^{iterk.2}$, $n_{inv}^{iterk.1}$ and

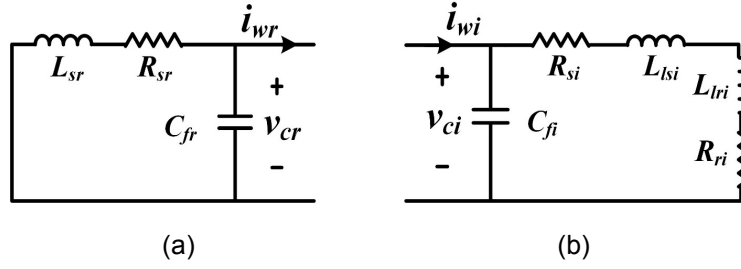


Fig. 3. 6. Equivalent per phase harmonic circuit: (a) line side, (b) motor side.

$n_{inv}^{iterk,2}$ are all zero during the k th iteration. According to Fig. 3. 5, no new harmonics will be introduced in dc link, and therefore, no new ac-side harmonics will be generated in the next iteration. In other words, to generate the harmonics with new frequencies, the harmonic components \bar{S}_{wh} ($h \neq 1$) in \bar{S}_w are required. Since \bar{S}_{wh} are much smaller than \bar{S}_{w1} , we can ignore their effects after a few (one or two) iterations. Moreover, since no new harmonics will be introduced with \bar{S}_{w1} , we can only consider the first few iterations to estimate the LC resonance conditions. In the following analysis, we consider the first two iterations of harmonics interaction to estimate the LC resonance.

Take the PWM current-source induction motor drive system for example (same analysis can also be used for other types of motors). The equivalent per phase harmonic circuits of the line side and the motor side can be shown as in Fig. 3. 6. In Fig. 3. 6(a), R_{sr} , L_{sr} , and C_{fr} are the line resistance, line inductance and filter capacitance in line side respectively. In Fig. 3. 6(b), R_{si} , L_{lsi} , R_{ri} , L_{lri} , and C_{fi} are the stator resistance, stator leakage inductance, rotor resistance, rotor leakage inductance and filter capacitance in motor side respectively. Considering the influence of dc choke inductance L_{dc} on the ac-side LC resonant frequency [114], the LC resonant frequency of each ac side, ω_{rec}^{res} and ω_{inv}^{res} , can be derived from (3-12). In (3-12), \bar{I}'_w represents the equivalent space-phasor PWM current in [114]. In addition, R_{eq} , L_{eq} , C_{eq} represent R_{sr} , L_{sr} , C_{fr} respectively in line side, $(R_{si}+R_{ri})$, $(L_{lsi}+L_{lri})$, C_{fi} respectively in motor side.

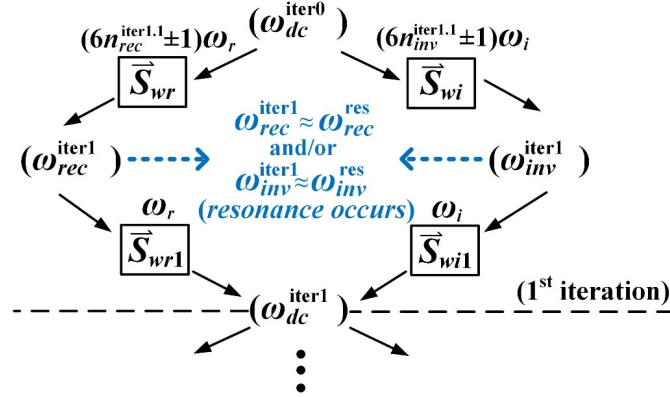


Fig. 3. 7. LC resonance occurs in the first iteration.

$$\frac{\bar{V}_c}{\bar{I}_w} = \frac{L_{dc}L_{eq}s^2 + L_{dc}R_{eq}s}{L_{dc}C_{eq}L_{eq}s^3 + L_{dc}C_{eq}R_{eq}s^2 + \left(\frac{8}{9}L_{eq} + L_{dc}\right)s + \frac{8}{9}R_{eq}} \quad (3-12)$$

If LC resonance occurs in the first iteration, it corresponds to the situation shown in Fig. 3. 7. In this situation, the frequencies of certain line-side harmonics and/or motor-side harmonics produced during the first iteration are close to the LC resonant frequency of corresponding side, which can be denoted as

$$\omega_{rec}^{iter1} \approx \omega_{rec}^{res} \quad \text{and/or} \quad \omega_{inv}^{iter1} \approx \omega_{inv}^{res}. \quad (3-13)$$

Since \bar{S}_{w1} is more significant than \bar{S}_{wh} ($h \neq 1$), after the LC resonance occurs in the first iteration, significant dc-link harmonics will be introduced through \bar{S}_{wr1} (fundamental component in \bar{S}_{wr}) and/or \bar{S}_{wi1} (fundamental component in \bar{S}_{wi}). Based on the developed frequency and sequence relationship between the ac-side components and the dc-link components, the frequencies of the significant dc-link harmonics among ω_{dc}^{iter1} , denoted as ω_{dcm}^{iter1} , are shown in (3-14) when the ac-side harmonics and \bar{S}_{w1} are of the same sequence, and in (3-15) when they are of different sequences.

$$\omega_{dcm}^{iter1} \approx \left| \omega_{rec}^{res} - \omega_r \right| \quad \text{and/or} \quad \omega_{dcm}^{iter1} \approx \left| \omega_{inv}^{res} - \omega_i \right| \quad (3-14)$$

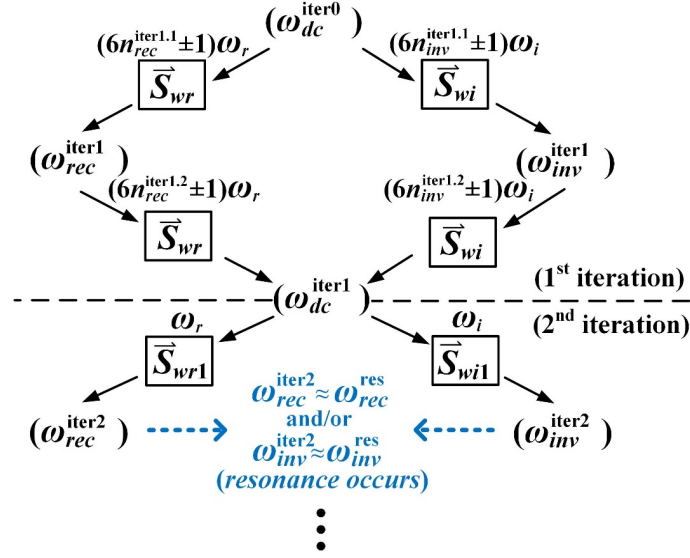


Fig. 3. 8. *LC* resonance occurs in the second iteration.

$$\omega_{dcm}^{iter1} \approx \left| \omega_{rec}^{res} + \omega_r \right| \quad \text{and/or} \quad \omega_{dcm}^{iter1} \approx \left| \omega_{inv}^{res} + \omega_i \right| \quad (3-15)$$

If *LC* resonance occurs in the second iteration, it corresponds to the situation shown in Fig. 3. 8. The *LC* resonance condition can be represented by

$$\omega_{rec}^{iter2} \approx \omega_{rec}^{res} \quad \text{and/or} \quad \omega_{inv}^{iter2} \approx \omega_{inv}^{res}. \quad (3-16)$$

In this situation, \bar{S}_{wr1} and \bar{S}_{wi1} are required to be used at least once during the first iteration to ensure that the components with new frequencies (ω_{dcm}^{iter1}) produced in the dc-link current are not too small. Similarly, \bar{S}_{wr1} and \bar{S}_{wi1} are needed to generate the line-side harmonics with ω_{rec}^{iter2} frequencies and the motor-side harmonics with ω_{inv}^{iter2} frequencies respectively during the second iteration. Therefore, based on the frequency relationship, (3-16) can be rewritten as

$$\left| \omega_{dcm}^{iter1} \pm \omega_r \right| \approx \omega_{rec}^{res} \quad \text{and/or} \quad \left| \omega_{dcm}^{iter1} \pm \omega_i \right| \approx \omega_{inv}^{res}. \quad (3-17)$$

Summarizing (3-14), (3-15) and (3-17), the *LC* resonance will occur if at least one of the four conditions shown in (3-18) is satisfied.

$$\left\{ \begin{array}{l} \left| \omega_{rec}^{res} + \omega_r \right| \approx \omega_{dcm}^{iter1} \\ \left| \omega_{rec}^{res} - \omega_r \right| \approx \omega_{dcm}^{iter1} \\ \left| \omega_{inv}^{res} + \omega_i \right| \approx \omega_{dcm}^{iter1} \\ \left| \omega_{inv}^{res} - \omega_i \right| \approx \omega_{dcm}^{iter1} \end{array} \right. \quad (3-18)$$

In (3-18), the possible values of ω_{dcm}^{iter1} are of the same expressions as the ω_{dc}^{iter1} shown in Fig. 3. 5, and at least one from $n_{rec}^{iterk.1}$, $n_{rec}^{iterk.2}$ and one from $n_{inv}^{iterk.1}$, $n_{inv}^{iterk.2}$ are zero since \bar{S}_{wr1} and \bar{S}_{wi1} are used at least once in the first iteration as discussed earlier. According to Fig. 3. 5, ω_{dcm}^{iter1} is determined by the SHE PWM pattern (n_{rec} , n_{inv}) and the motor operating frequency (ω_i). Therefore, if system parameters are known (ω_{rec}^{res} , ω_{inv}^{res} can be calculated from (3-12)) and the SHE patterns are determined, we can estimate ω_i that leads to the *LC* resonance based on (3-18), and obtain the frequencies of relevant significant dc-link current harmonics ω_{dcm}^{iter1} corresponding to ω_i .

3.3 Verification results

In order to verify the analysis of harmonics interaction and the *LC* resonance occurrence, simulated and experimental results are provided in this section.

3.3.1 Simulation results

The simulation is carried on a 1MVA/4160V/60Hz PWM current-source induction drive application with a PWM CSR, and the parameters are listed in TABLE. 3. 1. Also, the detailed model of power converters and the full-order model of induction motor are adopted in the simulations as well as in Chapter 2. Based on (3-12), the ac-side *LC* resonant frequency can be obtained from Fig. 3. 9 as ω_{rec}^{res} =285Hz for line side and ω_{inv}^{res} =228Hz for motor side. To simplify the analysis, we consider a certain range of motor operating frequency, [42Hz, 60Hz], in the following simulation. In such range, with the switching frequency limited within 540Hz,

TABLE. 3. 1. PARAMETERS OF A 1MVA/4160V PWM CURRENT-SOURCE DRIVE APPLICATION WITH AFE (SIMULATION)

Nominal power	1MVA		
Nominal grid voltage (line-to-line)	4160V		
Frequency	60Hz		
Motor rated voltage (line-to-line)	4000V		
Motor rated power	1100hp		
Motor rated speed	1190rpm		
	Line-side	DC-link	Motor-side
Voltage base value	2401.8V	5094.9V	2309.4V
Current base value	140A	198A	145.6A
Impedance base value	17.2Ω	25.7Ω	15.9Ω
Inductance base value	45.5mH	68.3mH	42.1mH
Capacitance base value	154.6μF		167.2μF
	Real value	P.U. value	
Line resistance	0.034Ω	0.002	
Line inductance	4.78mH	0.11	
Line-side filter capacitance	75.98μF	0.49	
DC choke	27.87mH	0.41	
Motor-side filter capacitance	60.08μF	0.36	
Motor stator leakage inductance	5.18mH	0.12	
Motor stator resistance	0.21Ω	0.013	
Motor magnetizing inductance	154.9mH	3.68	
Motor rotor leakage inductance	5.18mH	0.12	
Motor rotor resistance	0.146Ω	0.01	
Load torque	3000Nm		

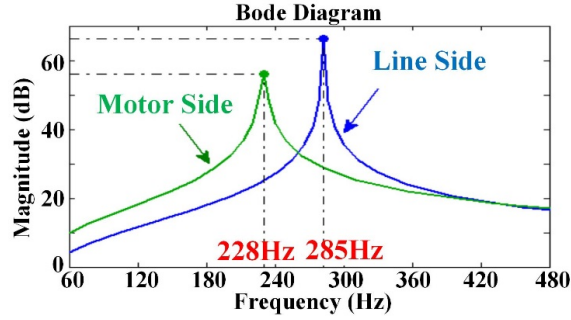


Fig. 3. 9. Bode plot of transfer function $\bar{V}_c(s) / \bar{I}_w(s)$ shown in (3-12).

the 9-pulse SHE scheme is used to modulate the PWM CSR and the PWM CSI. For convenience, the same 9-pulse SHE pattern designed to mitigate 5th, 7th, 11th, and 13th harmonics is adopted in both the CSR and the CSI. The harmonic content of the 9-pulse SHE pattern (also the modulation function \bar{S}_w) is shown in Fig. 3. 10. Since the 5th, 7th, 11th, and 13th harmonics cannot be fully eliminated simultane-

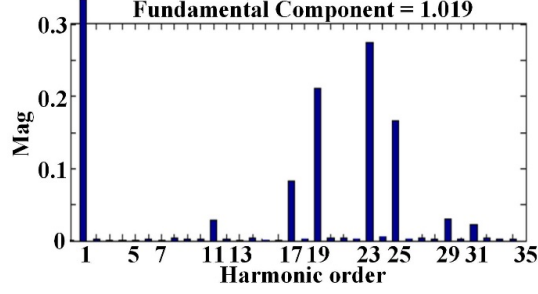


Fig. 3. 10. Harmonic content in the modulation function of a 9-pulse SHE PWM pattern.

ously according to [1], in this simulation, an insignificant 11th harmonic is remained in the PWM pattern. Note that the 9-pulse SHE pattern can be adjusted to fully eliminate the 5th, 7th and 11th harmonics but contains small quantity of 13th harmonic as well. As the residual 11th harmonic is insignificant, its influence on harmonics interaction can be ignored in the following analysis. According to Fig. 3. 10, it can be observed that the modulation function \bar{S}_w contains significant 17th, 19th, 23rd, and 25th harmonics. Since higher-order harmonics can be attenuated by the dc choke, we can only consider the fundamental component and the 17th, 19th, 23rd, and 25th harmonics in \bar{S}_w , which means that the n_{rec} and n_{inv} in the above analysis can be 0, 3,4.

According to the estimation of LC resonance occurrence in Section 3. 2, the left-hand-side of (3-18) is equal to $|285\text{Hz}\pm\omega_r|$ and $|228\text{Hz}\pm\omega_i|$ as the dash line drawn in Fig. 3. 11, and the right-hand-side ω_{dcm}^{iter1} can be $6\omega_r$, $6\omega_i$, $|18\omega_r\pm18\omega_i|$, $|18\omega_r\pm24\omega_i|$, $|24\omega_r\pm18\omega_i|$ and $|24\omega_r\pm24\omega_i|$ as the solid line in Fig. 3. 11, where $\omega_r=60\text{Hz}$, $\omega_i \in [42, 60]$ Hz. The (3-18) is satisfied at the circled intersection points in Fig. 3. 11, which means that the LC resonance will occur around the ω_i corresponding to Points (1)-(11). The simulation result of dc-link current at steady state versus ω_i is shown in Fig. 3. 12. It can be observed that the dc-link current contains significant harmonics when the motor operating frequency ω_i is around certain values, which are shown as the peaks in Fig. 3. 12. Each peak shows that the LC resonance occurs at the corresponding ω_i . From Fig. 3. 11 and Fig. 3. 12, we can observe that each peak of dc-link current harmonic Peaks (1)-(11) in Fig. 3. 12 has one-to-

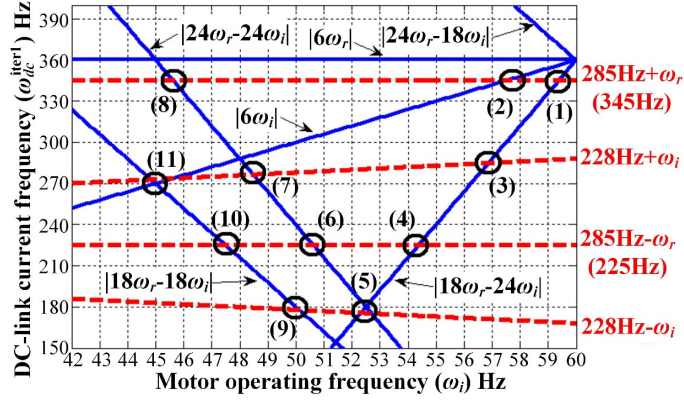


Fig. 3. 11. Frequency plot of (3-18) for simulation system.

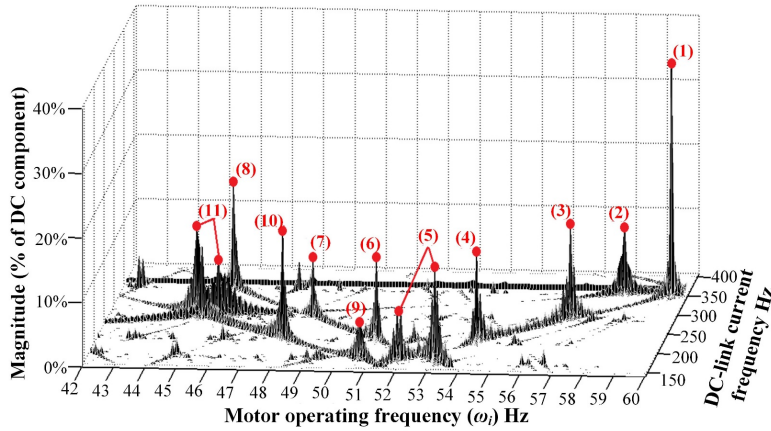


Fig. 3. 12. Steady-state dc-link current harmonics versus motor operating frequency (ω_i).

one correspondence to Points (1)-(11) in Fig. 3. 11. For example, when ω_i is close to 59Hz, the dc-link current harmonic with around 350Hz frequency has the significant magnitude as shown by Peak (1) in Fig. 3. 12. It corresponds to the situation around Point (1) in Fig. 3. 11, where the ω_i is close to 59Hz and the ω_{dc}^{iter1} is around 350Hz. The correspondence of analysis in Fig. 3. 11 and simulation result in Fig. 3. 12 verifies the effectiveness of the estimation of *LC* resonance occurrence presented in Section 3. 2. Note that Fig. 3.12 is plotted based on the dc-link current harmonics divided by the dc component in dc-link current. If divided by the rated current of the system, the magnitude of each peak in Fig. 3. 12 will have a certain rate of decrease, but the *LC* resonance problem still cannot be ignored. Fig. 3. 13 and Fig. 3. 14 show the simulation results of line current harmonics and motor stator

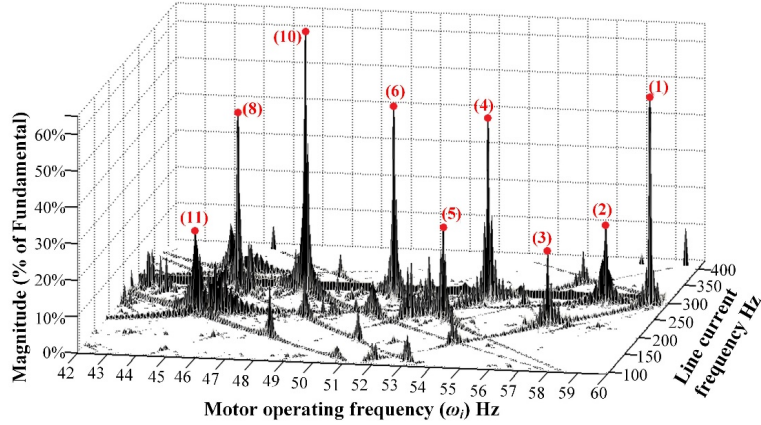


Fig. 3. 13. Line current harmonics vs. motor operating frequency (ω_i).

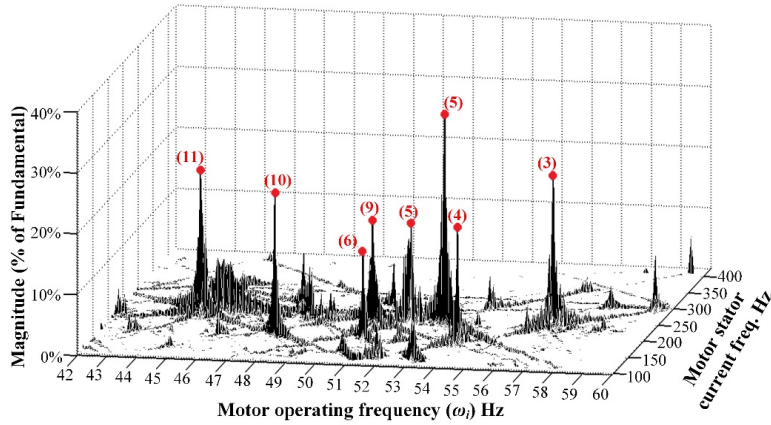


Fig. 3. 14. Motor stator current harmonics vs. motor operating frequency (ω_i).

current harmonics versus ω_i respectively. It can be observed that, through \bar{S}_{w1} , the LC resonance also results in the significant harmonics in the line side and the motor side with frequencies of $|\omega_{dcm}^{iter1} \pm \omega_r|$ and $|\omega_{dcm}^{iter1} \pm \omega_i|$ respectively, especially when their frequencies are close to the ac-side LC resonant frequency. The same peak number in Figs. 3. 12-3. 14, represents that the LC resonance occurs at same ω_i .

3.3.2 Experimental results

To experimentally validate the discussion above, plenty of real-time experiments have been carried out on a 10kVA/208V/60Hz PWM current-source induction motor drive prototype (with AFE), as shown in Fig. 3. 15, with parameters scaled down

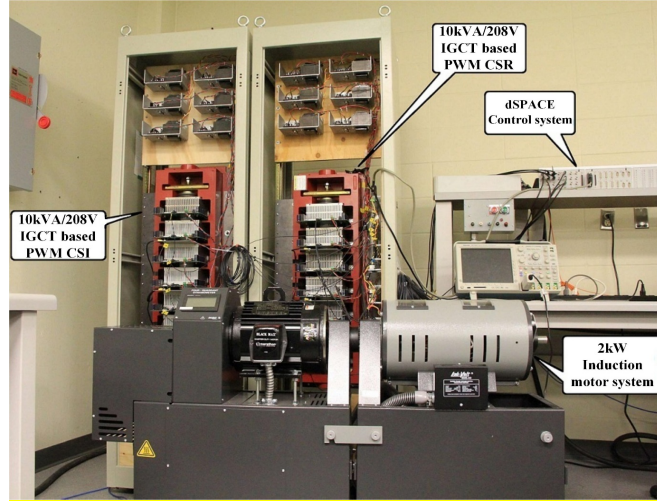


Fig. 3. 15. Setup of 10kVA/208V PWM current-source drive (with AFE) prototype.

from a high-power application as listed in TABLE. 3. 2. The background grid voltage is programmed harmonicless. The same 9-pulse SHE pattern as in the simulation section (Fig. 3. 10) is used for both the PWM CSR and CSI. To reduce the amount of data recorded for FFT analysis, we only test the system at integer motor operating frequency.

According to the analysis above, with the system parameters shown in TABLE. 3. 2, the ac-side LC resonant frequency can be obtained as $\omega_{rec}^{res} = 261\text{Hz}$ for line side and $\omega_{inv}^{res} = 209\text{Hz}$ for motor side, and the frequency plot of (3-18) can be drawn as Fig. 3. 16.

According to Fig. 3. 16, when motor operates at 42Hz frequency ($\omega_i = 42\text{Hz}$), two dc-link harmonics resulted from the harmonics interaction with 252Hz and 324Hz respectively are close to the dash lines so that will be amplified due to the LC resonance. With the fundamental component in modulation function, the LC resonance will also introduce the 192Hz ($=252\text{Hz}-60\text{Hz}$), 312Hz ($=252\text{Hz}+60\text{Hz}$), 264Hz ($=324\text{Hz}-60\text{Hz}$), 384Hz ($=324\text{Hz}+60\text{Hz}$) harmonics in line side; the 210 ($=252\text{Hz}-42\text{Hz}$), 294Hz ($=252\text{Hz}+42\text{Hz}$), 282Hz ($=324\text{Hz}-42\text{Hz}$), 366Hz ($=324\text{Hz}+42\text{Hz}$) harmonics in motor side. Fig. 3. 17 shows the waveforms of line current, dc-link current, and motor stator current when $\omega_i = 42\text{Hz}$. Figs. 3. 18(a), (b) and (c)

TABLE. 3. 2. PARAMETERS OF 10kVA/208V PWM CURRENT-SOURCE DRIVE PROTOTYPE WITH AFE (EXPERIMENT)

Nominal power	10kVA		
Nominal grid voltage (line-to-line)	208V		
Frequency	60Hz		
Motor rated voltage (line-to-line)	208V		
Motor rated power	2kW		
Motor rated speed	1720rpm		
	Line-side	DC-link	Motor-side
Voltage base value	120V	254.7V	120V
Current base value	27.8A	39.3A	27.8A
Impedance base value	4.32Ω	6.48Ω	4.32Ω
Inductance base value	11.47mH	17.20mH	11.47mH
Capacitance base value	613.6μF		613.6μF
	Real value	P.U. value	
Line inductance	1.67mH	0.15	
Line-side filter capacitance	240μF	0.40	
DC choke	10mH	0.60	
Motor-side filter capacitance	120μF	0.20	
Motor stator leakage inductance	4.0mH	0.35	
Motor stator resistance	0.78Ω	0.18	
Motor magnetizing inductance	53.5mH	4.66	
Motor rotor leakage inductance	4.0mH	0.35	
Motor rotor resistance	0.30Ω	0.07	
Load torque	1.6Nm		

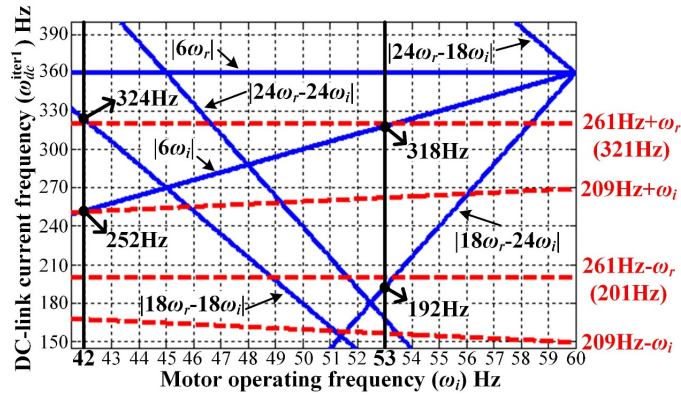


Fig. 3. 16. Frequency plot of (3-18) for experimental system.

are the FFT analysis of each current respectively. It can be observed from Fig. 3. 18(b) that dc-link current contains significant 252Hz and 324Hz harmonics. In addition, as shown in Figs. 3. 18(a) and (c), significant 192Hz, 264Hz, and 312Hz current harmonics are introduced in line side, and 210Hz, 282Hz, and 294Hz current harmonics are produced in motor side. Since the 384Hz harmonics is far from the line-side LC resonant frequency and the 366Hz harmonics is far from the motor-

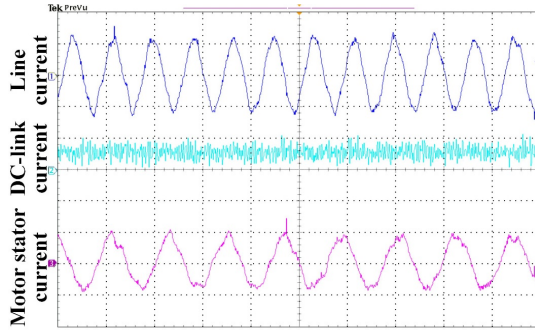
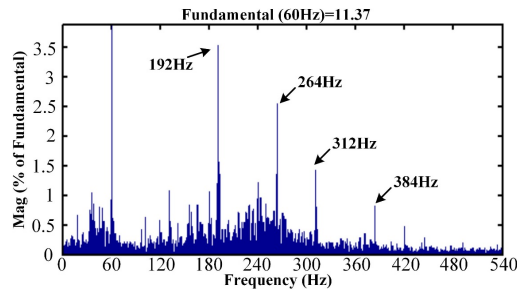
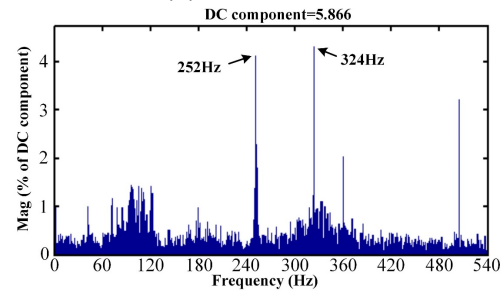


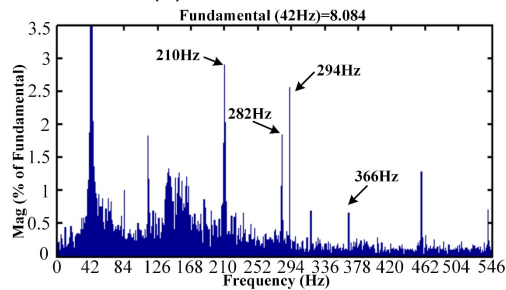
Fig. 3. 17. Waveforms of line current, dc-link current, and motor stator current at 42Hz motor operating frequency ($\omega_r=42\text{Hz}$) (10A/div., 20ms/div.).



(a) Line current



(b) DC-link current



(c) Motor stator current

Fig. 3. 18. FFT analysis of Fig. 3. 17.

side LC resonant frequency, they are not obvious in line side and motor side respectively. The experiment results at 42Hz motor operating frequency are corresponding to the analysis above.

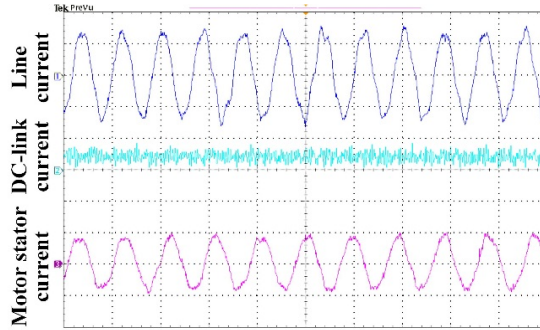


Fig. 3. 19. Waveforms of line current, dc-link current, and motor stator current at 53Hz motor operating frequency ($\omega_i=53\text{Hz}$) (10A/div., 20ms/div.).

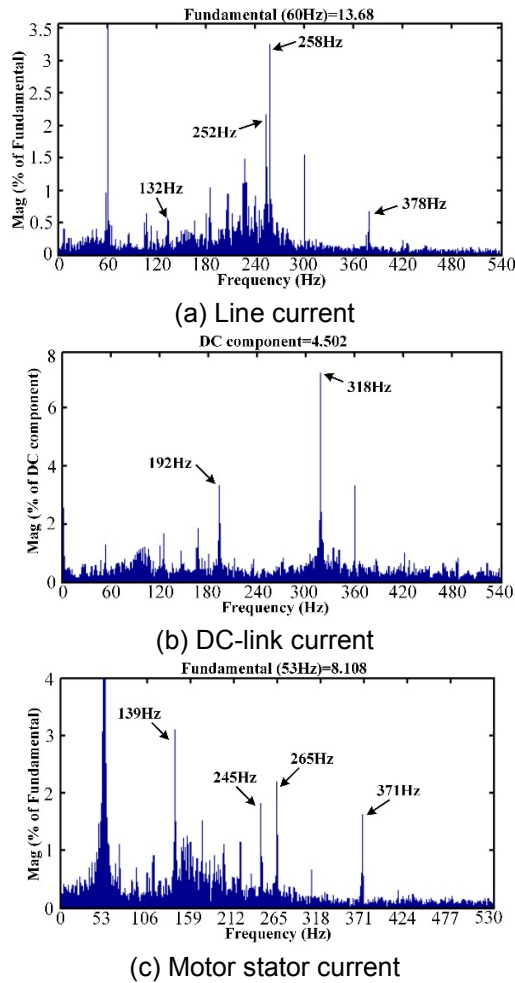


Fig. 3. 20. FFT analysis of Fig. 3. 19.

Similarly, when motor operates at 53Hz ($\omega_i=53\text{Hz}$), the 192Hz and 318Hz dc-link harmonics are close to the dash line as shown in Fig. 3. 16. Fig. 3. 19 shows the current waveforms of line side, dc link and motor side at 53Hz motor operating

frequency, and Fig. 3. 20 is the FFT analysis of each current. From Fig. 3. 20(b), we can observe that the 192Hz and 318Hz dc-link current harmonics are significant, and from Fig. 3. 20(a) and (c), the line current contains significant 252Hz (=192Hz+60Hz) and 258Hz (=318Hz-60Hz) harmonics and the motor stator current contains significant 139Hz (=192Hz-53Hz), 245Hz (=192Hz +53Hz), 265Hz (=318Hz-3Hz) and 371Hz (=318Hz+53Hz) harmonics which corresponds to above discussion as well.

3.4 Summary and discussion

In this chapter, with respect to the high-power PWM current-source drives with AFE, the harmonics interaction problem is thoroughly investigated based on a frequency iteration concept, and a detailed analysis of its impact on *LC* resonance occurrence is conducted. First, to facilitate the frequency analysis of the interharmonics caused by the harmonics interaction, the generalized frequency and sequence relationship between the ac-side voltage/current and the dc-link voltage/current through the modulation function of PWM current-source converter is developed. Then, an iteration concept is presented to analyze the possible frequencies of the interharmonics generated in line side, dc link and motor side due to the harmonics interaction. Also, based on the defined frequency iteration, the complexity of harmonics interaction analysis in the drives with the SHE-modulated high-power PWM current-source converters compared with the thyristor converters based drives is explained in details. Moreover, on the basis of the study on the harmonics interaction, an accurate estimation of the motor operating frequencies where the *LC* resonance is excited by the harmonics interaction is presented, and a frequency prediction of the significant interharmonics introduced in entire system due to the *LC* resonance is performed. Such method can also be applied to analyze other impacts of the interharmonics caused by the harmonics interaction in high-power PWM current-source drives with AFE. Finally, simulation and experimental results are provided to verify the effectiveness of the analysis in this chapter.

The investigation of the harmonics interaction phenomenon conducted in this chapter can help to prevent LC resonance, as well as the other impacts of the produced interharmonics, from being excited at certain motor operating frequencies through the design of filter circuit or PWM pattern. However, on the one hand, considering the extensive range of the possible interharmonic frequencies, it is difficult to completely inhibit the occurrence of LC resonance during the operation of motor through altering the resonant frequency of LC filter circuit. On the other hand, although it is possible to avoid the LC resonance by utilizing different SHE patterns in the different ranges of motor operating frequencies, it may require a considerable effort on the off-line design of PWM patterns and significantly increase the storage of SHE switching angles. Besides, the variation of system parameters may result in the failure of such method during the implementation. Since the passive damping involves amount of power loss in high-power applications, the active attenuation on the interharmonics so as to suppress the LC resonance is expected in high-power PWM current-source drives. In next chapter, an active attenuation strategy through the control of high-power PWM current-source converter is proposed based on the analysis in this chapter.

Chapter 4

Active Attenuation of Interharmonics in High-Power PWM Current-Source Drives

In high-power PWM current-source drives, the harmonics interaction between the rectifier and the inverter through the weak dc choke may introduce unexpected interharmonics in two ac sides and dc link. To reduce the impacts of the interharmonics, the following three approaches could be adopted according to previous analysis: 1) dc-link impedance could be increased to decouple the rectifier and inverter sides' harmonics so that the harmonics interaction could be prevented; 2) resistors could be added in each ac side to increase the damping on the interharmonics; 3) modulation schemes of the PWM current-source converters could be designed to prevent unexpected interharmonics from being generated at certain motor operating frequencies. For the first and second method, passive damping will result in additional costs and losses in the system, and physically increasing the dc-link impedance will aggravate its size and weight. For the third method, considerable efforts would be spent on the design of modulation schemes and the results may not be satisfactory with respect to solving some interharmonics-related problems (e.g. *LC* resonance) as discussed at the end of Chapter 2 and Chapter 3. If we could realize the active attenuation of the interharmonics through the control of high-power current-source converters, not only could the interharmonic problems be solved, but also the deficiencies of the three approaches would be overcome. However, although the PWM current-source converter is flexible in harmonic con-

Publications out of this chapter:

- (1) Y. Zhang, and Y. W. Li, "Detailed analysis of dc-link virtual impedance based suppression method for harmonics interaction in high-power PWM current-source motor drives," IEEE Transaction on Power Electronics, vol. 30, no. 9, pp. 4646-4658, Sept. 2015.

trol compared with the thyristor converter, the commonly-adopted selective harmonics elimination (SHE) modulation scheme in high-power applications constrains such ancillary function of PWM current-source converter in high-power drives. On the one hand, since the modulation index of SHE scheme is fixed in a fundamental cycle, the proposed active damping techniques through regulating the modulation index of space-vector-modulation (SVM)-based PWM converters [21],[57],[79]-[87] cannot be applied as discussed in Section 1. 2. 4. On the other hand, the proposed methods with focus on the active compensation ability of SHE-modulated PWM converters [93],[115], can realize the steady-state compensation of the harmonics in the systems, but is unable to mitigate the interharmonics resulted from the harmonics interaction.

To realize the active attenuation of interharmonics caused by the harmonics interaction in high-power PWM current-source drives, in this chapter, an SHE phase jittering method is proposed to enable the interharmonic compensation capability of SHE-modulated PWM current-source converter, and on the basis of which, a dc-link virtual impedance based strategy is developed to attenuate the interharmonics through weakening the harmonics interaction in the drive system. To illustrate the design and demonstrate the effectiveness, an application example of the proposed strategy to actively attenuate the interharmonics related to the LC resonance occurrence in high-power PWM current-source drive with active front end (AFE) is presented, and simulation and experimental results are provided.

4.1 Active interharmonic compensation based on SHE phase jittering method

As discussed earlier, the proposed methods with focus on the active compensation ability of SHE-modulated PWM converters lack the capability of interharmonics compensation. In this section, an SHE phase jittering method is proposed to enable the active interharmonic compensation capability of PWM converters

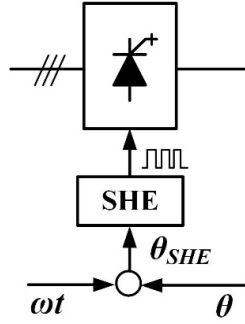


Fig. 4. 1. Diagram of SHE-modulated PWM current-source converter.

modulated by the SHE scheme. The proposed method is to actively generate the interharmonics in SHE PWM pattern, which are used for compensation, through introducing an alternating signal into SHE phase angle. The detailed theoretical derivation of the method is presented as follows.

According to Fig. 1. 6, the diagram of SHE scheme adopted to modulate the PWM current-source converter can be sketched as shown in Fig. 4. 1. Note that the modulation index of the SHE scheme is commonly not controlled but maintained at the maximum (around 1) in high-power PWM current-source drives as discussed in Section 1. 2. 2. In Fig. 4. 1, θ_{SHE} is named as SHE phase angle in the following analysis, and ω is the ac-side fundamental frequency, which is the line-side fundamental frequency for PWM current-source rectifier (CSR), and the motor-side fundamental frequency (motor operating frequency) for PWM current-source inverter (CSI). The phase angle ωt is provided from the phase-locked loop (PLL) for PWM CSR, and generated by the field-oriented control (FOC) scheme for PWM CSI. The phase angle θ is equal to the minus delay angle, $-\alpha$, for PWM CSR according to Fig. 1. 6, and is equal to the angle of the expected PWM current vector (\vec{I}_{wi}^*) in field-oriented synchronous reference frame for PWM CSI. At steady state of the drive system, the θ will be constant. Based on the previous analysis, the modulation function of SHE-modulated PWM converter can be represented as

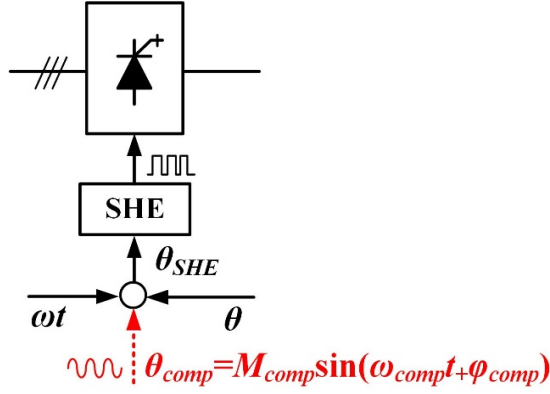


Fig. 4. 2. Diagram of SHE phase jittering method.

$$\begin{aligned}\bar{S}_w &= \sum_h -jM_{SHEh} e^{j(h\theta_{SHE} + \varphi_{SHEh})} \\ &= \sum_h -jM_{SHEh} e^{j(h(\omega t + \theta) + \varphi_{SHEh})} \quad (h = 1, -5, 7, -11, \dots),\end{aligned}\quad (4-1)$$

and at the steady state, the h th-order harmonic in the modulation function can be obtained as

$$\bar{S}_{wh} = -jM_{SHEh} e^{j(h\theta_{SHE} + \varphi_{SHEh})} = -jM_{SHEh} e^{j(h(\omega t + \theta) + \varphi_{SHEh})}, \quad (4-2)$$

where M_{SHEh} and φ_{SHEh} are the magnitude and phase of h th harmonics in SHE PWM pattern respectively. The positive h represents the positive sequence, and the negative h represents the negative sequence. When h is negative, $M_{SHEh} = -M_{SHE(-h)}$ and $\varphi_{SHEh} = -\varphi_{SHE(-h)}$.

Introducing an alternating signal θ_{comp} as

$$\theta_{comp} = M_{comp} \sin(\omega_{comp}t + \varphi_{comp}) \quad (4-3)$$

into the SHE phase angle θ_{SHE} as shown in Fig. 4. 2, the new SHE phase angle can be represented as

$$\theta'_{SHE} = \theta_{SHE} + \theta_{comp} = \omega t + \theta + M_{comp} \sin(\omega_{comp}t + \varphi_{comp}), \quad (4-4)$$

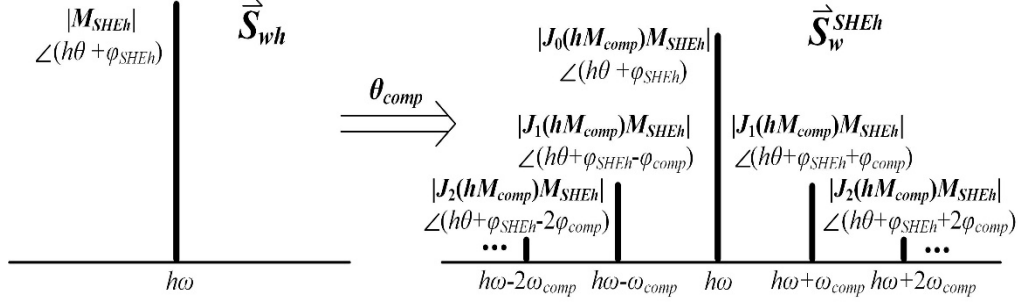


Fig. 4. 3. Diagram of \vec{S}_{wh} and \vec{S}_w^{SHEh} .

where M_{comp} , ω_{comp} , and φ_{comp} are the magnitude, frequency, and initial phase of θ_{comp} respectively. Then, the original h th harmonic as shown in (4-2) is rewritten as

$$\vec{S}_w^{SHEh} = -jM_{SHEh}e^{j(h\theta_{SHE} + \varphi_{SHEh})} = -jM_{SHEh}e^{j(h(\omega t + \theta + M_{comp} \sin(\omega_{comp}t + \theta_{comp})) + \varphi_{SHEh})}. \quad (4-5)$$

Taking Jacobi-Anger extension of (4-5) [116], we can obtain that

$$\begin{aligned} \vec{S}_w^{SHEh} &= -jJ_0(hM_{comp})M_{SHEh}e^{j(h(\omega t + \theta) + \varphi_{SHEh})} \\ &\quad - j \sum_{k=1}^{\infty} J_k(hM_{comp})M_{SHEh}e^{j((h\omega + k\omega_{comp})t + h\theta + \varphi_{SHEh} + k\varphi_{comp})}, \\ &\quad - j \sum_{k=1}^{\infty} (-1)^k J_k(hM_{comp})M_{SHEh}e^{j((h\omega - k\omega_{comp})t + h\theta + \varphi_{SHEh} - k\varphi_{comp})} \end{aligned}, \quad (4-6)$$

where $J_k(x)$ is the Bessel function. The frequency spectrum of h th harmonic before introducing θ_{comp} , \vec{S}_{wh} , and after introducing θ_{comp} , \vec{S}_w^{SHEh} , can be sketched as shown in Fig. 4. 3. It can be observed that, after introducing θ_{comp} , the sideband harmonics are produced at each ω_{comp} -frequency interval around the original h th harmonic in PWM pattern at steady state. For each sideband component, its magnitude ($|J_k(hM_{comp})M_{SHEh}|$), frequency ($|h\omega \pm k\omega_{comp}|$), and initial phase ($h\theta + \varphi_{SHEh} \pm k\varphi_{comp}$) are the independent function of the magnitude (M_{comp}), frequency (ω_{comp}), and initial phase (φ_{comp}) of θ_{comp} , respectively. It means that the sideband harmonics can be fully controlled by the introduced alternating signal θ_{comp} . In addition, since the frequency of θ_{comp} , ω_{comp} , can be either integer or non-integer multiples of the fundamental frequency ω , it provides a possibility to produce either the harmonics or

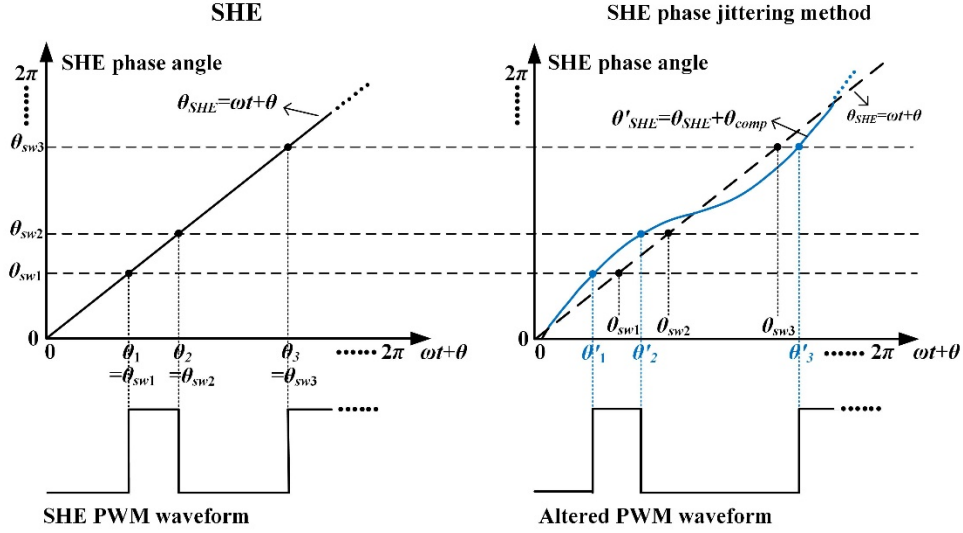


Fig. 4. 4. Illustration of the basic operating principle of the SHE phase jittering method.

the interharmonics as expected in PWM pattern based on the SHE scheme to realize the active harmonic or interharmonic compensation. The basic operating principle of the θ_{comp} to produce the expected harmonics or interharmonics in PWM pattern can be illustrated in Fig. 4. 4. In Fig. 4. 4, θ_{sw1} , θ_{sw2} , θ_{sw3} , ... , are the predesigned switching angles in SHE pattern, and by comparing the SHE phase angle θ_{SHE} with θ_{sw} , the SHE PWM pattern is generated in the left plot of Fig. 4. 4. After introducing the alternating signal θ_{comp} into the θ_{SHE} , the SHE phase angle will be jittered as the curve θ'_{SHE} shown in the right plot of Fig. 4. 4, and by comparing the jittering θ'_{SHE} with θ_{sw} , the SHE PWM pattern can be altered to produce the expected harmonics or interharmonics, which are used for compensation.

Since the magnitude of fundamental component \bar{S}_{w1} ($h=1$) in (4-1), M_{SHE1} (also known as modulation index), is much more significant than the magnitude of harmonic components M_{SHEh} ($h \neq 1$) in the modulation function, we can only consider the fundamental component in SHE modulation function during the design of the SHE-phase-jittering-based compensation method. Since the modulation index M_{SHE1} is fixed around 1 as discussed earlier and the fundamental phase angle φ_{SHE1}

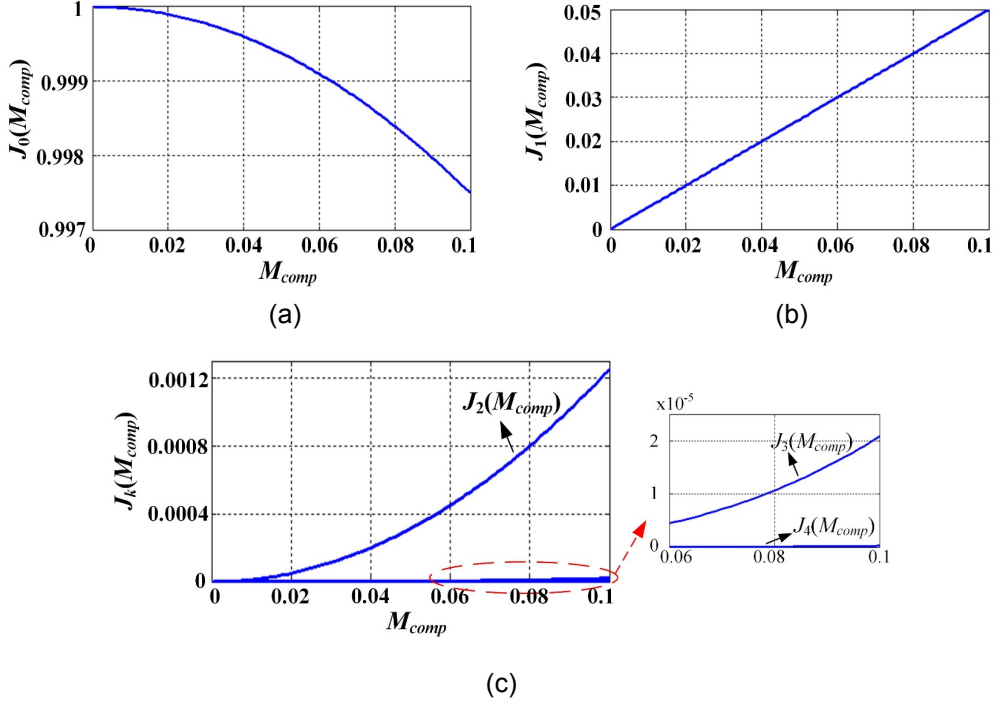


Fig. 4. 5. Properties of Bessel functions: (a) $J_0(M_{comp})$ vs. M_{comp} ; (b) $J_1(M_{comp})$ vs. M_{comp} ; (c) $J_k(M_{comp})$ vs. M_{comp} .

is designed to be 0 in SHE PWM pattern, the fundamental component \bar{S}_{w1} in (4-1) can be obtained as

$$\bar{S}_{w1} = -j e^{j(\omega t + \theta)}. \quad (4-7)$$

Based on (4-6), after introducing θ_{comp} , (4-7) can be rewritten as

$$\begin{aligned} \bar{S}_w^{SHE1} = & -j J_0(M_{comp}) e^{j(\omega t + \theta)} \\ & - \sum_{k=1}^{\infty} J_k(M_{comp}) e^{j((\omega + k\omega_{comp})t + \theta + k\varphi_{comp})} \\ & - \sum_{k=1}^{\infty} (-1)^k J_k(M_{comp}) e^{j((\omega - k\omega_{comp})t + \theta - k\varphi_{comp})} \end{aligned} \quad (4-8)$$

According to the properties of Bessel functions plotted in Fig. 4. 5, when M_{comp} is small, three approximations can be achieved as

$$\begin{cases} J_0(M_{comp}) \approx 1 \\ J_1(M_{comp}) \approx 0.5M_{comp} \\ J_k(M_{comp}) \approx 0 \quad (k \geq 2) \end{cases} \quad (4-9)$$

By utilizing the approximations in (4-9), (4-10) can be obtained from (4-8) as

$$\begin{aligned} \bar{S}_w^{SHE1} &\approx \bar{S}_{w1}^{SHE1} + \bar{S}_{w_Ls}^{SHE1} + \bar{S}_{w_Rs}^{SHE1} \\ \text{where } \begin{cases} \bar{S}_{w1}^{SHE1} \triangleq -je^{j(\omega t + \theta)} \\ \bar{S}_{w_Ls}^{SHE1} \triangleq j0.5M_{comp}e^{j((\omega - \omega_{comp})t + \theta - \varphi_{comp})} \\ \bar{S}_{w_Rs}^{SHE1} \triangleq -j0.5M_{comp}e^{j((\omega + \omega_{comp})t + \theta + \varphi_{comp})} \end{cases} \end{aligned} \quad (4-10)$$

According to (4-10), the two sideband components, $\bar{S}_{w_Ls}^{SHE1}$ and $\bar{S}_{w_Rs}^{SHE1}$, are produced around the fundamental component \bar{S}_{w1}^{SHE1} after introducing the θ_{comp} , which can be used for active compensation. Besides, three following features are offered:

- Easy design of real-time compensation:

With respect to the two sideband components, their magnitude ($0.5M_{comp}$), frequency ($\omega \pm \omega_{comp}$) and phase angle ($\theta \pm \varphi_{comp}$) have simple algebraic correspondence to the magnitude (M_{comp}), frequency (ω_{comp}) and phase angle (φ_{comp}) of the θ_{comp} according to (4-10), which greatly benefits the design of SHE-phase-jittering-based strategy and can also realize the real-time active compensation.

- No influence on the fundamental control of PWM converter:

Comparing the new fundamental component in (4-10) with the original fundamental component as shown in (4-7), we can obtain that $\bar{S}_{w1} = \bar{S}_{w1}^{SHE1}$. It means that the modulation index and the fundamental phase angle of the modulation scheme are not changed by the θ_{comp} , so that the fundamental control of PWM converter will not be affected.

- No increase on the pulse numbers of PWM pattern (switching frequency):

It can be proven that, if the magnitude of θ_{comp} , M_{comp} , is selected to satisfy $M_{comp} < \omega / \omega_{comp}$, the increasing function of the SHE phase angle θ_{SHE} will not be affected in θ'_{SHE} . As a result, there will be no increase on the pulse numbers of SHE PWM pattern (also the switching frequency).

4.2 DC-link virtual impedance based active attenuation of harmonics interaction

In previous section, the active interharmonic compensation capability of SHE-modulated PWM converter is enabled by the proposed SHE phase jittering method. In this section, based on a dc-link virtual impedance concept, the SHE phase jittering method is utilized to actively attenuate the interharmonics caused by the harmonics interaction in high-power PWM current-source drives.

According to the analysis in Chapter 2 and Chapter 3, the root cause of harmonics interaction in high-power PWM current-source drive systems is the weak attenuation effect of the small dc choke on current harmonics (especially low-frequency harmonics). Therefore, if the dc-link impedance could be increased, the harmonics produced by the rectifier and by the inverter will be decoupled so that the harmonics interaction can be attenuated. Furthermore, if the increase of dc-link impedance could be virtually realized through the feedback of dc-link current as illustrated in Fig. 4. 6, the additional costs/losses and the aggravation of size/weight involved with the physical increase of impedance can be avoided. In Fig. 4. 6, v_{dcr} , v_{dci} , i_{dc} , and Z_{dc} are the rectifier-side dc-link voltage, inverter-side dc-link voltage, dc-link current and real dc-link impedance (L_{dc} and R_{dc} are the inductance and resistance respectively) as defined above.

To realize the dc-link virtual impedance concept, the previously-proposed SHE phase jittering method can be adopted at either the PWM CSR (for high-power PWM current-source drives with AFE) or the PWM CSI. In the following analysis, the realization of dc-link virtual impedance is illustrated by the SHE phase jittering method used in the PWM CSR.

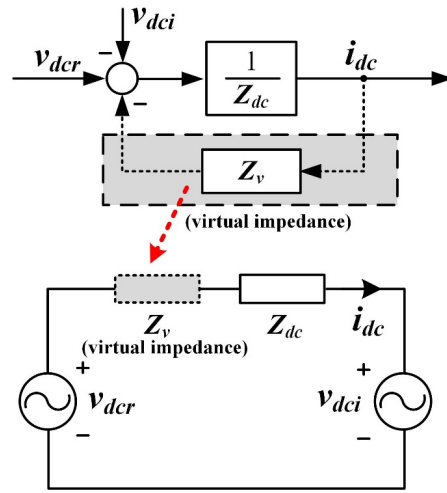


Fig. 4. 6. Concept of dc-link virtual impedance.

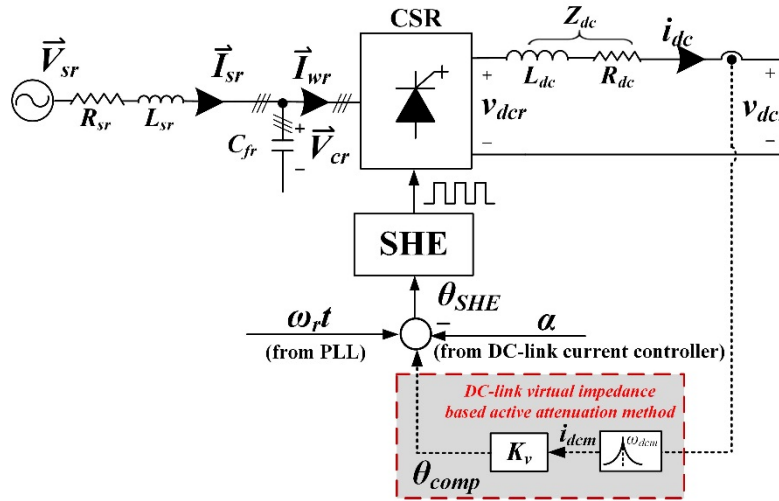


Fig. 4. 7. DC-link virtual impedance realized by the SHE phase jittering method adopted at PWM CSR.

Fig. 4. 7 shows the dc-link virtual impedance realized by the SHE phase jittering method adopted at PWM CSR. To facilitate the analysis, a certain dc-link current harmonic, defined as $i_{dcm} = I_{dcm} \sin(\omega_{dcm} t + \phi_{dcm})$ (I_{dcm} , ω_{dcm} , and ϕ_{dcm} are the magnitude, frequency, and initial phase, respectively), is extracted from i_{dc} . Such ω_{dcm} -frequency harmonic is multiplied by a coefficient K_v and then fed back into the CSR's SHE phase angle θ_{SHE} . According to the analysis in Section 4. 1, the introduced alternating signal θ_{comp} can be represented as

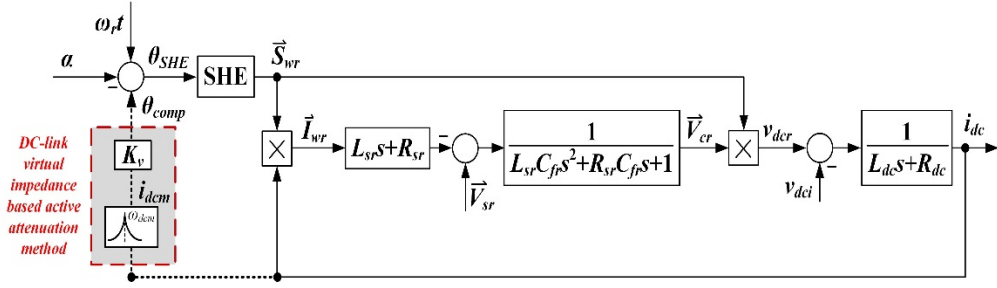


Fig. 4. 8. Transfer function model of Fig. 4. 7.

$$\theta_{comp} = K_v I_{dcm} \sin(\omega_{dcm} t + \varphi_{dcm}). \quad (4-11)$$

In Fig. 4. 7, \vec{V}_{sr} is the grid voltage; \vec{I}_{sr} is the line current; \vec{I}_{wr} is the line-side PWM current; \vec{V}_{cr} is the line-side capacitor voltage; ω_r is the line-side fundamental frequency; α is the delay angle of PWM CSR; R_{sr} , L_{sr} , and C_{fr} are the line resistance, line inductance, and capacitor voltage, respectively.

Based on the relationship between the line-side components and the dc-link components discussed in Chapter 2 as

$$\vec{I}_{wr} = i_{dc} \vec{S}_{wr}, \quad (4-12)$$

$$v_{dcr} = \vec{V}_{cr} \cdot \vec{S}_{wr}, \quad (4-13)$$

the transfer function model of Fig. 4. 7 can be described as Fig. 4. 8.

By taking (4-11) into (4-10), we can obtain that the two sideband components in CSR PWM pattern produced by the SHE phase jittering method at steady state are ($\theta=\alpha$ and $\omega=\omega_r$ for PWM CSR)

$$\begin{cases} \vec{S}_{wr_Ls}^{SHE1} = j0.5K_v I_{dcm} e^{-j((\omega_{dcm} - \omega_r)t + \alpha + \varphi_{dcm})} \\ \vec{S}_{wr_Rs}^{SHE1} = -j0.5K_v I_{dcm} e^{j((\omega_{dcm} + \omega_r)t - \alpha + \varphi_{dcm})} \end{cases}, \quad (4-14)$$

and Fig. 4. 8 can be simplified to Fig. 4. 9.

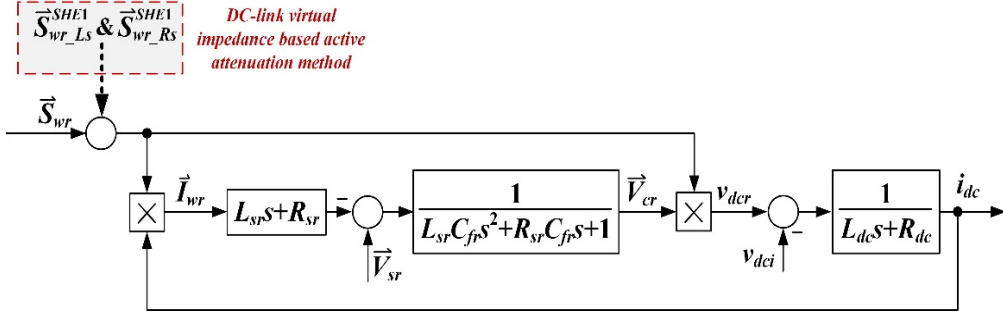


Fig. 4. 9. Simplified transfer function model of Fig. 4. 8.

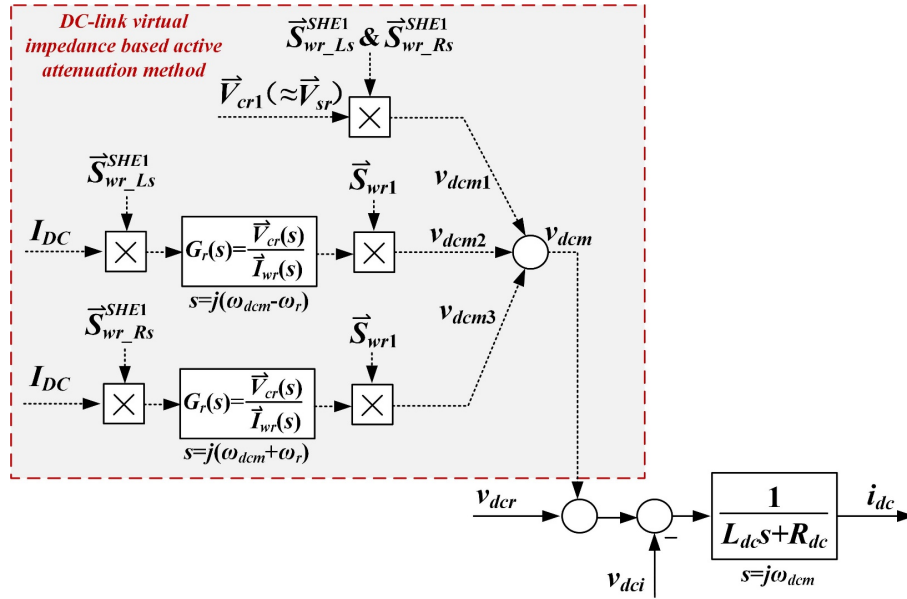


Fig. 4. 10. Simplified diagram of dc link at ω_{dcm} frequency.

Based on (4-12)-(4-14), it can be obtained that the $\vec{S}_{wr_Ls}^{SHE1}$ and $\vec{S}_{wr_Rs}^{SHE1}$ will produce the rectifier-side dc-link voltage harmonic at ω_{dcm} frequency (defined as v_{dcm}) mainly through three ways (defined as v_{dcm1} , v_{dcm2} , and v_{dcm3} , respectively), and Fig. 4. 9 can be further simplified to Fig. 4. 10 at ω_{dcm} frequency. With respect to v_{dcm1} , it is generated by the fundamental component in capacitor voltage, defined as \vec{V}_{cr1} , and the two sideband harmonics $\vec{S}_{wr_Ls}^{SHE1}$ and $\vec{S}_{wr_Rs}^{SHE1}$ as shown in Fig. 4. 10. Assuming that the grid voltage is harmonicless and neglecting the small voltage drop on the line impedance in high-power drive systems, we can obtain that

$$\vec{V}_{cr1} \approx \vec{V}_{sr} \triangleq -jV_{sr}e^{j\omega_r t}, \quad (4-15)$$

where V_{sr} is the magnitude of grid voltage. Then, based on (4-13) and (4-14), it can be obtained that

$$v_{dcm1} = \vec{V}_{cr1} \cdot \vec{S}_{wr_Ls}^{SHE1} + \vec{V}_{cr1} \cdot \vec{S}_{wr_Rs}^{SHE1} \approx (-1.5K_v V_{sr} \sin \alpha) I_{dcm} \sin(\omega_{dcm} t + \varphi_{dcm}). \quad (4-16)$$

With respect to the generation of v_{dcm2} and v_{dcm3} , according to (4-12), the dc component in dc-link current, defined as I_{DC} , will produce two interharmonics in PWM current (\vec{I}_{wr}) with $(\omega_{dcm} \pm \omega_r)$ frequencies through $\vec{S}_{wr_Ls}^{SHE1}$ and $\vec{S}_{wr_Rs}^{SHE1}$ respectively, at first. Then, through the line-side circuit, the two interharmonics with $(\omega_{dcm} \pm \omega_r)$ frequencies will be produced in the capacitor voltage (\vec{V}_{cr}) correspondingly. The introduced two interharmonic components in capacitor voltage generate v_{dcm2} and v_{dcm3} at dc link through the fundamental component in CSR PWM pattern (\vec{S}_{wr1}). The line-side circuit can be represented by the transfer function as

$$G_r(s) = \frac{\vec{V}_{cr}(s)}{\vec{I}_{wr}(s)} = \frac{L_{sr}s + R_{sr}}{L_{sr}C_{fr}s^2 + R_{sr}C_{fr}s + 1} \quad (s \neq j\omega_r) \quad (4-17)$$

according to Fig. 4. 9 as shown in Fig. 4. 10. Based on (4-12)-(4-14), v_{dcm2} and v_{dcm3} can be obtained as (4-18) and (4-19), respectively.

$$v_{dcm2} = (I_{DC} \vec{S}_{wr_Ls}^{SHE1} G_r^-) \cdot \vec{S}_{wr1} \approx (0.75K_v I_{DC} |G_r^-|) I_{dcm} \cos(\omega_{dcm} t + \varphi_{dcm} + \angle G_r^-) \quad (4-18)$$

$$G_r^- \triangleq G_r(s) \Big|_{s=j(\omega_{dcm}-\omega_r)}$$

$$v_{dcm3} = (I_{DC} \vec{S}_{wr_Rs}^{SHE1} G_r^+) \cdot \vec{S}_{wr1} \approx (-0.75K_v I_{DC} |G_r^+|) I_{dcm} \cos(\omega_{dcm} t + \varphi_{dcm} + \angle G_r^+) \quad (4-19)$$

$$G_r^+ \triangleq G_r(s) \Big|_{s=j(\omega_{dcm}+\omega_r)}$$

The division of v_{dcm} by the previously-defined i_{dcm} ($i_{dcm} = I_{dcm} \sin(\omega_{dcm} t + \varphi_{dcm})$) can be considered as a virtual impedance Z_v introduced at dc link by the SHE phase jittering method as illustrated in Fig. 4. 11. Based on (4-16), (4-18), and (4-19), Z_v can be obtained as (4-20). It can be observed from (4-20) that the tunable coefficient K_v in the feedback of dc-link current as shown in Fig. 4. 7 greatly affects the introduced dc-link virtual impedance Z_v . The proper selection of K_v can enhance the

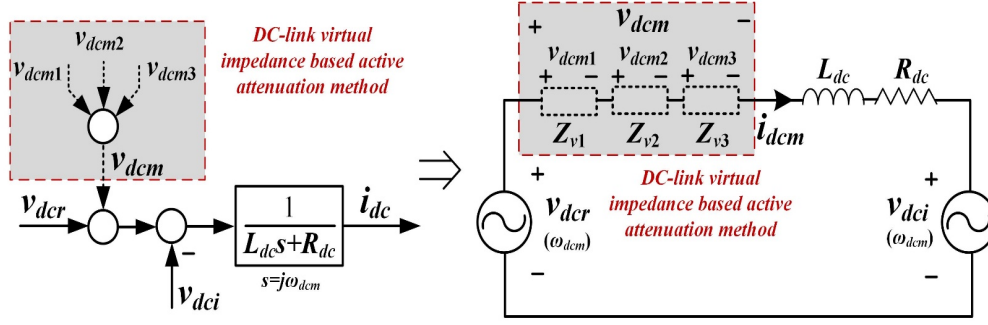


Fig. 4. 11. Illustration of dc-link virtual impedance introduced by the active attenuation method.

attenuation effect of dc link on current harmonics through the virtually-introduced Z_v . As K_v can be designed as a complex number (magnitude amplification and phase shift of i_{dcm}), not only can the magnitude of Z_v be controlled by K_v , but also K_v may alter the physical property of Z_v (resistive, or inductive, or capacitive). In next section, with respect to an application example: suppression of LC resonance in high-power PWM current-source drives with AFE, the design of K_v in the proposed dc-link virtual impedance based active attenuation method is discussed in details.

$$\begin{cases} Z_{v1} = \frac{v_{dcm1}}{i_{dcm}} = -1.5K_v V_{sr} \sin \alpha \\ Z_{v2} = \frac{v_{dcm2}}{i_{dcm}} = 0.75K_v I_{DC} |G_r^-| \left(\cos(\angle G_r^-) \cot(\omega_{dcm} t + \varphi_{dcm}) - \sin(\angle G_r^-) \right) \\ Z_{v3} = \frac{v_{dcm3}}{i_{dcm}} = -0.75K_v I_{DC} |G_r^+| \left(\cos(\angle G_r^+) \cot(\omega_{dcm} t + \varphi_{dcm}) - \sin(\angle G_r^+) \right) \end{cases} \quad (4-20)$$

4.3 Detailed analysis on the design of dc-link virtual impedance

As analyzed in Chapter 3, the interharmonics caused by the harmonics interaction phenomenon may give rise to the LC resonance at the line side and/or the motor side in high-power PWM current-source drives with AFE. To avoid the significant impact on the drive system due to the occurrence of LC resonance, the proposed

dc-link virtual impedance based active attenuation of harmonics interaction could be adopted without additional costs and losses involved. In this section, with respect to such application example, the design of the coefficient K_v in the proposed method is discussed in details. Since the LC resonance could occur at either the line side or the motor side, the different resonance conditions will affect the relationship between the K_v and Z_v , and therefore, the relationship between K_v and Z_v under different resonance conditions is analyzed at first. Then, the important factors required to be considered during the selection of K_v will be discussed. For the convenience of analysis, the active attenuation is still realized through the control of PWM CSR as discussed above.

4.3.1 Relationship between K_v and Z_v under different resonance conditions

In Chapter 3, the estimation of LC resonance conditions in high-power PWM current-source drives with AFE is carried out. It can accurately predict the motor operating frequencies at which the LC resonance will be excited by the interharmonics caused by the harmonics interaction. Also, the frequencies of the significant dc-link current harmonics can be predetermined based on the estimation. By feeding back such dc-link current harmonics through the proposed dc-link virtual impedance method, they can be greatly attenuated due to the virtually-increased dc-link impedance at the corresponding frequencies. As a result, due to the enhanced decoupling of rectifier-side harmonics and inverter-side harmonics by the dc-link, the significant ac-side interharmonics would also be reduced, so that the LC resonance can be suppressed.

According to Figs. 3. 11 and 3. 16, the estimation of LC resonance conditions can be briefly illustrated by Fig. 4. 12. In Fig. 4. 12, the horizontal axis represents the motor operating frequency (ω_i), and the vertical axis is the frequency of dc-link harmonics. As discussed in Chapter 3, the frequencies of the dc-link current harmonics introduced by the harmonics interaction are only related to the PWM pattern of two converters and the motor operating frequencies. Since the SHE PWM pattern

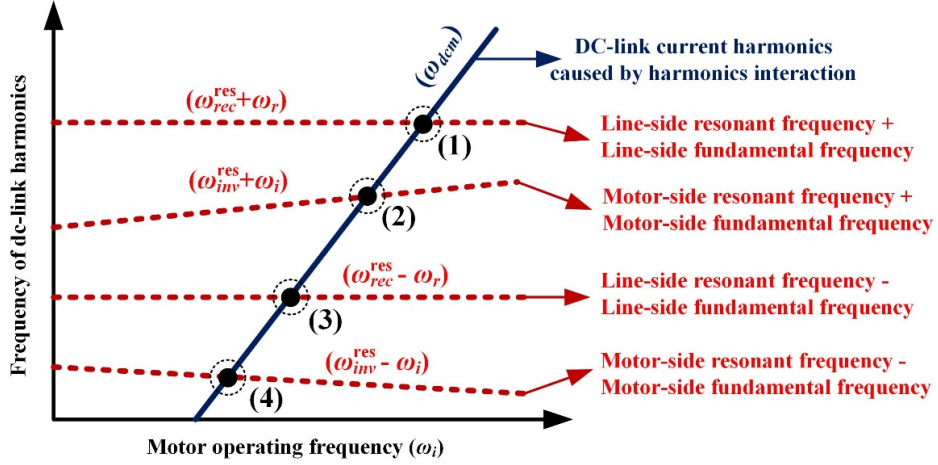


Fig. 4. 12. Illustration of *LC* resonance conditions' estimation.

is off-line designed and fixed during online implementation, the frequencies of the dc-link current harmonics (ω_{dcm}) are known under different motor operating frequencies. The ω_{dcm} can be represented by the solid lines, and for the convenience of explanation, only one of the lines is drawn in Fig. 4. 12 which represents one of the dc-link current harmonics. The four dash lines in Fig. 4. 12 represent the line-side *LC* resonant frequency (ω_{rec}^{res}) plus/minus the line-side fundamental frequency (ω_r), and the motor-side *LC* resonant frequency (ω_{inv}^{res}) plus/minus the motor-side fundamental frequency (ω_i). They can be considered as the reflection of ac-side resonant frequency to dc link through PWM process, and their overlap can be guaranteed not to occur with the selected ac-side filter parameters. The *LC* resonance will be excited when the solid line intersects with the dash line as the four intersection points shown in Fig. 4. 12, and the corresponding ω_i and ω_{dcm} can be known according to Fig. 4. 12. To suppress the resonance, the proposed method can be enabled when the motor operates at the frequency (ω_i) around each intersection point, by feeding back the significant ω_{dcm} -frequency dc-link current harmonics during the online implementation. If considering the variation and inaccuracy of system parameters, the ac-side resonant frequency (ω_{rec}^{res} and ω_{inv}^{res}) may change so that causes the shift of the dash lines in Fig. 4. 12. Note that the solid line has no relationship with the system parameters so that it will not be affected. As a result, the intersection points will shift along the solid line. To avoid being affected by this

issue, the proposed method can stay active at any motor operating frequency (ω_i). With respect to the LC resonance conditions shown in Fig. 4. 12, since $\omega_{dcm} = \omega_{rec}^{res} + \omega_r$ at Point (1), it means that the LC resonance is excited by the $(\omega_{dcm} - \omega_r)$ -frequency interharmonic at line side. Similarly, the Point (2), Point (3) and Point (4) represents the LC resonance is resulted from the $(\omega_{dcm} - \omega_i)$ -frequency interharmonic at motor side, $(\omega_{dcm} + \omega_r)$ -frequency interharmonic at line side, and $(\omega_{dcm} + \omega_i)$ -frequency interharmonic at motor side respectively. At each intersection point, the relationship between Z_v and K_v as shown in (4-20) can be further simplified as follows.

1) Resonance occurs at motor side (Point (2) and Point (4)):

Since the overlap of dash lines will not occur as mentioned above, the resonance will not be excited at the line side and the motor side simultaneously. Therefore, if the LC resonance occurs at motor side, the two frequencies of the line-side interharmonics, $(\omega_{dcm} - \omega_r)$ and $(\omega_{dcm} + \omega_r)$, will be far from the line-side resonant frequency. As a result, the $|G_r^-|$ and $|G_r^+|$ in (4-20) will be small, and the virtual impedance Z_v will be dominated by Z_{v1} as shown in (4-21).

$$Z_v \approx Z_{v1} = -1.5K_v V_{sr} \sin \alpha \quad (4-21)$$

2) Resonance excited by line-side $(\omega_{dcm} - \omega_r)$ -frequency interharmonic (Point (1)):

If the resonance occurs at line side by the $(\omega_{dcm} - \omega_r)$ -frequency interharmonic, due to the significant amplification effect of the line-side LC resonance, Z_{v2} will be dominant. Moreover, according to [114], the dc choke in PWM current-source system will result in a certain shift up of ac-side resonant frequency so that the phase shift of the ac-side interharmonics at resonant frequency will approach positive 90 degree. The $\angle G_r^-$ in (4-20) can be approximately considered as 90 degree, and we can obtain (4-22) as

$$Z_v \approx Z_{v2} = -0.75K_v I_{DC} |G_r^-|. \quad (4-22)$$

3) Resonance excited by line-side $(\omega_{dcm} + \omega_r)$ -frequency interharmonic (Point (3)):

Similarly, if the resonance occurs at line side by the $(\omega_{dcm}+\omega_r)$ -frequency inter-harmonic, we can obtain that

$$Z_v \approx Z_{v3} = +0.75K_v I_{DC} |G_r^+|. \quad (4-23)$$

4.3.2 Selection of K_v to enable Z_v 's attenuation effect

As mentioned above, K_v can be designed as a complex number. Since the phase shift of an ac signal is usually realized in time domain through signal delay or differential which may affect the system stability, K_v is recommended as a real coefficient in this work. It can be observed that, after choosing K_v as a negative real number in (4-21) and (4-22) and a positive real number in (4-23), Z_v becomes a virtually introduced resistance that can enhance the attenuation effect of dc link on current harmonics, so that realizes the active suppression of the LC resonance caused by the harmonics interaction.

With respect to the magnitude of K_v , it is obvious that the larger the $|K_v|$ is, the stronger resonance suppression the Z_v will perform. However, according to (4-11), the magnitude of the compensation signal θ_{comp} equals to $|K_v I_{dcm}|$ ($M_{comp} = |K_v I_{dcm}|$). The large $|K_v|$ will increase M_{comp} so that the approximations based on the Bessel function's properties in Section 4. 1 may be invalid, which may result in some negative impacts as follows:

1) Degrade the performance of attenuation:

According to the analysis above, the virtual impedance Z_v shown in (4-20)-(4-23) is derived based on the approximation of $J_1(M_{comp}) \approx 0.5M_{comp}$ in Section 4. 1. Taking Z_{v1} in (4-21) as an example, without this assumption, Z_{v1} will be as

$$Z_v \approx Z_{v1} = -3J_1(K_v I_{dcm}) V_{sr} \sin \alpha / I_{dcm}. \quad (4-24)$$

Note that polarity of K_v is selected to be negative in this case as mentioned above. When $|K_v|$ increases, according to the property of $J_1(x)$, the linear approximation will lose effectiveness gradually; and when it is further increased, the monotonicity

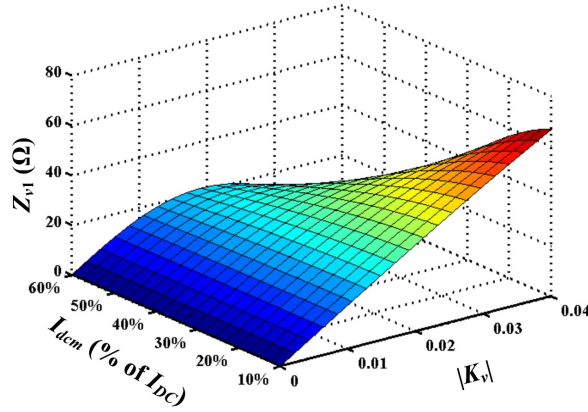


Fig. 4. 13. Illustration of $|K_v|$'s influence on the virtual impedance.

of $J_1(x)$ will be lost and the polarity may even be changed. If so, the attenuation performance of Z_v will be degraded, and Z_v may even result in detrimental effect with the selected polarity of K_v . Take the real high-power PWM current-source drive application simulated in Section 3. 3. 1 for example, the parameters of which are listed in TABLE 3. 1. Fig. 4. 13 shows the influence of $|K_v|$ and I_{dcm} on Z_{v1} under the rated condition. It can be observed that, when $|K_v|$ is large, the linear relationship between Z_{v1} and $|K_v|$ as shown in (4-21) will lose effectiveness and Z_{v1} even drops as $|K_v|$ increases. Such problem will be aggravated when I_{dcm} is larger and $|K_v|$ is further increased.

2) Affect the control of drive system:

The conclusion that θ_{comp} will not affect the modulation index of PWM converter is obtained by comparing \bar{S}_{w1}^{SHE1} in (4-10) with \bar{S}_{w1} in (4-7). Such conclusion is based on the approximation of $J_0(M_{comp}) \approx 1$. However, when $|K_v|$ increases, such approximation will become invalid and the $J_0(x)$ will be far less than 1 with a large $|K_v|$. As a result, the modulation index will be significantly altered by θ_{comp} , which will affect the control of drive system. Considering the previously-mentioned drive application as an example again, the influence of $|K_v|$ and I_{dcm} on CSR's modulation index (M_{sr1}) under rated condition is shown in Fig. 4. 14. We can observe that the large $|K_v|$ will significantly deviate the modulation index from 1 (the modulation index of the SHE scheme is fixed at 1 as mentioned above). If neglecting the system

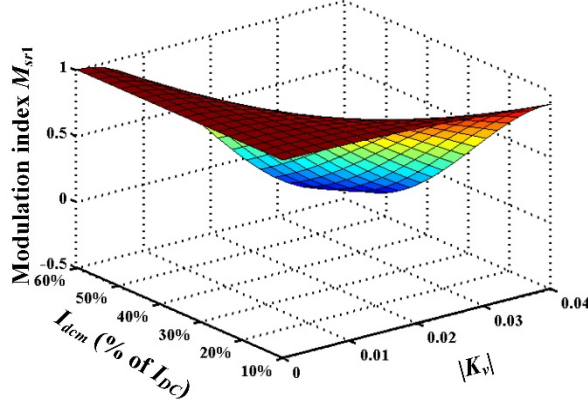


Fig. 4. 14. Illustration of $|K_v|$'s influence on the modulation index.

power loss, the voltage drop on line impedance and the system harmonics, (4-25) can be obtained at steady state based on the system active power balance as

$$\cos \alpha = \frac{P_{motor}}{1.5V_{sr} I_{DC} M_{sr1}}, \quad (4-25)$$

where P_{motor} is the active power consumption of the motor. Since the dc component of dc-link current (I_{DC}) is controlled to track the reference I_{dc_ref} , which is generated by the motor drive FOC scheme as shown in Fig. 1. 6, it has no relationship with the CSR's modulation index (M_{sr1}). As a result, according to (4-25), the significant deviation of M_{sr1} will greatly change the delay angle α , which will affect the dc-link current control. Furthermore, the decrease of M_{sr1} will increase the $\cos \alpha$ at the left-hand side of (4-25). Since the value of $\cos \alpha$ has an upper limit of 1, the significant deviation of M_{sr1} may even break the system active power balance as shown in (4-25). Therefore, the large $|K_v|$ may even result in the instability of the drive system control after adopting the proposed active attenuation method.

3) Introduce unexpected interharmonics in the system:

During the analysis of SHE-modulated converters' interharmonics compensation capability enabled by the θ_{comp} , we only considered the two nearest sideband harmonics produced by the fundamental component in SHE PWM pattern and the θ_{comp} , $\bar{S}_{wr_Ls}^{SHE1}$ and $\bar{S}_{wr_Rs}^{SHE1}$, and neglected other sideband harmonics in far region.

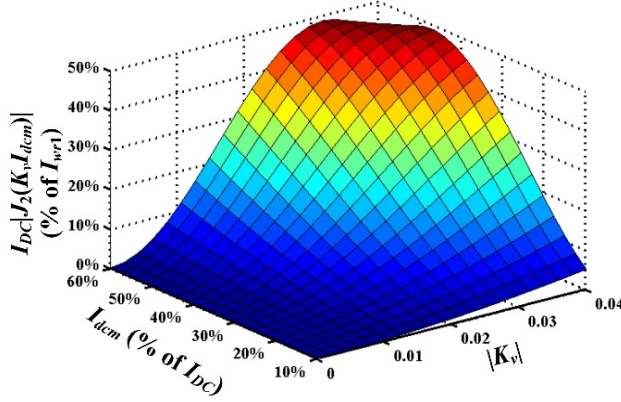


Fig. 4. 15. Illustration of $|K_v|$'s influence on the interharmonics in line-side PWM current.

This is based on the approximation of $J_k(M_{comp}) \approx 0$ ($k \geq 2$). However, such approximation will also be invalid when $|K_v|$ increases, especially for the second nearest sideband harmonics. According to (4-8) and (4-11), the second nearest sideband harmonics will have the magnitude of $|J_2(K_v I_{dcm})|$ and the frequencies of $(\omega_r \pm 2\omega_{dcm})$ with respect to the dc-link virtual impedance based strategy. When $|K_v|$ is large, their magnitude cannot be ignored. Reacting with the dc-link current, it may introduce significant $(\omega_r \pm 2\omega_{dcm})$ -frequency interharmonics with the magnitude of $I_{DC}|J_2(K_v I_{dcm})|$ in line-side PWM current \bar{I}_{wr} . For the drive application mentioned above, Fig. 4. 15 shows the influence of $|K_v|$ and I_{dcm} on the magnitude of such interharmonics (I_{wr1} in Fig. 4. 15 is the magnitude of fundamental line-side PWM current). It can be observed that the large $|K_v|$ will result in the significant $(\omega_r \pm 2\omega_{dcm})$ -frequency interharmonics in line-side PWM current. Since $\omega_r \pm 2\omega_{dcm}$ are comparatively low frequencies as can be observed in next section, the line-side LC circuit cannot effectively attenuate such interharmonics, so that the interharmonics with the same frequencies will be introduced into the line current which will affect the grid power quality. Besides their influence on the line side, such second nearest sideband harmonics will also react with the line-side capacitor voltage to produce interharmonics in dc link and may further introduce interharmonics in motor side through PWM CSI.

Moreover, other sideband harmonics in PWM pattern produced by the harmonic components in SHE PWM pattern and the θ_{comp} may also result in unexpected inter-harmonics in the system with a large $|K_v|$. With respect to the drive application, their situations are similar to Fig. 4. 15.

As a result, the magnitude of K_v has to be selected with the consideration of the above tradeoff.

4.4 Verification results

To demonstrate the effectiveness of the proposed dc-link virtual impedance based active attenuation method, simulations and experiments are respectively conducted on the same simulation system and experimental system in Chapter 3. Also, to verify the design of the coefficient K_v discussed in previous section, the performance of the proposed method to suppress the LC resonance caused by the harmonics interaction in the simulation and experimental system is presented in this section. Moreover, the same 9-pulse SHE scheme used in Chapter 3 as shown in Fig. 3. 10 is adopted at both the PWM CSR and the PWM CSI.

4.4.1 Simulation results

The parameters of the simulation system can refer to TABLE 3. 1. According to the estimation of LC resonance conditions in the simulation system shown in Fig. 3. 11 and the discussion of K_v 's design in previous section, K_v is selected to be a negative number when the solid lines intersect with the first (uppermost), second and fourth (lowermost) dash line in Fig. 3. 11; K_v is selected to be a positive number when the solid lines intersect with the third dash line in Fig. 3. 11. With respect to the selection of K_v 's magnitude ($|K_v|$), the three aspects discussed in Section 4. 3 need to be considered. According to the discussion based on the simulation system as the example (see Figs. 4. 13-4. 15), $|K_v|$ is selected to be 0.008 here. Note that the selection of $|K_v|$ is analyzed at the rated condition of the drive system in aforementioned discussions. The appropriate range of $|K_v|$ can be extended according to the normal operation conditions.

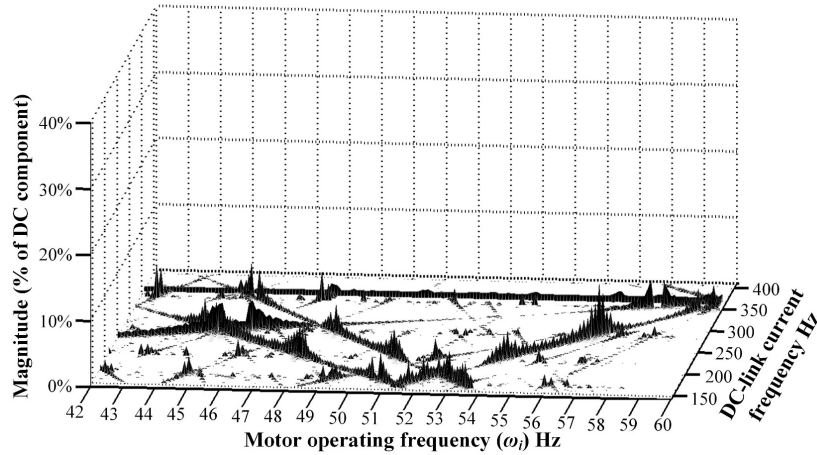


Fig. 4. 16. Steady-state dc-link current harmonics versus motor operating frequency (ω_i) after using the proposed method.

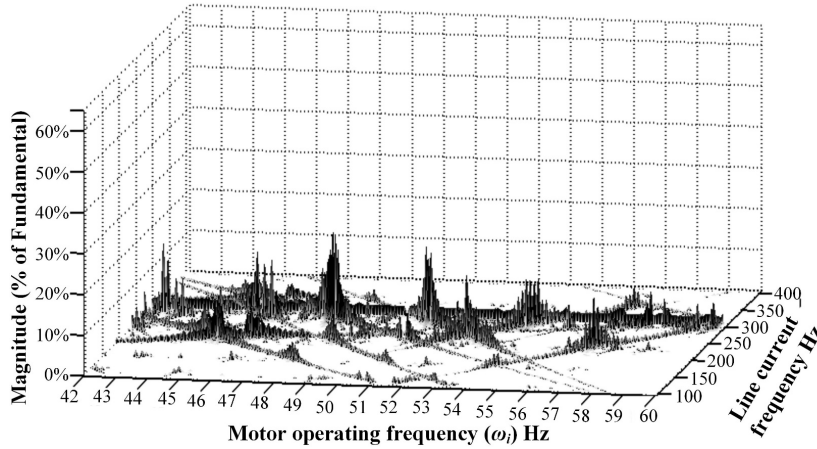


Fig. 4. 17. Line current harmonics vs. motor operating frequency (ω_i) after using the proposed method.

Figs. 4. 16-4. 18 show the simulation results of steady-state dc-link current harmonics, line current harmonics and motor-side stator current harmonics under different motor operating frequencies after using the proposed attenuation method. Comparing with the Figs. 3. 12-3. 14 (without using the attenuation method), we can observe that the dc-link virtual impedance concept is effectively realized by the proposed active attenuation method at all resonance conditions, as the high peaks in Figs. 3. 12-3. 14 are greatly attenuated in Fig. 4. 16-4. 18. It verifies the analysis in this chapter.

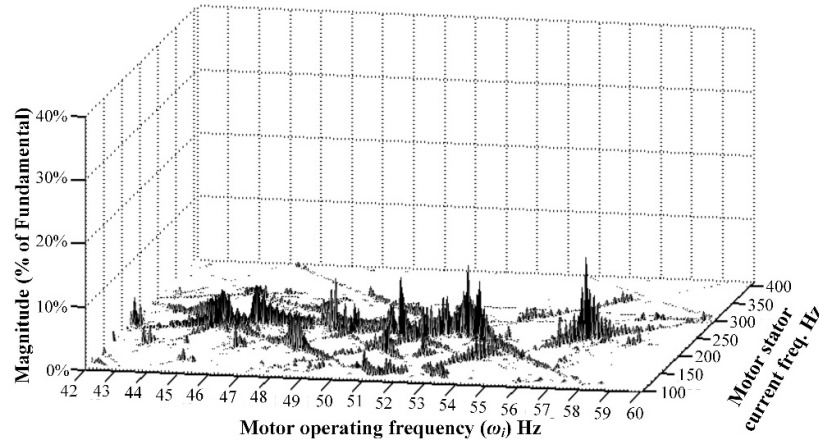


Fig. 4. 18. Motor stator current harmonics vs. motor operating frequency (ω_i) after using the proposed method.

4.4.2 Experimental results

To further verify the validity of the analysis, plenty of real-time experiments have been carried out on the experimental system with parameters shown in TABLE 3. 2. To demonstrate the effectiveness of the proposed attenuation method, two examples at 42Hz and 53Hz motor operating frequency as the same as in Chapter 3 are provided respectively. According to the estimation of LC resonance conditions in Fig. 3. 16 and following the same procedure of K_v 's selection for the simulation system, K_v is selected to be -0.1 for 252Hz and 324Hz dc-link current harmonics at 42Hz motor operating frequency to virtually increase the dc-link impedance. Similarly, K_v is selected to be +0.1 for 192Hz and -0.1 for 318Hz dc-link current harmonics at 53Hz motor operating frequency.

Figs. 4. 19 and 4. 20 show the waveforms and FFT analysis of the steady-state line current, dc-link current and motor-stator current at 42Hz motor operating frequency, Figs. 4. 21 and 4. 22 show the results at 53Hz motor operating frequency. According to Figs. 3. 17-3. 20 (without using the attenuation method) and Figs. 4. 19-4. 22 (after using the attenuation method), the magnitude of those harmonics before and after using the attenuation method is summarized in TABLE 4. 1. We

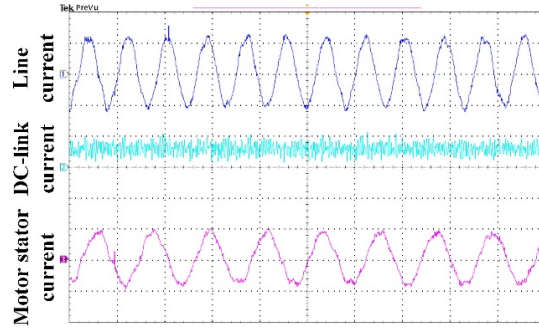
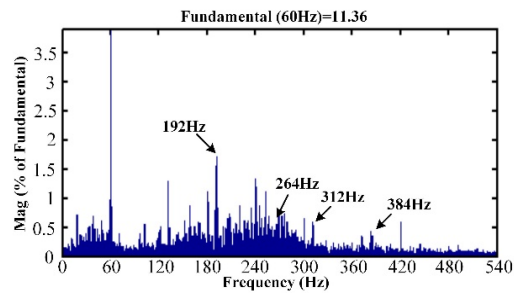
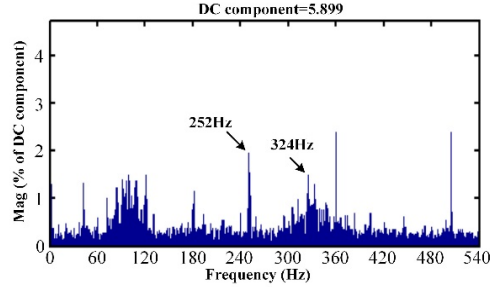


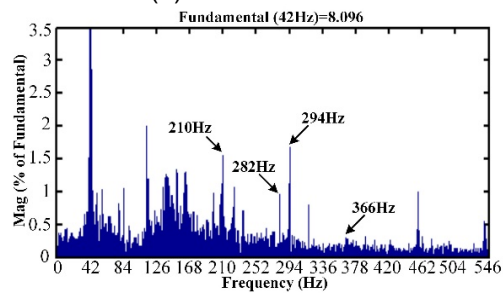
Fig. 4. 19. Waveforms of line current, dc-link current, and motor stator current at $\omega_i=42\text{Hz}$ after using the proposed method (10A/div., 20ms/div.).



(a) Line current



(b) DC-link current



(c) Motor stator current

Fig. 4. 20. FFT analysis of Fig. 4. 19.

can observe that the proposed method significantly reduces the dc-link current harmonics so that attenuates the harmonics interaction phenomenon in PWM current-

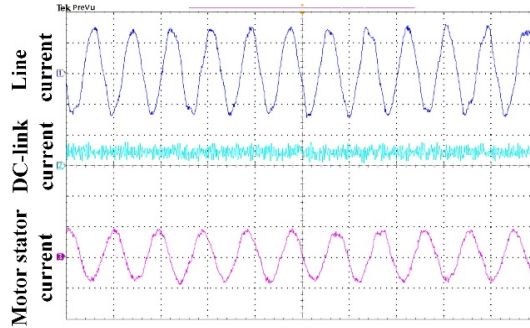
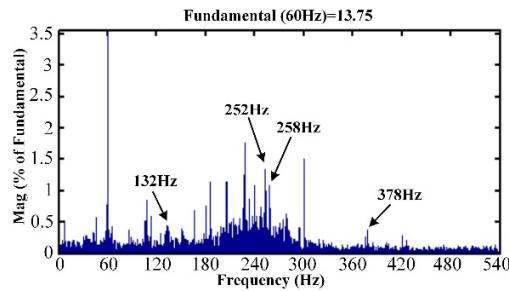
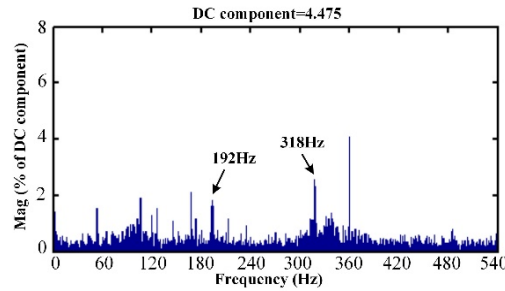


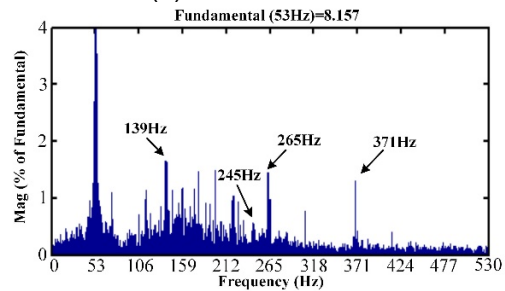
Fig. 4. 21. Waveforms of line current, dc-link current, and motor stator current at $\omega_i=53\text{Hz}$ after using the proposed method (10A/div., 20ms/div.).



(a) Line current



(b) DC-link current



(c) Motor stator current

Fig. 4. 22. FFT analysis of Fig. 4. 21.

source drive system, which can be observed from the greatly-attenuated interharmonics at both the line side and the motor side.

TABLE. 4. 1. MAGNITUDE OF HARMONICS BEFORE AND AFTER ATTENUATION

42Hz motor operating frequency ($\omega_r=42\text{Hz}$)				
	Before Attenuation		After Attenuation	
Line current (% of Fundamental)	Fundamental=11.37A		Fundamental=11.36A	
	192Hz	264Hz	192Hz	264Hz
	3.51%	2.49%	1.65%	0.32%
	312Hz	384Hz	312Hz	384Hz
	1.45%	0.72%	0.53%	0.31%
DC-link current (% of DC component)	DC component=5.87A		DC component=5.89A	
	252Hz	324Hz	252Hz	324Hz
	4.08%	4.16%	1.89%	1.33%
Motor stator current (% of Fundamental)	Fundamental=8.08A		Fundamental=8.07A	
	210Hz	282Hz	210Hz	282Hz
	2.82%	1.80%	1.48%	0.99%
	294Hz	366Hz	294Hz	366Hz
	2.51%	0.60%	1.71%	0.28%
53Hz motor operating frequency ($\omega_r=53\text{Hz}$)				
	Before Attenuation		After Attenuation	
Line current (% of Fundamental)	Fundamental=13.68A		Fundamental=13.75A	
	252Hz	258Hz	252Hz	258Hz
	2.18%	3.27%	1.20%	1.01%
DC-link current (% of DC component)	DC component=4.502A		DC component=4.475A	
	192Hz	318Hz	192Hz	318Hz
	3.68%	7.30%	1.89%	2.12%
Motor stator current (% of Fundamental)	Fundamental=8.108A		Fundamental=8.157A	
	139Hz	245Hz	139Hz	245Hz
	3.12%	1.88%	1.60%	0.45%
	265Hz	371Hz	265Hz	371Hz
	2.11%	1.66%	1.45%	1.33%

4.5 Summary and discussion

In this chapter, a dc-link virtual impedance based active attenuation method is proposed to attenuate the interharmonics caused by harmonics interaction in high-power PWM current-source drives. The proposed method can virtually increase the dc-link impedance through the control of PWM current-source converter so as to enhance the ability of dc link to decouple the harmonics produced by the rectifier and the inverter. At first, an SHE phase jittering method is proposed to enable the active interharmonic compensation capability of SHE-modulated PWM current-source converters. Then, aiming to attenuate the interharmonics caused by the harmonics interaction in high-power PWM current-source drives, a dc-link virtual impedance concept is developed and its realization based on the SHE phase jittering

method is thoroughly studied. To illustrate the design and demonstrate the performance, the proposed dc-link virtual impedance based active attenuation method is applied in high-power PWM current-source drive system with AFE to actively suppress the LC resonance caused by the interharmonics due to the harmonics interaction. By comparing the provided simulation and experimental results in this chapter with the results in Chapter 3 (without using the attenuation method), the effectiveness of the proposed method is verified.

Comparing with the passive damping methods and the design of SHE PWM pattern to solve the harmonics interaction problems, the proposed active attenuation strategy based on the dc-link virtual impedance concept is easy to be designed and implemented without additional costs/losses involved. The dc-link virtual impedance concept also has potential to be used in voltage-source drive systems to guarantee a good interharmonic performance with a smaller dc-link capacitance. In addition, the SHE phase jittering method proposed in this chapter can not only enable the SHE-modulated PWM current-source converter to actively attenuate the interharmonics, but also offers a lot of advantages in the active compensation of system background harmonics which will be discussed in next chapter.

Chapter 5

Active Compensation of System Background Harmonics in High-Power PWM Current-Source Drives

In high-power PWM current-source drives, not only the interharmonics caused by the harmonics interaction will result in the unexpected impacts on the drive system, but the system background harmonics (e.g. harmonics from utility supply and harmonics contained in motor back electromotive force (EMF) due to the imperfect winding distribution) may also significantly distort the current due to the LC circuits. As discussed in Chapter 1, the resonant frequency of the LC circuit in the ac side of PWM current-source converter is normally designed in the range of 3.6pu to 5.8pu, which will greatly amplify the low-order system background harmonics (e.g. 5th, 7th) in ac-side current. Since the passive damping will involve costs and power losses, utilizing the PWM converter to actively compensate the system background harmonics has been well studied in previous work [21],[57],[79]-[87]. In most of the studies, the realization of such ancillary function of PWM converter are based on the on-line PWM schemes, such as the sinusoidal pulse width modulation (SPWM) and the space vector modulation (SVM), where the harmonics can be easily controlled through the reference wave. However, those active compensation methods are difficult to be implemented in PWM converters modulated by the off-line modulation technique, selective harmonics elimination (SHE) scheme. On the one hand, as the PWM pattern of the SHE scheme is fixed in a fundamental cycle,

Publications out of this chapter:

- (1) Y. Zhang, Y. W. Li, N. R. Zargari, and Z. Cheng, "Improved selective harmonics elimination scheme with on-line harmonic compensation for high-power PWM converters," IEEE Transaction on Power Electronics, vol. 30, no. 7, pp. 3508-3517, Jul. 2015.

the modulation-index-based active compensation methods based on the SVM-modulated PWM converters cannot be applied on the SHE-scheme-based modulation. On the other hand, the constraint of quarter-wave symmetry in SHE scheme as shown in Fig. 1. 4(c) confines all the harmonics in PWM pattern to be either in phase or antiphase with the fundamental [88]-[90], which can be observed from (2-24). It means that the phase of each harmonic is uncontrollable. Since the high-power PWM converters are normally modulated by the SHE scheme and significant power losses are involved with the passive damping methods in high-power applications, the active compensation capability of SHE-modulated PWM converters is expected to be enabled. Heretofore, with respect to the active compensation capability of SHE scheme, Zhou *et al.* [93] proposed a selective harmonics compensation (SHC) PWM scheme by relaxing the quarter-wave symmetry in SHE scheme so that both the magnitude and the phase angle of each order harmonic in PWM pattern can be controlled. Based on the SHC scheme, Zhou *et al.* [93] and Ni *et al.* [115] realized the active attenuation of line current harmonic caused by the utility harmonic in high-power PWM current-source drive systems. Nevertheless, due to a look-up table required in the SHC scheme, it has some drawbacks in applications which will be elaborated later. According to the discussions in Chapter 4, the proposed SHE phase jittering method can realize the active harmonic compensation of high-power PWM converters in real time without look-up table required. Thus, if the SHE phase jittering method could be developed to actively compensate the system background harmonics, the drawbacks related to the look-up table in SHC scheme will be overcome.

In this chapter, a strategy of the SHE phase jittering method to actively compensate the system background harmonics is proposed. By comparing with the SHC scheme, which is briefly reviewed in this chapter, the advantages of the SHE-phase-jittering-based active harmonic compensation are presented. In addition, a combination approach based on the SHE phase jittering method and the SHC scheme is also developed to realize the active compensation of multiple harmonics. To demonstrate the performance of the proposed methods, they are adopted to actively attenuate the line current distortion caused by the utility harmonics in high-power

PWM current-source drive system with AFE. Plenty of experimental results are provided.

5.1 Review of SHC-scheme-based active harmonic compensation

In order to illustrate the advantages of the SHE-phase-jittering-based active harmonic compensation over the previous SHC-scheme-based active harmonic compensation, the basic operating principle of the SHC scheme is briefly reviewed in this section based on an application in high-power PWM current-source drive system. In addition, a detailed discussion of its drawbacks is presented.

Based on the SHC scheme, Zhou *et al.* [93] and Ni *et al.* [115] realized the active attenuation of the negative-sequence 5th line current harmonic caused by utility harmonic in high-power PWM current-source drive system with AFE. Fig. 5. 1 shows the diagram of the method presented in [115]. Since the active compensation method is realized through the modulation of PWM current-source rectifier (CSR), for the convenience of illustration, only the inner dc-link current control loop in

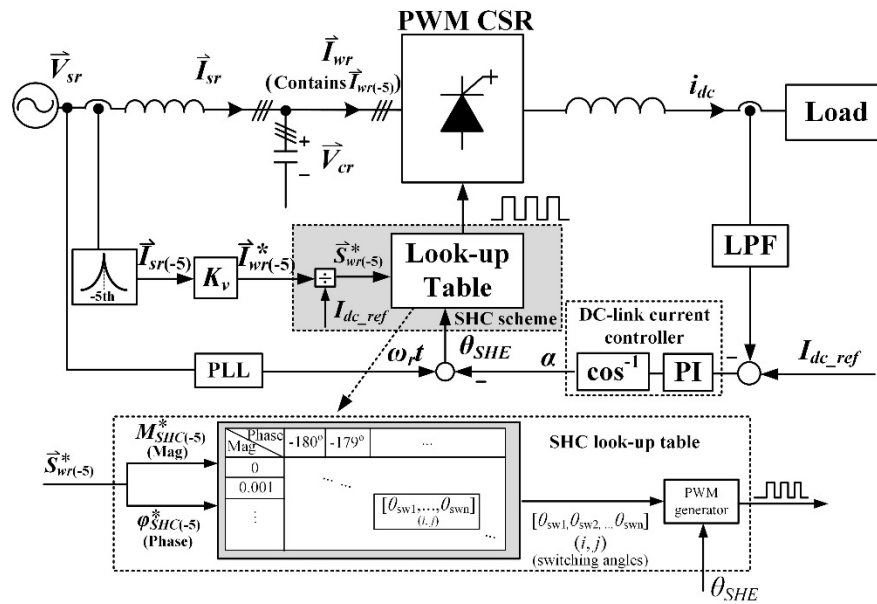


Fig. 5. 1. Diagram of SHC-scheme-based active attenuation on 5th line current harmonic in high-power PWM current-source drive system.

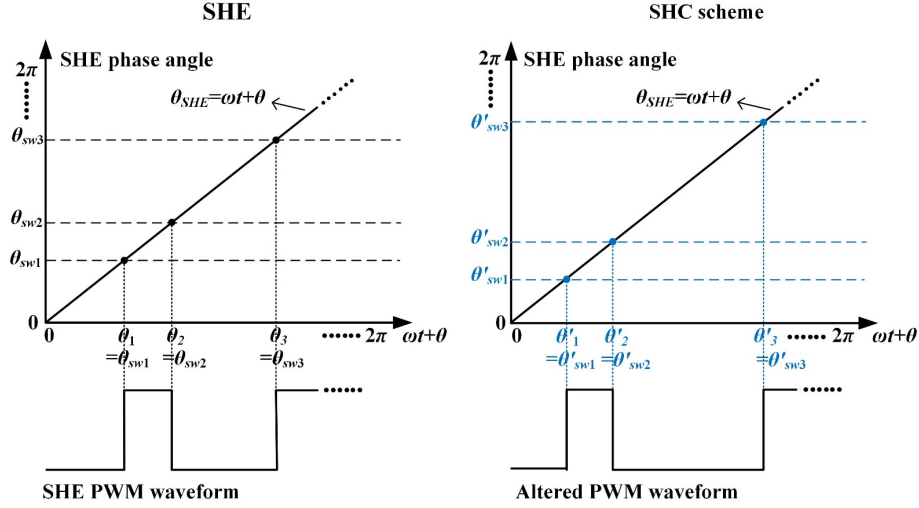


Fig. 5. 2. Basic operating principle of SHC-scheme-based active harmonic compensation.

entire drive control system (shown in Fig. 1. 6) is drawn in Fig. 5. 1, and the PWM current-source inverter (CSI) fed motor drive is equivalent to a load connected to the dc link. As shown in Fig. 5. 1, through multiplying the measured negative-sequence 5th line current harmonic ($\bar{I}_{sr(-5)}$) by a designed coefficient K_v , the reference of 5th PWM current harmonic ($\bar{I}_{wr(-5)}^*$) is produced. To attenuate the $\bar{I}_{sr(-5)}$ in closed loop, the SHC scheme is used to enable the PWM CSR to actively generate 5th harmonic in PWM current \bar{I}_{wr} , $\bar{I}_{wr(-5)}$, according to the reference $\bar{I}_{wr(-5)}^*$. In the SHC scheme, the reference of 5th harmonic in PWM pattern $\bar{S}_{wr(-5)}^*$ is obtained through dividing $\bar{I}_{wr(-5)}^*$ by the dc-link current reference I_{dc_ref} at first. Then, its magnitude $M_{SHC(-5)}^*$ and phase angle $\varphi_{SHC(-5)}^*$ are input into a two dimensional look-up table. With respect to the different magnitude and phase reference of 5th harmonic in PWM pattern, each set of switching angles saved in the look-up table is off-line calculated by solving non-linear trigonometry equation set. During on-line implementation, according to the $M_{SHC(-5)}^*$ and the $\varphi_{SHC(-5)}^*$, the look-up table indexes the corresponding set of switching angles once every fundamental cycle to alter the PWM pattern, so that the PWM CSR can be enabled to actively produce $\bar{I}_{wr(-5)}$ as expected. The basic operating principle of the SHC scheme to produce the expected

harmonics in PWM pattern can be illustrated as shown in Fig. 5. 2. In Fig. 5. 2, θ_{SHE} represents the SHE phase angle, which repeatedly increases from 0 to 2π at system fundamental frequency (at steady state); $\theta_{sw1}, \theta_{sw2}, \dots$, are the predesigned switching angles in SHE pattern; θ and ω are the same as defined in Section 4. 1. As discussed in Section 4. 1 and shown in Fig. 4. 4, the SHE PWM pattern is generated by comparing θ_{SHE} with θ_{sw} as shown in left plot of Fig. 5. 2. To produce the expected harmonics in PWM pattern so as to realize the active compensation, the SHC scheme alters the PWM waveform by on-line changing the switching angles saved in the look-up table at each fundamental cycle (shown as $\theta'_{sw1}, \theta'_{sw2}, \dots$) as shown in right plot of Fig. 5. 2.

Due to the required look-up table, the SHC scheme has certain drawbacks. First up, a considerable off-line calculation of trigonometric equation sets is required to create the table, and a compromise has to be made between the resolution and the size of the table. In addition, since the switching angles can only be updated once in a fundamental cycle, one fundamental delay may be caused in the worst case during the attenuation of line current harmonic, which will affect the compensation performance. Moreover, if two line current harmonics (such as 5th and 7th) are expected to be attenuated, the SHC scheme will require a four dimensional look-up table according to Fig. 5. 1, which challenges both the calculation and the storage during the implementation. For the calculation, not only the amount and complexity of non-linear equations will be greatly increased, but also the solution becomes harder to be obtained. For the storage, if the look-up table used in [93] and [115] is extended to four dimensions with the same resolution, around 230 MB memory space will be needed which greatly challenges the real implementation.

5.2 Active harmonic compensation based on SHE phase jittering method

In Chapter 4, the active interharmonic compensation capability of SHE-modulated PWM converters is enabled by the SHE phase jittering method. According to

the analysis, the SHE phase jittering method can not only enable the high-power PWM converters to actively attenuate interharmonics in the system, but also can be utilized to compensate system harmonics. In this section, the SHE-phase-jittering-based active harmonic compensation method is developed and applied to actively attenuate the line current distortion caused by utility harmonics. Its advantages over the previously-proposed SHC scheme are discussed. In addition, the design of SHE PWM pattern and compensation coefficient related to the implementation of the SHE-phase-jittering-based active harmonic compensation is also presented in this section.

5.2.1 Real-time active harmonic compensation through SHE phase jittering method

The basic operating principle of SHE phase jittering method can refer to Fig. 4. 4. As shown in Fig. 4. 4, to actively generate the expected harmonics for the compensation, the SHE phase jittering method on-line changes the PWM pattern through jittering the SHE phase angle θ_{SHE} by an alternating signal θ_{comp} ($\theta_{comp}=M_{comp}\sin(\omega_{comp}t+\varphi_{comp})$), instead of changing the switching angles θ_{sw} in SHC scheme as shown in Fig. 5. 2. According to the analysis in Section 4. 1, after introducing the θ_{comp} , two main sideband harmonics will be produced around the fundamental component in SHE modulation function as

$$\begin{cases} \bar{S}_{w_Ls}^{SHE1} = j0.5M_{comp} e^{j((\omega-\omega_{comp})t+\theta-\varphi_{comp})} \\ \bar{S}_{w_Rs}^{SHE1} = -j0.5M_{comp} e^{j((\omega+\omega_{comp})t+\theta+\varphi_{comp})} \end{cases} \quad (5-1)$$

Take the active compensation of negative-sequence 5th harmonic for instance, which is the same situation in the previous discussions of SHC scheme. Assume that the 5th harmonic expected to be produced in PWM pattern is

$$\bar{S}_{w(-5)}^* = jM_{s(-5)}^* e^{-j(5\omega t + \varphi_{s(-5)}^*)}, \quad (5-2)$$

where $M_{s(-5)}^*$ and $\varphi_{s(-5)}^*$ are the magnitude and phase angle of 5th PWM harmonic reference. To actively generate the 5th PWM harmonic as expected through the SHE phase jittering method, the magnitude, frequency and phase of θ_{comp} , M_{comp} , ω_{comp} , and φ_{comp} , can be selected as

$$\begin{cases} M_{comp} = 2M_{s(-5)}^* \\ \omega_{comp} = 6\omega \\ \varphi_{comp} = \varphi_{s(-5)}^* + \theta \end{cases}, \quad (5-3)$$

and then, the left sideband harmonic in (5-1) can be rewritten as

$$\bar{S}_{w_Ls}^{SHE1} = j0.5M_{comp} e^{j((\omega - \omega_{comp})t + \theta - \varphi_{comp})} = jM_{s(-5)}^* e^{-j(5\omega t + \varphi_{s(-5)}^*)}. \quad (5-4)$$

By redefining such harmonic as $\bar{S}_{w(-5)}^{SHE1}$, we can obtain that the negative-sequence 5th harmonic in PWM pattern produced by the θ_{comp} is equal to the reference $\bar{S}_{w(-5)}^*$ ($\bar{S}_{w(-5)}^{SHE1} = \bar{S}_{w(-5)}^*$), which means that the active compensation of negative-sequence 5th harmonic is realized by the SHE phase jittering method.

With respect to the application of the 5th line current harmonic attenuation in high-power PWM current-source drive system with AFE, the SHC scheme shown in Fig. 5. 1 can be replaced by the developed active compensation through the SHE phase jittering method as depicted in Fig. 5. 3.

Comparing Fig. 5. 3 with Fig. 5. 1, to generate $\bar{I}_{wr(-5)}$ according to $\bar{I}_{wr(-5)}^*$ through the SHE phase jittering method, only a simple algebraic calculation as shown in (5-3) is needed instead of the SHC look-up table. Not only will it save the effort on creating the SHC look-up table, but also the real-time active harmonic compensation based on the SHE scheme is realized without introducing any delay due to the update of switching angles in SHC scheme. Besides, as discussed in Section 4. 1, if the magnitude of θ_{comp} , M_{comp} , is limited to be small, one the one

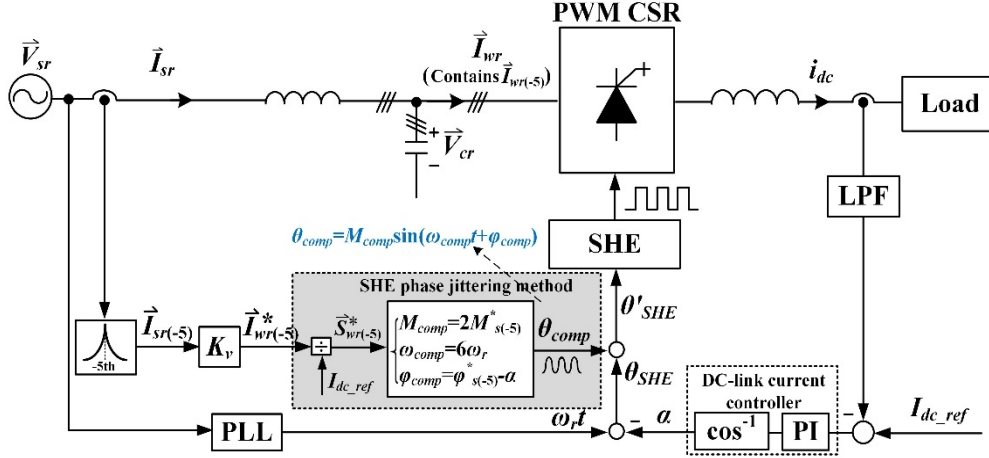


Fig. 5. 3. Diagram of SHE-phase-jittering-based active attenuation on 5th line current harmonic in high-power PWM current-source drive system.

hand, the dc-link current control will not be affected due to the unchanged fundamental component in PWM pattern after using the SHE phase jittering method. On the other hand, the pulse numbers of PWM waveforms (switching frequency) will not be increased.

For the SHE-phase-jittering-based active harmonic compensation, one possible complication is that an unexpected parasitic harmonic is produced in PWM pattern. Regarding the compensation of negative-sequence 5th harmonic, while the left sideband harmonic in (5-1) $\bar{S}_{w_Ls}^{SHE1}$ (also defined as $\bar{S}_{w(-5)}^{SHE1}$ above) is utilized to actively produce 5th PWM harmonic through introducing the 6ω -frequency signal θ_{comp} as shown in (5-3), a parasitic 7th harmonic, defined as \bar{S}_{w7}^{SHE1} , is also produced in PWM pattern by the right sideband harmonic in (5-1) $\bar{S}_{w_Rs}^{SHE1}$ as

$$\bar{S}_{w_Rs}^{SHE1} \triangleq \bar{S}_{w7}^{SHE1} = -j0.5M_{comp} e^{j((\omega+\omega_{comp})t+\theta+\phi_{comp})} = -j0.5M_{s(-5)}^* e^{j(7\omega t+2\theta+\phi_{s(-5)}^*)}. \quad (5-5)$$

Such 7th harmonic may distort the 7th line current harmonic. However, with respect to the high-power PWM current-source drive system with AFE, although the SHE-modulated PWM CSR has been enabled to actively compensate the lowest characteristic utility harmonic (5th), the resonant frequency of the line-side LC filter still

needs to be designed as low as possible to prevent other low-order line current harmonics (such as 7th) from being amplified. In previous works [93],[115], the LC resonant frequency is normally designed around 4pu, which is close to the lower bound of LC resonant frequency range discussed in Section 1. 2. 1 (3.6pu-5.8pu). As a result, the influence of the 7th parasitic harmonic on line current is greatly reduced by the LC filter, and if the magnitude of θ_{comp} , M_{comp} , could be limited small, its influence will be further insignificant according to (5-5).

5.2.2 Influence of harmonics in SHE pattern on SHE-phase-jittering-based active harmonic compensation

For the SHE phase jittering method, according to (4-6) and Fig. 4. 3 in Chapter 4, each harmonic in SHE PWM pattern will generate sideband components after introducing the alternating signal θ_{comp} into the SHE phase angle θ_{SHE} . During the design of SHE-phase-jittering-based active interharmonic compensation in previous chapter, we only consider the sideband components produced by the fundamental component in SHE PWM pattern and the θ_{comp} as discussed in Section 4. 1. On the one hand, since the harmonics in SHE PWM pattern are much less significant than the fundamental, their produced sideband components are comparatively small, especially when the magnitude of θ_{comp} , M_{comp} , is well limited. On the other hand, since the frequencies of the interharmonics being compensated are not integer multiples of the fundamental frequency, the frequencies of the sideband components produced by the different harmonics in SHE PWM pattern will be at different non-integer multiples of the fundamental frequency, so that the compensation performance, the fundamental component in modulation function, and the low-order current harmonics will not be affected. In addition, they will not cause cumulative detriments on system interharmonics, due to the small magnitude and different interharmonic frequencies. As a result, the sideband components produced by the harmonics in SHE PWM pattern are not taken into account in Chapter 4. However, with respect to the SHE-phase-jittering-based active harmonic compensation discussed in this chapter, since the frequency of θ_{comp} , ω_{comp} , is the integer multiples of the ac-side fundamental frequency ω , the sideband components produced by the

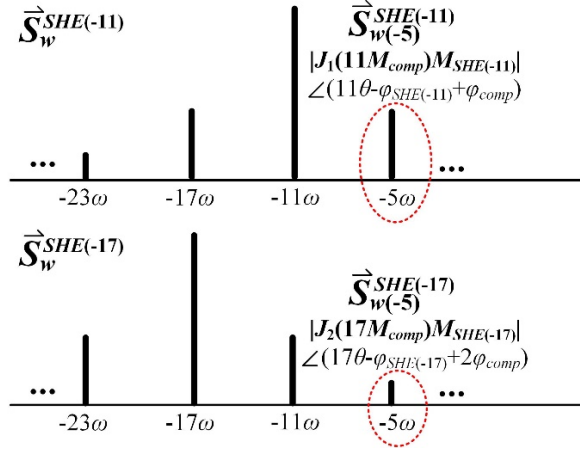


Fig. 5. 4. Influence of harmonics in SHE PWM pattern on 5th harmonic compensation after introducing θ_{comp} .

different harmonics in SHE PWM pattern can be at the same frequency, and the accumulation of their influence may affect the compensation performance, fundamental component in modulation function, and other low-order harmonics in the system. Therefore, such influence of harmonics in SHE PWM pattern needs to be considered in this chapter.

Regarding the active compensation of negative-sequence 5th harmonic, to avoid the compensation performance being affected by the harmonics in SHE PWM pattern, the 5th PWM harmonic should be fully eliminated during the design of SHE pattern at first ($M_{SHE(-5)}=0$). Besides, according to (4-6) and Fig. 4. 3, after introducing the θ_{comp} , the sideband component generated by the 11th and 17th harmonics in SHE PWM pattern ($\bar{S}_{w(-11)}$ and $\bar{S}_{w(-17)}$) at negative-sequence 5th order, defined as $\bar{S}_{w(-5)}^{SHE(-11)}$ and $\bar{S}_{w(-5)}^{SHE(-17)}$, will have the most significant influence on the compensation as shown in Fig. 5. 4. For the higher-order SHE harmonic, e.g. 23rd harmonic $\bar{S}_{w(-23)}$, since the negative-sequence 5th component is in the farer region of side band, their influence can be ignored by compared with $\bar{S}_{w(-5)}^{SHE(-11)}$ and $\bar{S}_{w(-5)}^{SHE(-17)}$. In Fig. 5. 4, $M_{SHE(-11)}$ and $M_{SHE(-17)}$ are the magnitude of 11th and 17th harmonic, respectively; $\varphi_{SHE(-11)}$ and $\varphi_{SHE(-17)}$ are the phase of 11th and 17th harmonics, respectively. According to Fig. 5. 4, since the phase of $\bar{S}_{w(-5)}^{SHE(-11)}$ and $\bar{S}_{w(-5)}^{SHE(-17)}$ can be any value

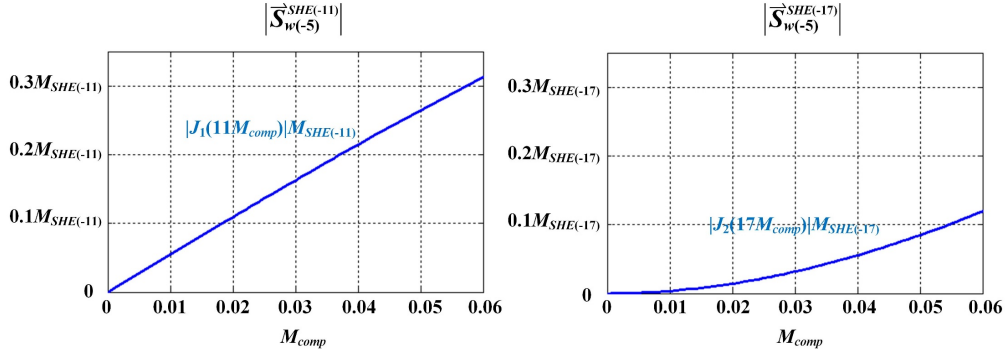


Fig. 5.5. Magnitude of $\bar{S}_{w(-5)}^{SHE(-11)}$ and $\bar{S}_{w(-5)}^{SHE(-17)}$ versus M_{comp} .

respectively, in certain conditions, they may significantly affect the 5th harmonic, $\bar{S}_{w(-5)}^{SHE1}$, that is actively produced by the SHE phase jittering method to realize the compensation. Fig. 5.5 shows the magnitude of $\bar{S}_{w(-5)}^{SHE(-11)}$ and $\bar{S}_{w(-5)}^{SHE(-17)}$ versus the magnitude of θ_{comp} , M_{comp} . According to Fig. 5.5, the most direct way of reducing the influence of $\bar{S}_{w(-5)}^{SHE(-11)}$ and $\bar{S}_{w(-5)}^{SHE(-17)}$ on the 5th harmonic compensation performance is to greatly attenuate the 11th harmonic in SHE PWM pattern ($M_{SHE(-11)} \approx 0$), and mitigate the 17th harmonic as much as possible during the design of SHE pattern ($M_{SHE(-17)} \rightarrow 0$).

With respect to the low-order harmonics affected by the SHE phase jittering method, beside the produced 7th parasitic harmonic \bar{S}_{w7}^{SHE1} as discussed in previous section, the sideband component generated by the harmonics in SHE PWM pattern can also be at 7th order. Their cumulative influence on 7th line current harmonic may not be well attenuated by the LC filter in high-power PWM current-source drives even with a designed low LC resonant frequency. Note that, the 7th harmonic in SHE PWM pattern is also required to be eliminated during the design of SHE scheme ($M_{SHE7} = 0$). The 7th sideband components produced by the 13th harmonic and 19th harmonic in SHE PWM pattern (\bar{S}_{w13} and \bar{S}_{w19}) are the most significant, defined as \bar{S}_{w7}^{SHE13} and \bar{S}_{w7}^{SHE19} respectively, as shown in Fig. 5.6. The magnitude of \bar{S}_{w7}^{SHE13} and \bar{S}_{w7}^{SHE19} versus M_{comp} are drawn in Fig. 5.7. To reduce their influence on 7th harmonic, the 13th harmonic in SHE PWM pattern is expected to be greatly

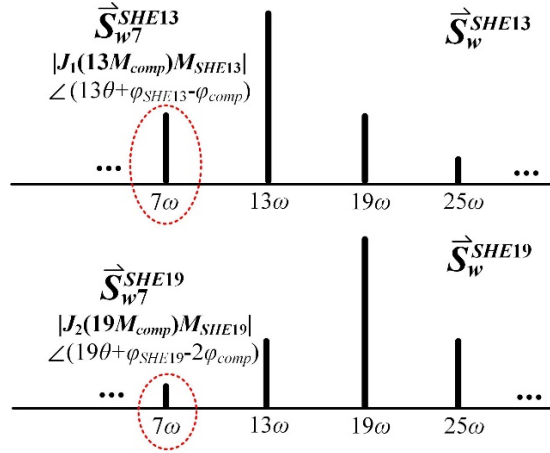


Fig. 5. 6. Influence of harmonics in SHE PWM pattern on 7th harmonic after introducing θ_{comp} .

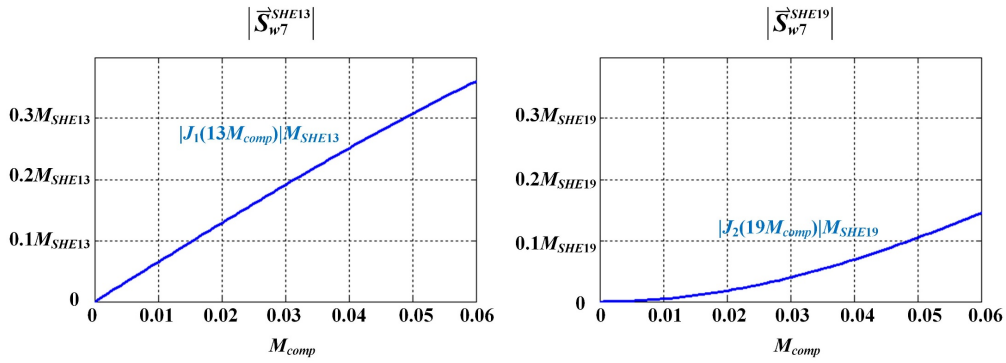


Fig. 5. 7. Magnitude of \vec{S}_{w7}^{SHE13} and \vec{S}_{w7}^{SHE19} versus M_{comp} .

attenuated ($M_{SHE13} \approx 0$), and the 19th SHE harmonic is expected to be reduced as much as possible ($M_{SHE19} \rightarrow 0$). For the other low-order harmonics, such as 11th and 13th, if the 11th and 13th harmonics in SHE PWM pattern could be greatly attenuated, and the 17th and 19th SHE harmonics could be reduced as much as possible, they would not be affected much by the SHE phase jittering method, and the influence can be further minimized by the *LC* filter on the 11th and 13th line current harmonics.

For the fundamental component (modulation index and fundamental phase angle) in the modulation function, if the SHE PWM pattern can be designed by following the criteria discussed above as:

- 1) Fully eliminate 5th and 7th harmonics,
- 2) Greatly attenuate 11th and 13th harmonic,
- 3) Reduce 17th and 19th harmonics as much as possible,

it will not be affected by the harmonics in SHE PWM pattern after adopting the SHE phase jittering method.

It can be observed that the summarized design criteria of SHE pattern are similar as the traditional SHE scheme which is aiming to greatly reduce the low-order harmonics. Therefore, the SHE phase jittering method can be well combined with the traditional SHE scheme to actively compensate 5th harmonic.

5.2.3 Coefficient design in the implementation of SHE-phase-jittering-based active harmonic compensation

As aforementioned, the SHC-scheme-based active compensation of high-power PWM converter has been adopted to actively attenuate the 5th line current harmonic due to the utility harmonic in high-power PWM current-source drives with AFE as shown in Fig. 5. 1. The design of coefficient K_v in the attenuation strategy was discussed in [115]. To overcome the disadvantages of the SHC scheme, the developed SHE-phase-jittering-based active compensation can substitute for the SHC scheme in the same application as shown in Fig. 5. 3. Regarding the design of K_v in such implementation of SHE phase jittering method, some considerations are made in this part based on the analysis in [115].

According to [115], the coefficient K_v can be a complex number as $K_v = M_{K_v} e^{j\varphi_{K_v}}$, where M_{K_v} and φ_{K_v} represent the magnitude and phase respectively. In the following analysis, we consider the selection of its magnitude and phase angle separately.

A. Phase angle selection

According to Fig. 5. 3, if we assume that the 5th PWM current harmonic $\bar{I}_{wr(-5)}$ (actively produced by the PWM CSR) could well track its reference $\bar{I}_{wr(-5)}^*$, the Fig. 5. 3 would be simplified as shown in Fig. 5. 8 at the frequency of 5th harmonic.

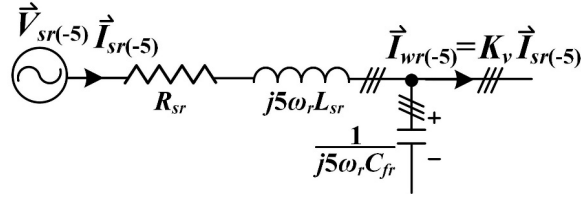


Fig. 5. 8. Simplified steady-state diagram of Fig. 5. 3 at 5th harmonic.

Based on Fig. 5. 8, by defining $\omega_{r(-5)} = -5\omega_r$, the relationship between the 5th grid voltage harmonic $\vec{V}_{sr(-5)}$ and the 5th line current harmonic $\vec{I}_{sr(-5)}$ can be obtained as

$$\frac{\vec{I}_{sr(-5)}}{\vec{V}_{sr(-5)}} = \frac{-j\omega_{r(-5)}C_{fr}}{(1 - \omega_{r(-5)}^2 L_{sr} C_{fr}) - j\omega_{r(-5)} R_{sr} C_{fr} - K_v}. \quad (5-6)$$

By defining $K_{const} = \sqrt{(1 - \omega_{r(-5)}^2 L_{sr} C_{fr})^2 + (\omega_{r(-5)} R_{sr} C_{fr})^2}$, the modulus of (5-6) can be obtained as

$$\frac{|\vec{I}_{sr(-5)}|}{|\vec{V}_{sr(-5)}|} = \frac{|\omega_{r(-5)}| C_{fr}}{\sqrt{K_{const}^2 + M_{Kv}^2 - 2K_{const} M_{Kv} \sin\left(\varphi_{Kv} + \tan^{-1}\left(\frac{\omega_{r(-5)}^2 L_{sr} C_{fr} - 1}{\omega_{r(-5)} R_{sr} C_{fr}}\right)\right)}}. \quad (5-7)$$

It can be observed that, when

$$\varphi_{Kv} = \frac{3\pi}{2} - \tan^{-1}\left(\frac{\omega_{r(-5)} L_{sr}}{R_{sr}} - \frac{1}{\omega_{r(-5)} R_{sr} C_{fr}}\right), \quad (5-8)$$

the value of (5-7) is minimum at fixed M_{Kv} . If we define such phase as φ_{Kv_opt} , it means that when the phase of K_v (φ_{Kv}) is selected to be φ_{Kv_opt} , the best attenuation performance of line current harmonic $\vec{I}_{sr(-5)}$ will be achieved at certain M_{Kv} as

$$\left.\frac{|\vec{I}_{sr(-5)}|}{|\vec{V}_{sr(-5)}|}\right|_{\varphi_{Kv}=\varphi_{Kv_opt}} = \frac{|\omega_{r(-5)}| C_{fr}}{K_{const} + M_{Kv}}. \quad (5-9)$$

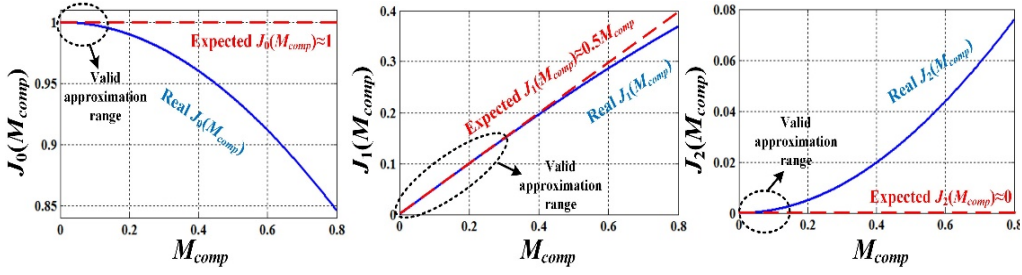


Fig. 5. 9. $J_0(M_{comp})$, $J_1(M_{comp})$, and $J_2(M_{comp})$ versus M_{comp} .

B. Magnitude selection

According to (5-9), the larger the M_{Kv} is, the better the attenuation performance will be. However, the large M_{Kv} will cause a series of problems.

As shown in Fig. 5. 3, the magnitude of θ_{comp} , M_{comp} , can be represented as

$$M_{comp} = 2M_{s(-5)}^* = \frac{2M_{Kv}I_{sr(-5)}}{I_{dc_ref}}, \quad (5-10)$$

where $I_{sr(-5)}$ is the magnitude of 5th line current harmonic. According to (5-10), the large M_{Kv} will increase the M_{comp} , which may have a strong impact on SHE-phase-jittering-based active harmonic compensation.

On the one hand, according to the analysis on the design of coefficient K_v in dc-link virtual impedance based active attenuation method in Section 4. 3. 2., the large M_{comp} will invalidate the three approximations $J_0(M_{comp}) \approx 1$, $J_1(M_{comp}) \approx 0.5M_{comp}$, and $J_k(M_{comp}) \approx 0$ ($k \geq 2$) as shown in Fig. 5. 9. As discussed in Section 4. 3. 2, the invalidation of $J_0(M_{comp}) \approx 1$ will greatly affect the modulation index of PWM CSR which may cause impacts on the line-side power factor and even result in the instability of the system. If $J_1(M_{comp}) \approx 0.5$ loses effect, the $\bar{S}_{w(-5)}^{SHE1}$ will no longer be equal to the $\bar{S}_{w(-5)}^*$, so that the $\bar{I}_{wr(-5)}$ cannot well track the $\bar{I}_{wr(-5)}^*$. Accordingly, the assumption that $\bar{I}_{wr(-5)} = \bar{I}_{wr(-5)}^*$ in previous part (phase angle selection) will be invalid.

The performance of 5th line current attenuation will be degraded, and the line current distortion may even be deteriorated. Also, if $J_k(M_{comp})$ ($k \geq 2$) are not zero, unexpected harmonics will be introduced in the system.

On the other hand, as discussed in Section 5.2.2, the impact of harmonics in SHE pattern on the SHE phase jittering method can be minimized by designing the SHE scheme to: fully eliminate 5th and 7th harmonics; greatly attenuate 11th and 13th harmonics; reduce 17th and 19th harmonics as much as possible. However, with limited pulse numbers of SHE scheme, the aforementioned design criteria cannot be perfectly realized. Taking the 9-pulse SHE scheme for instance, it is unable to fully eliminate 5th, 7th, 11th, and 13th harmonics in PWM pattern simultaneously [1]. If the elimination of 5th and 7th harmonics is given first priority, there will be a residual 11th harmonic as shown in Fig. 3.10, or a residual 13th harmonic as shown in Fig. 2.9, or both 11th and 13th harmonics if optimization algorithm is used as shown in (2-22). In addition, with four free switching angles, the 9-pulse SHE scheme is difficult to effectively reduce the 17th and 19th harmonics in PWM pattern. Based on Figs. 5.5 and 5.7, to avoid the impact of those harmonics in SHE pattern with low pulse numbers, the M_{comp} is expected to be small.

To limit M_{comp} , one way is to introduce a saturation block after the generation of $M_{s(-5)}^*$ in Fig. 5.3, but it may result in a slow dynamic of compensation and the different steady-state compensation performance under different dc-link current according to (5-10). To overcome the problems, an alternative method is through the design of M_{Kv} , the magnitude of coefficient K_v . According to (5-10), M_{Kv} is expected to be small to avoid the problems caused by the large M_{comp} . Besides, as shown in Fig. 5.3, a harmonic filter is required to extract the negative-sequence 5th line current harmonic while effectively block the signals of other frequencies, especially the signal at LC resonant frequency. A large M_{Kv} may also weaken the attenuation effect of the harmonic filter on the unexpected-frequency signals, which can result in unexpected harmonics and interharmonics in the system and may even destabilize the system. But the M_{Kv} cannot be too small to guarantee a good attenuation performance on line current harmonic according to (5-9). Therefore, a

tradeoff has to be made during the selection of M_{Kv} . Moreover, according to (5-10), since M_{comp} is also related to the dc-link current reference I_{dc_ref} , for the applications in high-power motor drive systems, the M_{Kv} can be designed at rated dc-link current and scaled down as dc-link current decreasing to maintain M_{comp} at a proper value.

5.3 Compensation of two harmonics based on the combination of SHE phase jittering method and SHC scheme

As discussed at the end of Section 5. 1, to actively compensate two harmonics (such as 5th and 7th) through the SHC scheme, a four-dimension look-up table will be required. Not only the off-line calculation is much more complex and the solution becomes harder to be obtained, but also the memory space required by the look-up table will be dramatically increased. For the SHE-phase-jittering-based active harmonic compensation, as discussed earlier, a parasitic 7th PWM harmonic will be produced when it is used to actively compensate 5th harmonic. Consequently, the SHE phase jittering method is incapable of actively compensating 5th and 7th harmonics simultaneously. Since both the SHC scheme and the SHE phase jittering method are only applicable to compensate one harmonic (usually the lowest characteristic harmonic, negative-sequence 5th) in high-power PWM converter systems, the resonant frequency of the system filter circuit has to be designed as low as possible in order not to amplify other low-order harmonics (such as 7th). As aforementioned, for their applications in high-power PWM current-source drives to actively attenuate the 5th line current harmonic caused by the utility harmonic, the line-side LC resonant frequency is usually designed around 4pu in previous works [93],[115]. The limitation of low filter resonant frequency will result in a larger value of passive components in the filter, which may increase the size and decrease the system power factor.

In order to further attenuate the harmonic distortion and reduce the constraint on filter circuit design, the high-power PWM converters are expected to be capable of

actively compensating more system background harmonics. Based on the analysis in Section 5. 1 and Section 5. 2, if the SHC scheme and the SHE phase jittering method could be combined in high-power PWM converter systems and be effectively utilized to compensate one harmonic respectively, the active compensation of two harmonics would be realized. Also, the combination approach will not increase the dimensions of the SHC look-up table in the compensation of two harmonics. However, a main problem faced by this combination approach is the interference between the two methods during the compensation. In this section, the interference between the two methods is analyzed, and strategies are proposed to guarantee an independent operation of each method without being interfered during the active compensation. To facilitate the following analysis, we assume that the SHE phase jittering method is used to compensate a negative-sequence 5th harmonic and the SHC scheme is used to compensate a positive-sequence 7th harmonic respectively. In the compensation, the reference of 7th harmonic in PWM is defined as $\vec{S}_{w7}^* = -jM_{s7}^* e^{j(7\omega t + \phi_{s7}^*)}$, and the reference of 5th harmonic is the same as $\vec{S}_{w(-5)}^*$ defined in (5-2).

A. Decoupling of SHC-scheme-based active compensation and SHE-phase-jittering-based active compensation

To avoid the two active compensation method interfering with each other during the compensation of two harmonics, the parasitic harmonic produced by the SHE phase jittering method needs to be solved at first. According to the above analysis, to track the reference of negative-sequence 5th harmonic in PWM pattern $\vec{S}_{w(-5)}^*$, the SHE phase jittering method can produce a 5th PWM harmonic $\vec{S}_{w(-5)}^{SHE1}$ through introducing a 6ω -frequency θ_{comp} (shown in (5-3)) into the SHE phase angle, but at the same time, a parasitic positive-sequence 7th harmonic is also generated in PWM pattern as \vec{S}_{w7}^{SHE1} shown in (5-5). Such parasitic harmonic may degrade the performance of SHC-scheme-based active compensation on 7th harmonic, or even amplify the 7th system background harmonic at certain conditions. To eliminate such

impact, we can subtract \bar{S}_{w7}^{SHE1} from the 7th harmonic reference \bar{S}_{w7}^* to obtain the new reference input to the SHC look-up table as

$$\bar{S}_{w7_new}^* = \bar{S}_{w7}^* - \bar{S}_{w7}^{SHE1} \triangleq -jM_{SHC7}^* e^{j(7\omega t + \phi_{SHC7}^*)}. \quad (5-11)$$

By using this strategy, the parasitic harmonic produced by the SHE phase jittering method during the compensation will not affect the performance of SHC-scheme-based compensation when they are used simultaneously.

Moreover, as discussed in Section 5. 2. 2, the harmonics in SHE PWM pattern will generate unexpected sideband components at low order after introducing the θ_{comp} . In the same manner, such issue also needs to be considered in the design of each set of switching angles saved in the SHC look-up table, in order to prevent the active compensation from being affected. According to the analysis in Section 5. 2. 2, to minimize the impact on SHE-phase-jittering-based 5th harmonic compensation, each set of switching angles is expected to be designed to fully eliminate 5th harmonic, and greatly attenuate 11th harmonic, and reduce 17th harmonic as much as possible in PWM pattern. Regarding the SHC-scheme-based active compensation, beside the 7th harmonic in PWM pattern is required to be generated according to $\bar{S}_{w7_new}^*$ in (5-11) for each set of switching angles in the look-up table, they are expected to greatly attenuate 13th harmonic and reduce 19th harmonic as much as possible in the PWM pattern to avoid the influence on the performance of 7th harmonic compensation after introducing θ_{comp} .

Based on the previous analysis, an application example of the combination approach to actively attenuate 5th and 7th line current harmonics due to the utility harmonics in high-power PWM current-source drive system is illustrated as shown in Fig. 5. 10. In Fig. 5. 10, the $K_{v(-5)}$ and the K_{v7} are two tunable coefficients for SHE-phase-jittering-based 5th harmonic compensation and SHC-scheme-based 7th harmonic compensation respectively.

B. Coefficient design in the implementation of combination approach

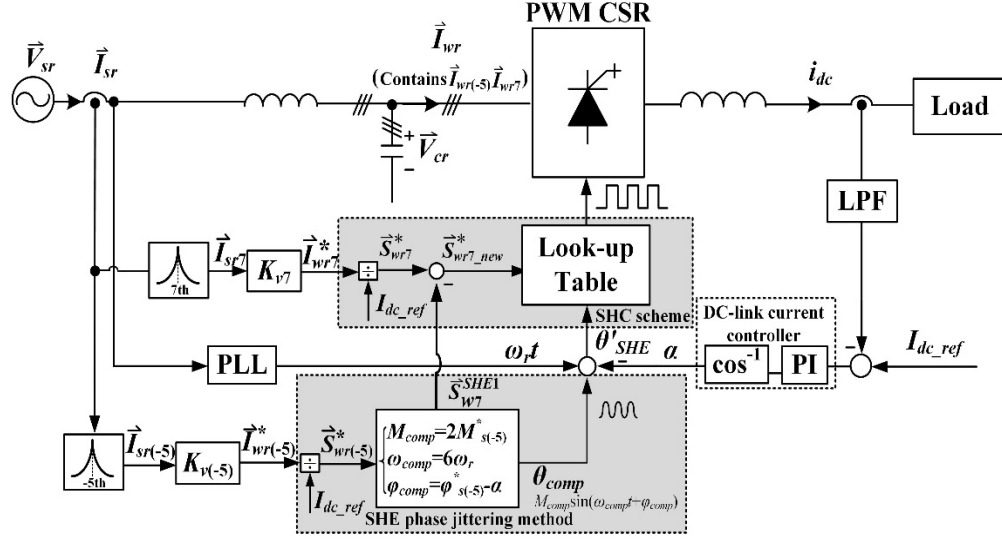


Fig. 5. 10. Diagram of active attenuation on 5th and 7th line current harmonic based on combination approach in high-power PWM current-source drive.

In Section 5. 2. 3, based on the application on high-power PWM current-source drive systems, the design of coefficient K_v in the SHE-phase-jittering-based active attenuation of line current harmonic is discussed. According to the discussion, a tradeoff in the selection of K_v is required to guarantee a good compensation performance while not affect the control of drive system. With respect to the proposed combination-approach-based active attenuation of line current harmonics in this section as shown in Fig. 5. 10, some minor changes of the coefficient design are needed.

As discussed in previous part (part A), each set of switching angles in SHC look-up table is required to generate 7th harmonic in PWM pattern according to the reference $\vec{S}_{wr7_new}^*$, and is expected to fully eliminate 5th harmonic, and greatly attenuate 11th and 13th harmonics, and reduce 17th and 19th harmonics as much as possible in PWM pattern. Take an 11-pulse SHC scheme for instance. Theoretically, it has enough free switching angles to generate 7th harmonic as expected and greatly attenuate 5th, 11th and 13th PWM harmonics. Define a function f_{cost} as

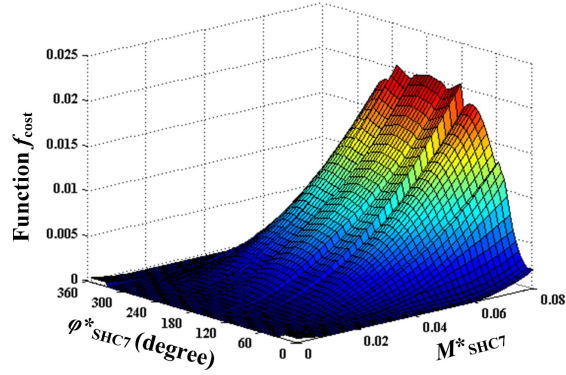


Fig. 5. 11. Function f_{cost} of 11-pulse SHC switching angles' solution under different M^*_{SHC7} and φ^*_{SHC7} .

$$f_{cost} = \left(M_{SHC(-5)}\right)^2 + \left(M_{SHC7} \angle \varphi_{SHC7} - M^*_{SHC7} \angle \varphi^*_{SHC7}\right)^2 + \left(M_{SHC(-11)}\right)^2 + \left(M_{SHC13}\right)^2. \quad (5-12)$$

Ideally, the f_{cost} should be zero at each value of reference M^*_{SHC7} and φ^*_{SHC7} . However, the real value of f_{cost} with the solutions of switching angles under different M^*_{SHC7} and φ^*_{SHC7} is shown in Fig. 5. 11. It can be observed that the larger the M^*_{SHC7} is, the poorer the solutions of switching angles will be as f_{cost} deviates farther from 0. If the reduction of 17th and 19th harmonics in PWM pattern is further considered, there will be a worse result. Note that if the pulse numbers of SHC scheme is decreased (e.g. 9 pulses) to lower the switching frequency, the result will be worse. As a result, the M^*_{SHC7} is expected to be limited within a small value. Based on Fig. 5. 10, (5-3) and (5-11), we can obtain that

$$-jM^*_{SHC7} e^{j(7\omega t + \varphi^*_{SHC7})} = -j \frac{M_{Kv7} I_{sr7}}{I_{dc_ref}} e^{j(7\omega t + \varphi_{Isr7} + \varphi_{Kv7})} + j \frac{M_{Kv(-5)} I_{sr(-5)}}{2I_{dc_ref}} e^{j(7\omega t - 2\alpha + \varphi_{Isr(-5)} - \varphi_{Kv(-5)})}, \quad (5-13)$$

where I_{sr7} and φ_{Isr7} are the magnitude and phase angle of 7th line current harmonic; $M_{Kv(-5)}$, M_{Kv7} , $\varphi_{Kv(-5)}$ and φ_{Kv7} are the magnitude and phase angle of $K_{v(-5)}$ and K_{v7} respectively. Since the initial phase of two complex numbers on the right hand side of (5-13) can be any value from 0 to 2π due to the different conditions of utility

TABLE 5. 1 EXPERIMENT PARAMETERS

Rated value	10kVA/208V/60Hz	
	Real value	P.U. value
Line inductance	1.67mH	0.15
Filter capacitance	240 μ F	0.40
DC-link inductance	10mH	0.58
DC-link resistance load	5.76 Ω	0.89

harmonics, to reduce M_{SHC7}^* , both $M_{K_V(-5)}$ and M_{K_V7} needs to be confined. Considering this issue, the magnitude of $K_{V(-5)}$ and K_{V7} in the combination-approach-based compensation of two harmonics is required to be reduced properly, compared with the selection of K_V in the one harmonic compensation through the SHC scheme (shown in Fig. 5. 1) or the SHE phase jittering method (shown in Fig. 5. 3). Note that the phase angle of $K_{V(-5)}$ and K_{V7} , $\phi_{K_V(-5)}$ and ϕ_{K_V7} , can still be selected based on (5-8) (for the selection of ϕ_{K_V7} , the $\omega_{r(-5)}$ in (5-8) is replaced by $\omega_7=7\omega_r$).

5.4 Verification results

To verify the effectiveness of the developed active harmonic compensation based on the SHE phase jittering method and the combination approach, simulations and experiments are conducted on the PWM current-source drive system with AFE to actively attenuate the line current distortion caused by the utility harmonics as shown in Figs 5. 3 and 5. 10 respectively. As the simulations and experiments have very similar performance, only the experimental results are provided in this section. The experiments are carried out on the same 10kVA/208V/60Hz experimental system as in Chapter 3 and Chapter 4, and the dc-link resistance load is adopted instead of CSI-fed induction motor for convenience.

5.4.1 Experimental results of the attenuation on 5th line current harmonic through the SHE phase jittering method

The parameters of the experimental system are listed in TABLE 5. 1. A 9-pulse SHE scheme is used with the harmonic content shown in Fig. 5. 12. According to the discussion in Section 5. 2. 2, the phase of coefficient K_V in Fig. 5. 3, ϕ_{K_V} is

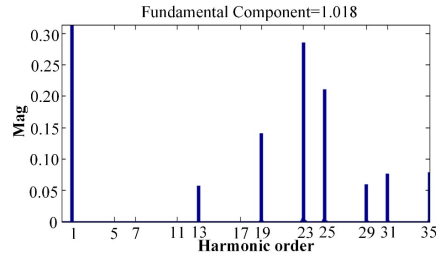


Fig. 5. 12. Harmonic content of 9-pulse SHE PWM pattern.

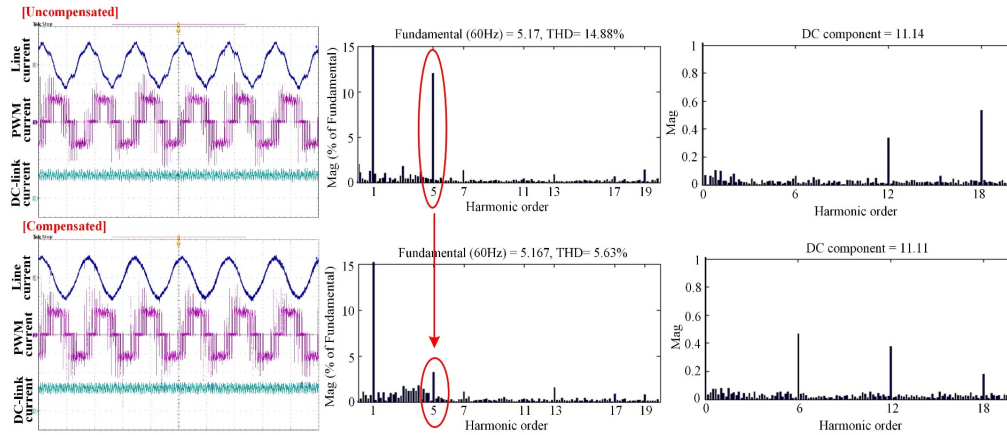


Fig. 5. 13. Steady-state compensation performance under 1% 5th grid voltage harmonic (i_s : 5A/div., i_w : 10A/div., i_{dc} : 10A/div., time: 10ms/div.).

selected as -35° based on (5-8), and its magnitude M_{Kv} is selected as 1.3 in the following experiments.

A. Steady-state attenuation performance

At first, the grid voltage is programmed to contain 1% 5th harmonic. The dc-link current is controlled at 10A. Fig. 5. 13 shows the experimental results before and after using the SHE phase jittering method. It can be observed that the 5th line current is greatly reduced and there is no significant increase on the other order line current harmonics.

To further verify the SHE-phase-jittering-based active compensation method, the grid voltage is programmed to contain 1% 5th harmonic and 1% 7th harmonic. Fig. 5. 14 shows the current waveforms under four different sets of 5th grid voltage

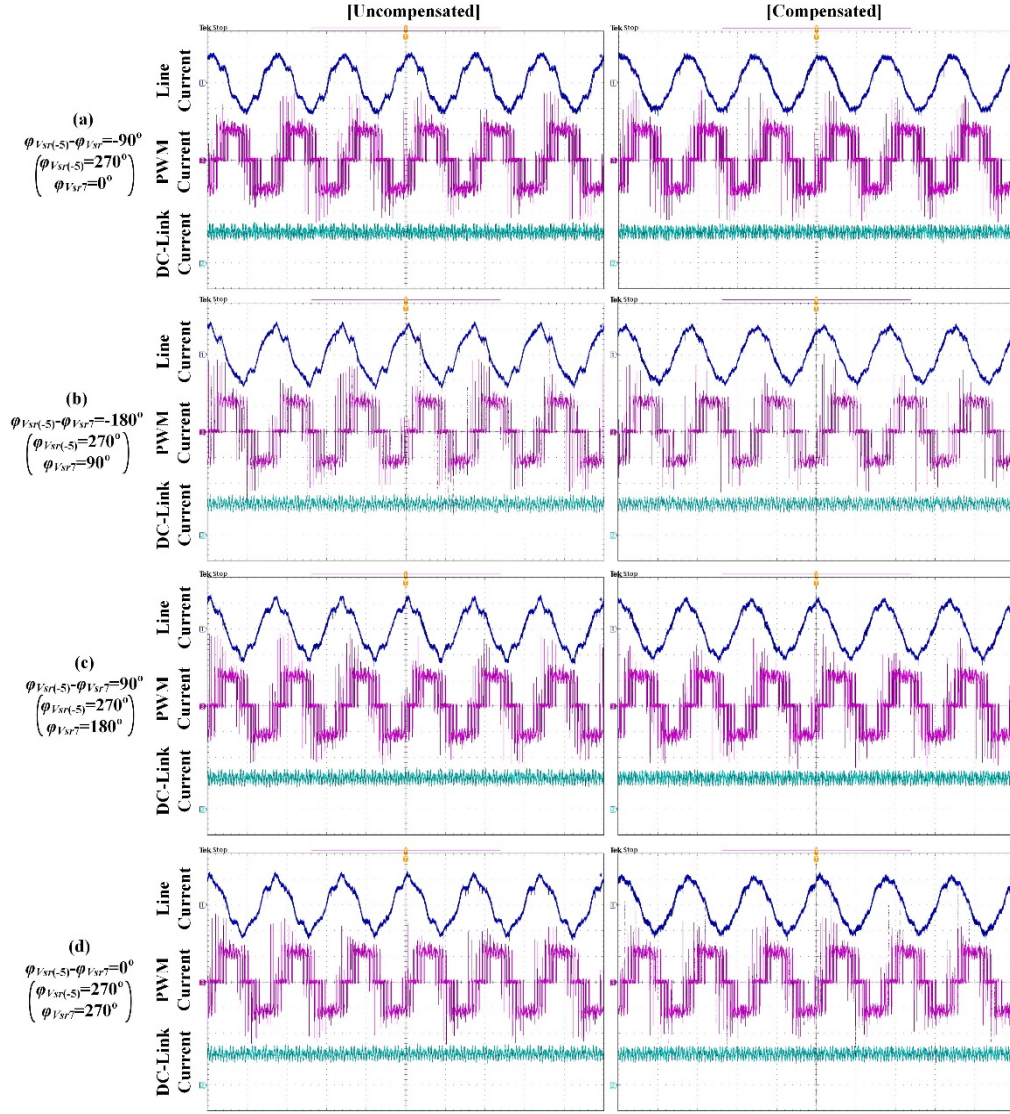


Fig. 5. 14. Current waveforms before and after using the SHE-phase-jittering-based active harmonic compensation under different 5th (1%) and 7th (1%) grid voltage harmonics' phases.

harmonic's initial phase ($\varphi_{V_{sr(-5)}}$) and 7th grid voltage harmonic's initial phase ($\varphi_{V_{sr7}}$). It can be observed that, after using the SHE phase jittering method, the distortion of line current are highly reduced. Fig. 5. 15 shows the FFT analysis of line current in Fig. 5. 14. We can observe from Fig. 5. 15 that the 5th line current harmonic can be well attenuated under all conditions and there is no significant increase on the other line current harmonics.

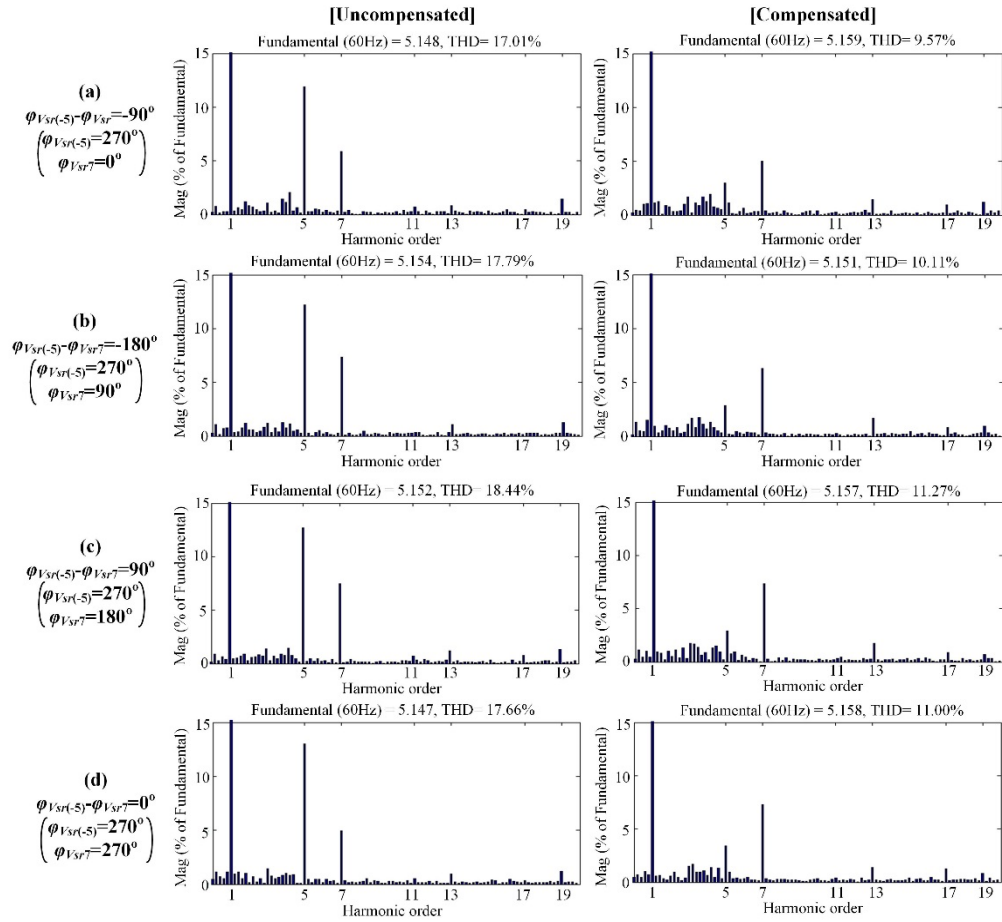


Fig. 5. 15. FFT analysis of line current in Fig. 5. 14.

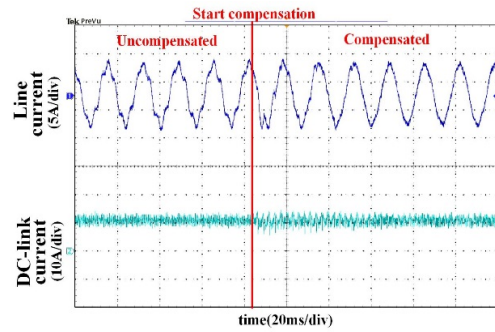


Fig. 5. 16 Transient of applying compensation method.

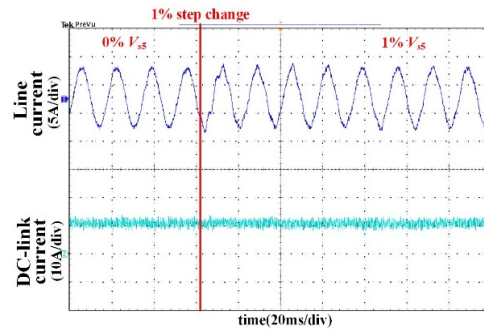


Fig. 5. 17 Transient of 1% step change of 5th grid voltage harmonic.

B. Dynamic attenuation performance

To test the dynamic performance, two experiments are carried out. Fig. 5. 16 shows the transient of applying the SHE phase jittering method. Fig. 5. 17 shows

TABLE 5. 2 EXPERIMENT PARAMETERS

Rated value	10kVA/208V/60Hz	
	Real value	P.U. value
Line inductance	1.67mH	0.15
Filter capacitance	150 μ F	0.24
DC-link inductance	10mH	0.58
DC-link resistance load	5.76 Ω	0.89

the transient of 1% step change of 5th grid voltage harmonic under the adoption of the SHE phase jittering method. It can be observed from the two figures that the dynamic of the SHE-phase-jittering-based active compensation is fast and the dc-link current control is not affected.

5.4.2 Experimental results of the attenuation on 5th and 7th line current harmonics based on the combination approach

In this part, the developed combination approach is tested to actively attenuate 5th and 7th line current harmonics simultaneously (SHE phase jittering method is used to attenuate 5th harmonic and SHC scheme is used to attenuate 7th harmonic). Since both the 5th and 7th harmonics are aiming to be compensated, the line-side LC resonant frequency is increased from previous 4.08pu (line inductance: 0.15pu; filter capacitance: 0.4pu) to 5.3pu (line inductance: 0.15pu; filter capacitance: 0.24pu) as shown in TABLE 5. 2. As the filter capacitance is decreased from 0.4pu to 0.24pu in this work, the reactive power flow in line side will be significantly reduced.

At first, the background grid voltage is programmed to contain 0.7% 5th harmonic $v_{sr(-5)}$ and 0.7% 7th harmonic v_{sr7} respectively. For the coefficients $K_{v(-5)}$ and K_{v7} , according to the analysis in Section 5. 3, their phase is selected to be $\varphi_{Kv(-5)}=-121^\circ$ and $\varphi_{Kv7}=-19^\circ$ respectively; the magnitude, $M_{Kv(-5)}$ and M_{Kv7} , are selected as 0.75 and 1.1 respectively. The attenuation performance of the proposed method are tested under different phases of 5th and 7th grid voltage harmonics ($\varphi_{Vsr(-5)}$ and φ_{Vsr7}), and a part of the results are presented as shown in Figs. 5. 18 and 5. 19. It can be

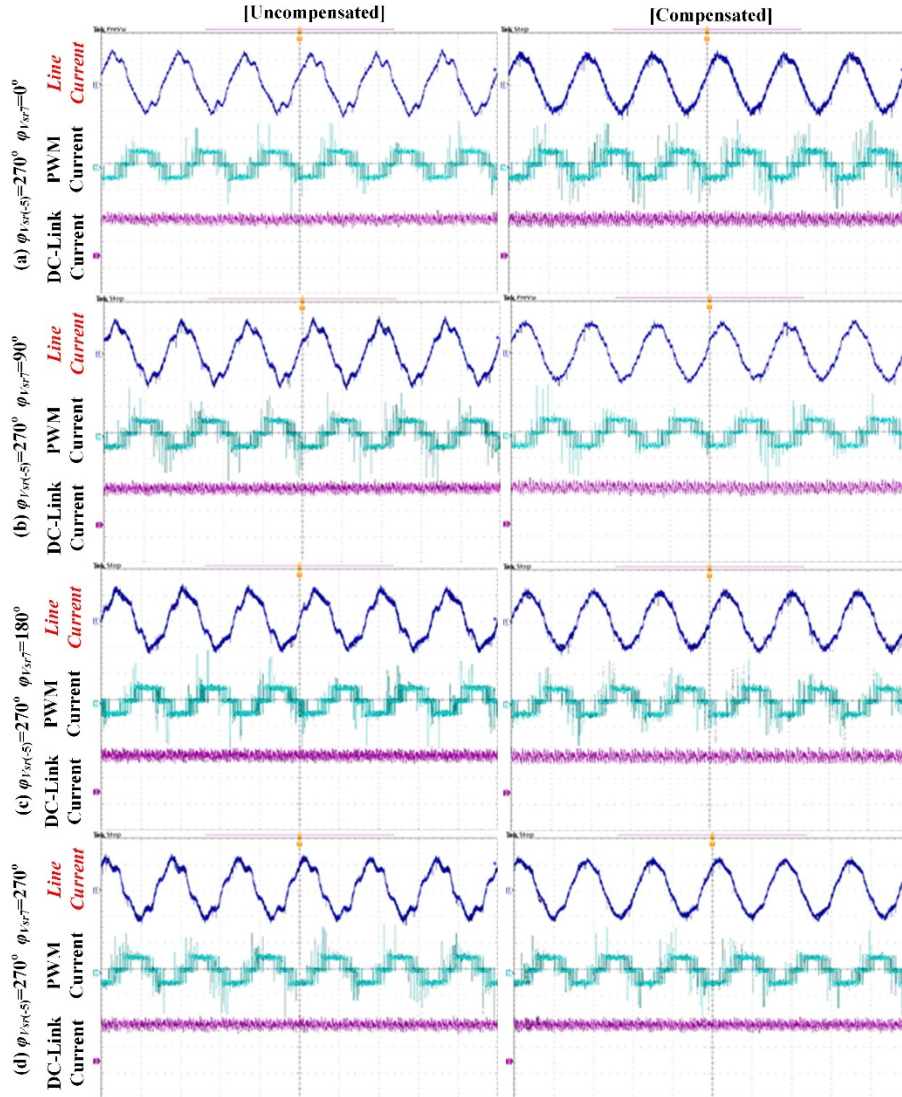


Fig. 5. 18. Current waveforms before and after using the combination approach under different 5th (0.7%) and 7th (0.7%) grid voltage harmonics' phases.

observed that, without being compensated, there are significant 5th and 7th line current harmonics due to the increased line-side LC resonant frequency. After using the combination approach, both the 5th and 7th line current harmonics are effectively attenuated, and there is no significant increase on the other line current harmonics.

To further test the performance, both the 5th and 7th grid voltage harmonics are increased to 1.1%. The large grid voltage harmonics will increase the magnitude of the corresponding line current harmonics. As a result, $M_{KV(-5)}$ and M_{KV7} are expected to be reduced to limit M_{comp} and M_{SHC7}^* as discussed above. With the reselected

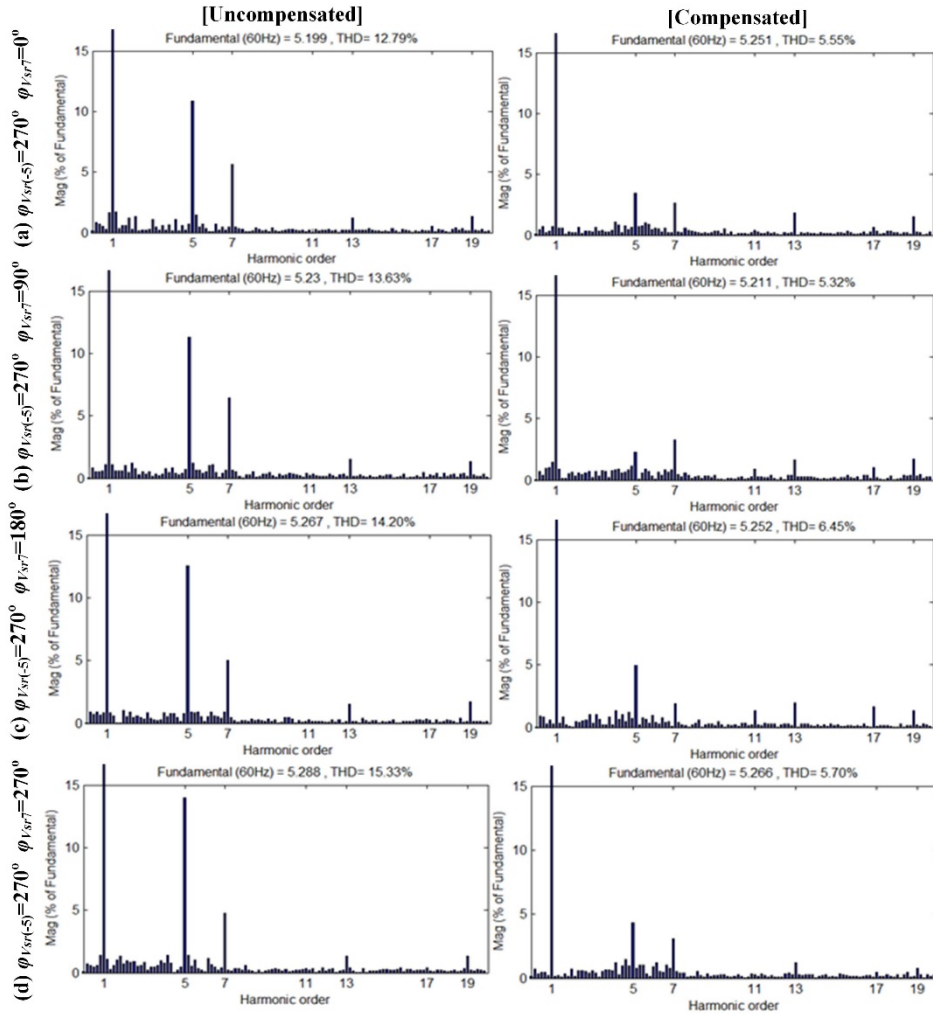


Fig. 5. 19. FFT analysis of line current in Fig. 5. 18.

$M_{Kv(-5)}$ and M_{Kv7} as 0.5 and 0.7 respectively, the experimental results are shown in Figs. 5. 20 and 5. 21. We can observe that both the 5th and 7th line current harmonics are effectively attenuated by the combination approach.

5.5 Summary and discussion

In this chapter, the SHE phase jittering method is developed to enable the high-power PWM converters to actively compensate the system background harmonics. For the SHE-phase-jittering-based active harmonic compensation method, only a simple algebraic calculation is required to generate the expected compensation harmonics through the high-power PWM converter. Compared with the SHC-scheme-

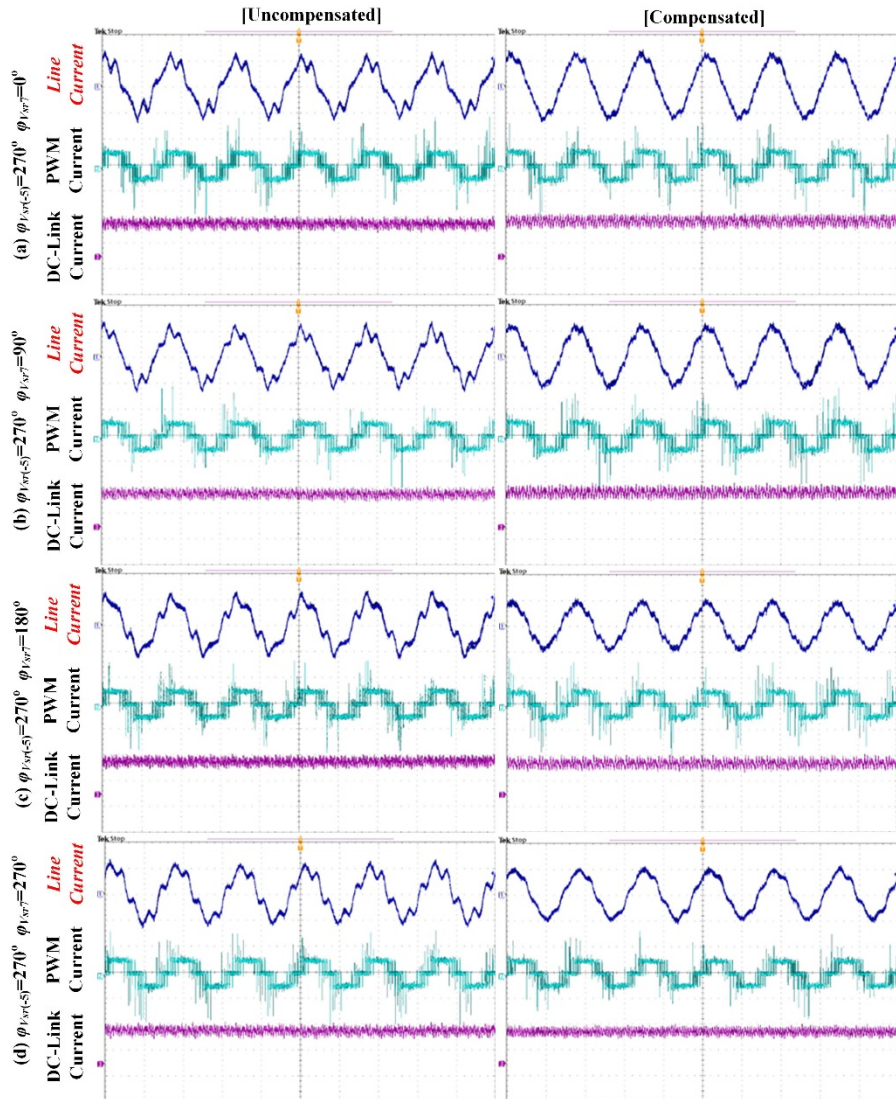


Fig. 5. 20. Current waveforms before and after using the combination approach under different 5th (1.1%) and 7th (1.1%) grid voltage harmonics' phases.

based active harmonic compensation, the SHE phase jittering method not only saves the effort on the creation of look-up table, but also realizes the real-time compensation without any delay introduced. In addition, combined with the SHC scheme, it enables the high-power PWM converter to actively compensate two harmonics without increasing the dimensions of SHC look-up table. By using such developed combination approach, not only the line current distortion could be further reduced compared with previous work, but also the low-resonant-frequency

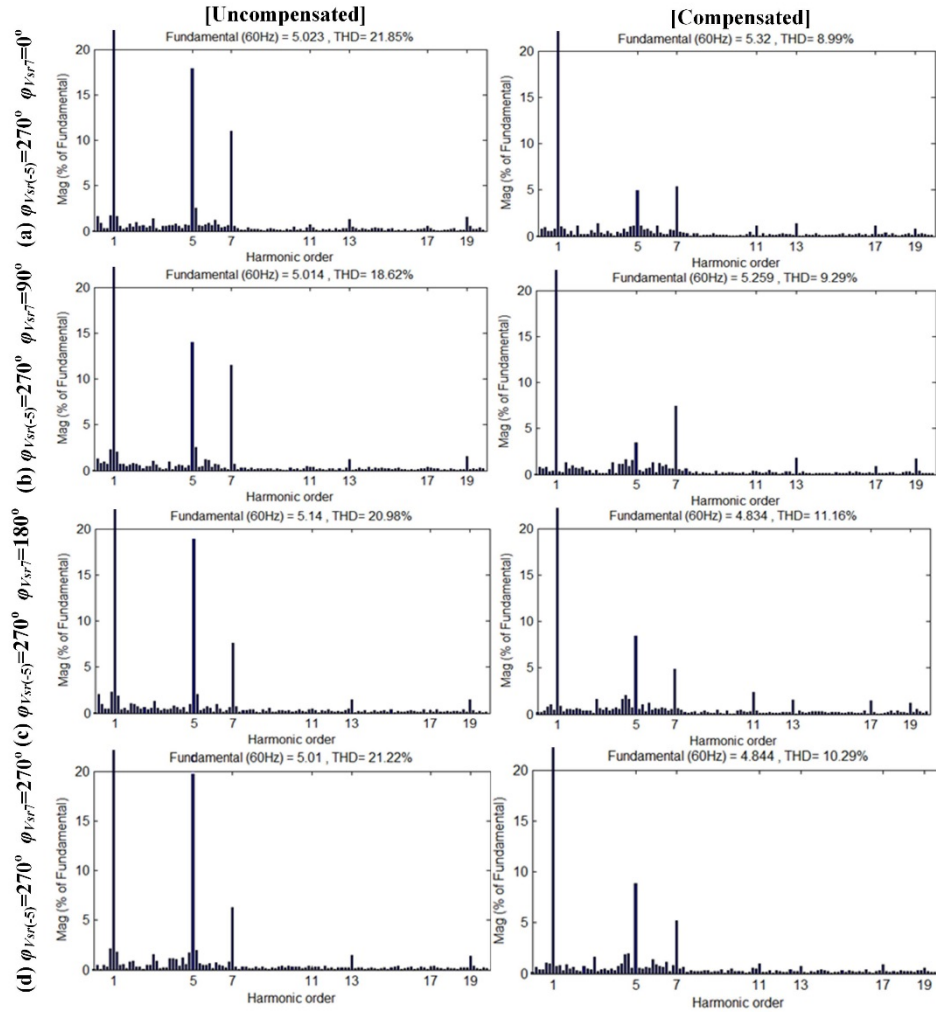


Fig. 5. 21. FFT analysis of line current in Fig. 5. 20.

constraint of system filter circuit can be relaxed. The possible increase of filter circuit's resonant frequency can help to reduce the reactive power flow so as to further increase the system power factor.

To verify the effectiveness of the proposed methods, experimental results of their application in high-power PWM current-source drive with AFE to actively attenuate the line current harmonics caused by utility harmonics are provided. Although their adoption in PWM CSR is used as an example, according to the earlier analysis, the proposed methods have a great potential to be used in both the high-power current-source converters and voltage-source converters at either rectifier side or inverter side for more flexible control of the converter's output harmonic

pattern. It is also important to note that this real-time on-line harmonic compensation can realize the grid harmonic control using the grid interfacing high-power converters with a very low switching frequency. This can be a very important ancillary functions in future grid interfacing high-power converter systems, such as PV plant, wind farm, STATCOM, HVDC, etc.

Chapter 6

Conclusions and Future Work

To guarantee a good harmonic performance with low converter switching frequency, the selective harmonic elimination (SHE) scheme is commonly adopted to modulate PWM current-source converters in high-power PWM current-source drives. Nevertheless, the harmonic and interharmonic distortion is still a typically challenge faced by such drive system. On the one hand, with a small dc choke to reduce costs and weights, the harmonics produced by the rectifier and the inverter will interact with each other through the weak dc-link, so that introduces harmonics and interharmonics in entire drive system. On the other hand, the system background harmonics (from utility and load) may be amplified by the ac-side LC circuit so that results in significant current harmonic distortion. The harmonics and interharmonics may cause the deterioration of power quality, significant power loss, communication interference, and motor derating, and can even give rise to the LC resonance and the load torsional vibration. With respect to the problem of harmonics and interharmonics in high-power PWM current-source drives, a thoroughly investigation of their generation is presented in this thesis, and a detailed analysis of their impacts is also provided. To overcome the harmonic and interharmonic problem, an SHE phase jittering method is proposed to enable the active compensation capability of SHE-modulated high-power PWM converters, and such method is developed to actively attenuate both the harmonics and the interharmonics through the control of PWM converters in high-power PWM current-source drives.

6.1 Conclusions

The conclusions from the research addressed in each chapter of the thesis are presented below.

Chapter 2

Chapter 2 analyzes the interharmonic problem caused by the harmonic interaction in high-power PWM current-source drives with thyristor front end. In this chapter, the generation of dominant interharmonics at the line side and the motor side due to the weak dc link is investigated. Based on the investigation, the impacts of the produced interharmonics are discussed based on two specific cases, line-side communication interference and motor-side torsional vibration problem, and analysis on the occurrence of impacts are presented in each case. According to the analysis, the SHE PWM pattern of current-source inverter (CSI) plays an important role in the generation of interharmonics. As a result, a simple method through designing the CSI SHE PWM pattern is proposed to reduce the impacts of interharmonics at last.

Chapter 3

Chapter 3 discusses the harmonics interaction phenomenon in high-power PWM current-source drives with active front end (AFE). Since the high-power PWM current-source converters are adopted at both the rectifier and the inverter and the potential LC resonance exists in two ac sides, the analysis on the interharmonics caused by the harmonics interaction and their impacts, especially the excitation of LC resonance, in AFE-based PWM current-source drives is more complex than the current-source drives with TFE. With respect to such characteristic, a frequency iteration method is developed to analyze the possible interharmonics generated at line side, dc link and motor side due to the harmonics interaction. In addition, an estimation method is proposed to predict the conditions that the produced interharmonics give rise to the LC resonance, and to predetermine the frequencies of the significant interharmonics caused by the LC resonance in entire drive system.

Chapter 4

To reduce the interharmonics due to the harmonics interaction in high-power PWM current-source drives without additional costs and losses involved, an active interharmonic compensation strategy is proposed in Chapter 4. The active interharmonic compensation capability of SHE-modulated high-power PWM current-

source converters is first enabled by a proposed SHE phase jittering method. Such method generates the compensation interharmonics through the PWM converter by introducing an alternating signal into the SHE phase angle. Based on this active interharmonic compensation method, a dc-link virtual impedance based strategy is developed to attenuate the interharmonics caused by the harmonics interaction in high-power PWM current-source drive systems. The developed strategy can effectively reduce the impacts of interharmonics due to the harmonics interaction, such as the LC resonance.

Chapter 5

In Chapter 5, the proposed SHE phase jittering method is further developed to realize the active compensation of system background harmonics through the SHE-modulated high-power PWM converters. Compared with the SHC-scheme-based active harmonic compensation proposed in previous works, the SHE phase jittering method not only saves the effort on the considerable off-line calculation, but can also be easily implemented on-line to realize the real-time compensation without any delay introduced. Nevertheless, both the SHE phase jittering method and the SHC scheme are only applicable to compensate one harmonic, which constrains the design of LC circuit's resonant frequency. To actively compensate more system background harmonics in high-power drive systems, a combination approach based on the SHE phase jittering method and the SHC scheme is also developed in this chapter. The effectiveness of the proposed methods is verified in a high-power PWM current-source drive application to actively attenuate the low-order line current harmonics caused by the utility harmonics.

6.2 Thesis contributions

The research reported in this thesis contributes to the research of harmonic and interharmonic problem faced by the high-power PWM current-source drives in four main aspects.

1) Thorough investigation of harmonics interaction phenomenon in high-power PWM current-source drives

The harmonics interaction phenomenon in high-power PWM current-source drives is thoroughly investigated in this thesis. Previous related researches mainly focus on the PWM voltage-source inverter (VSI) fed drives and the load-commutated inverter (LCI) fed drives. Compared with the PWM VSI-fed drive, which is usually equipped with a sufficient large dc-link capacitor, the harmonics interaction problem appears stronger in high-power PWM current-source drive due the small dc choke (to reduce the size and weight). Compared with the LCI-fed drive, where all of the characteristic harmonics are contained in the modulation function of thyristor-based converters, the SHE scheme that is normally adopted to modulate high-power PWM current-source converter can eliminate certain order harmonics in PWM pattern. It complicates the analysis on the generation of harmonics and interharmonics due to the harmonics interaction, especially for the high-power PWM current-source drives with AFE, where the SHE scheme is used to modulate both the PWM CSR and PWM CSI. In this thesis, based on the developed frequency relationship between ac-side components and dc-link components, the frequencies of dominant harmonics and interharmonics caused by the harmonics interaction in high-power PWM current-source drives are analyzed. Moreover, with respect to the system with AFE, a frequency iteration concept is proposed to study the generation of harmonics and interharmonics.

2) In-depth study on the impacts of harmonics interaction

Based on the analysis of the harmonics and interharmonics produced by the harmonics interaction, their impacts on the high-power PWM current-source drives are carefully studied with respect to three main cases: line-side communication interference, load torsional vibration, and *LC* resonance excitation. For each case, the mechanism of impact's occurrence is presented, and the conditions that the produced harmonics and interharmonics give rise to the impacts at certain motor operating frequencies are accurately estimated. Such estimation can help to avoid the

impacts occurring at certain motor operating frequencies through the design of PWM pattern, and also contributes to the implementation of the active compensation strategies proposed in this thesis. Note that, although the line-side communication and load torsional vibration are discussed with respect to the drives with TFE, and the *LC* resonance is analyzed in the drives with AFE, the same procedure can be used to study all of the impacts in the drives with either TFE or AFE.

3) Active interharmonic compensation enabled by the SHE phase jittering method

Most of the active compensation strategies proposed in previous works are based on the on-line PWM schemes (e.g. sinusoidal PWM, space vector modulation), which cannot be applied on the SHE-modulated PWM converters, and the previously-proposed methods with focus on the active compensation ability of SHE-modulated PWM converters lack the capability of interharmonic compensation. To realize the active attenuation of the interharmonics caused by the harmonics interaction in high-power PWM current-source drives, an SHE phase jittering method is proposed to enable the active interharmonic compensation capability of SHE-modulated high-power PWM converters. In this method, the compensation interharmonics can be easily generated through the PWM converters by introducing an alternating signal in the SHE phase angle. Based on the SHE-phase-jittering-based active interharmonic compensation, a dc-link virtual impedance based strategy is developed to attenuate the interharmonics due to the harmonics interaction in high-power PWM current-source drives. Such strategy virtually introduces an impedance in dc-link through the control of PWM converters, which can enhance the harmonic attenuation effect of the dc-link so as to reduce the harmonic interaction.

4) SHE-phase-jittering-based active compensation of system background harmonics

Beside the realization of the interharmonic attenuation through the high-power PWM converters, the SHE phase jittering method is also developed to actively compensate system background harmonics in this thesis. Compared with the SHC-

scheme-based active harmonic compensation in previous works, the SHE phase jittering method enables the SHE-modulated high-power PWM converters to generate the compensation harmonics based on a simple algebraic equation. Not only it can be easily designed and implemented on-line, but also realizes the real-time compensation without any delay introduced. Moreover, combined with the SHC scheme, it also makes the high-power PWM converters be able to compensate two harmonics without increasing the complexity of SHC scheme design. The SHE-phase-jittering-based active harmonic compensation can effectively attenuate the line current distortion caused by the utility harmonics in high-power PWM current-source drives, and also contributes to the grid harmonic control in future using the grid interfacing high-power converters in other systems, such as PV plant and wind farm.

6.3 Future work

Three areas where further work is needed are indicated.

1) Further testing the SHE-phase-jittering-based active compensation

In Chapter 4, the attenuation of interharmonics based on the SHE phase jittering method is tested on a high-power PWM current-source drive application with a harmonicless utility. The influence of the utility harmonics on the compensation method is expected to be tested. In Chapter 5, the SHE phase jittering method is adopted to attenuate the line current harmonics caused by the utility harmonics. To facilitate the tests, a dc-link resistance load is used to emulate the PWM CSI-fed motor drive. The influence of the SHE-phase-jittering-based active harmonic compensation on the motor-side harmonics through dc link needs to be tested, and the influence of the motor-side harmonics on the line-side harmonic attenuation is also expected to be considered. Moreover, if the compensation of harmonics and the attenuation of interharmonics are realized simultaneously, the possible interference between the two methods is required to be investigated.

2) Stability analysis of SHE-phase-jittering-based active compensation

In Chapter 4 and Chapter 5, with respect to the stability issue related to the design of coefficient K_v in the compensation methods, discussions about the influence of K_v on the modulation index are presented. According to the discussions, the large K_v will result in significant deviation of modulation index so that affects the steady-state active power balance and causes instability of the drive system. Nevertheless, a more rigorous analytical study of system stability is expected. It is very challenging, since both the ac sides and the dc link are involved in the active compensation method which makes the system highly nonlinear. Moreover, the SHE scheme used in this work is an off-line PWM and is a nonlinear element in the control system that cannot be approximated as the linear element like for other types of PWM methods. Therefore, the traditional stability analysis based on linear system theory cannot be directly applied. The rigorous stability study needs to be carefully considered and can be a main research task in future.

3) Further applications of the SHE-phase-jittering-based active compensation

In this thesis, the SHE-phase-jittering-based active compensation is mainly adopted at PWM CSR to suppress the LC resonance caused by the interharmonics, and attenuate the line current harmonic distortion due to the utility harmonics. Such active compensation method can also be applied at PWM CSI by regulating the SHE phase angle of CSI's modulation. It can be designed to mitigate the motor-side current distortion resulted from the non-ideal motor characteristics, and also can be applied to generate compensation electromagnetic torque through PWM CSI to attenuate the load torsional vibration. The related research and tests can be conducted in future.

References

- [1] B. Wu, *High-Power Converters and AC Drives*, Piscataway, NJ: IEEE Press, 2006, pp. 3-283.
- [2] J. Rodriguez, S. Bernet, B. Wu, J. Pontt, and S. Kouro, "Multilevel voltage-source-converter topologies for industrial medium-voltage drives," *IEEE Trans. Ind. Electron.*, vol. 54, no. 6, pp. 2930-2945.
- [3] B. Wu, J. Pontt, J. Rodriguez, S. Bernet, and S. Kouro, "Current-source converter and cycloconverter topologies for industrial medium-voltage drives," *IEEE Trans. Ind. Electron.*, vol. 55, no. 7, pp. 2786-2797.
- [4] R. D. Klug, and N. Klaassen, "High power medium voltage drives-innovations, portfolio, trends," in *Proc. Conf. Rec. EPE*, Dresden, Germany, 2005, CD-ROM.
- [5] S. Rizzo, and N. Zargari, "Medium voltage drives: what does the future hold?" in *Proc. 4th IPEMC*, 2004, pp. 82-89.
- [6] P.K. Steimer, H. E. Gruning, *et al.*, "IGCT-a new emerging technology for high power, low cost inverters," *IEEE Ind. Appl. Mag.*, vol. 5, no. 4, pp. 12-18, Jul./Aug. 1999.
- [7] H. Akagi, "Large static converters for industry and utility applications," *Proc. IEEE.*, vol. 89, no. 6, pp. 976-983, Jun. 2001.
- [8] J. K. Steinke, and P. K. Steimer, "Medium voltage drive converter for industrial applications in the power range from 0.5MW to 5MW based on a three-level converter equipped with IGCTs," in *Proc. IEE Seminar PWM Medium Voltage Drives*, 2000, pp. 6/1-6/4.
- [9] N. Zargari and S. Rizzo, "Medium voltage drives in industrial applications," in *Proc. Tech. Seminar, IEEE Toronto Section*, Nov. 2004, CD-ROM.
- [10] J. Rodriguez, J. S. Lai, and F. Z. Peng, "Multilevel inverters: a survey of topologies, controls and applications," *IEEE Trans. Ind. Electron.*, vol. 49, no. 4, pp. 724-738, Aug. 2002.

- [11] S. Bernet, "State of the art and developments of medium voltage converters-an overview," *Prz. Elektrotech. (Electrical Review)*, vol. 82, no. 5, pp. 1-10, May 2006.
- [12] N. R. Zargari, S. C. Rizzo, *et al.*, "A new current-source converter using a symmetric gate-commutated thyristor (SGCT)," *IEEE Trans. Ind. Appl.*, vol. 37, no. 3, pp. 896-903, May/Jun. 2001.
- [13] H. Stemmler, "High-power industrial drives," *Proc. IEEE*, vol. 82, no. 8, pp. 1266-1286, Aug. 1994.
- [14] B. Wu, S. B. Dewan, and G. R. Slemon, "PWM-CSI inverter for induction motor drives," *IEEE Trans. Ind. Appl.*, vol. 28, no. 1, pp. 64-71, Jan./Feb. 1992.
- [15] Y. W. Li, M. Pande, N. R. Zargari, and B. Wu, "An input power factor control strategy for high-power current-source induction motor drive with active front-end," *IEEE Trans. Power Electron.*, vol. 25, no. 2, pp. 352-359, Feb. 2010.
- [16] A. M. Qiu, Y. W. Li, B. Wu, D. Xu, N. R. Zargari, and Y. Liu, "High performance current source inverter fed induction motor drive with minimal harmonic distortion," in *Proc. Power Electron. Spec. Conf.*, pp. 79-95, Jun. 2007.
- [17] Z. Wang, B. Wu, D. Xu, and N. R. Zargari, "A current-source-converter-based high-power high-speed PMSM drive with 420-Hz switching frequency," *IEEE Trans. Ind. Electron.*, vol. 59, no. 7, pp. 2970-2981, Jul. 2012.
- [18] H. J. Lee, S. Jung, and S. K. Sul, "A current controller design for current source inverter-fed AC machine drive system," *IEEE Trans. Power Electron.*, vol. 28, no. 3, pp. 1366-1381, Mar. 2013.
- [19] Y. W. Li, and M. Pande, N. R. Zargari, and B. Wu, "Power-factor compensation for PWM CSR-CSI-fed high-power drive system using flux adjustment," *IEEE Trans. Power Electron.*, vol. 24, no. 12, pp. 3014-3019, Dec. 2009.
- [20] Y. W. Li, and M. Pande, N. R. Zargari, and B. Wu, "DC-link current minimization for high-power current-source motor drives," *IEEE Trans. Power Electron.*, vol. 24, no. 1, pp. 232-240, Jan. 2009.

- [21] J. D. Ma, B. Wu, N. R. Zargari, and S. C. Rizzo, "A space vector modulated CSI-based ac drive for multimotor applications," *IEEE Trans. Power Electron.*, vol. 16, no. 4, pp. 535-543, Jul. 2001.
- [22] Z. Wang, B. Wu, D. Xu, and N. R. Zargari, "Hybrid PWM for high-power current-source-inverter-fed drives with low switching frequency," *IEEE Trans. Power Electron.*, vol. 26, no. 6, pp. 1754-1763, Jun. 2011.
- [23] A. R. Beig, and V. T. Ranganathan, "A novel CSI-fed induction motor drive," *IEEE Trans. Power Electron.*, vol. 21, no. 4, pp. 1073-1082, Jul. 2006.
- [24] IEEE Standard 519-2014, *IEEE Recommended Practice and Requirements for Harmonic Control in Electrical Power Systems* (Revision of IEEE Std 519-1992), IEEE Inc., 2014.
- [25] IEC 61000-2-4 EMC Part 2, *Compatibility Levels in Industrial Plants for Low-Frequency Conducted Disturbances*, IEC Inc., 1994.
- [26] IEC 61000-3-6, *Assessment of Emission Limits for Distorting Loads in MV and HV Power Systems-Basic EMC Publication*, IEC Inc., 1996.
- [27] M. McGranaghan, and G. Beaulieu, "Update on IEC 61000-3-6: harmonic emission limits for customers connected to MV, HV, and EHV," in *Proc. Transmission and Distribution Conf. and Exhibition*, 2006, pp. 1158-1161.
- [28] Engineering Recommendation G5/4-1, *Planning Levels for Harmonic Voltage Distortion and the Connection of Non-linear Equipment to Transmission Systems and Distribution Networks in the United Kingdom*, Energy Networks Association, 2009.
- [29] Online available: <http://www.mvdrives.com>.
- [30] F. Kieferndorf, M. Basler, *et al.*, "A new medium voltage drive system based on ANPC-5L technology," in *Proc. Industrial Technology (ICIT)*, pp. 643-649, Chile, 2010.
- [31] F. Kieferndorf, M. Basler, *et al.*, "ANPC-5L technology applied to medium voltage variable speed drives applications," in *Proc. Power Electron. Electrical Drives Automation and Motion (SPEEDAM)*, pp. 1718-1725, 2010.
- [32] *Medium Voltage AC Drive ACS 2000*, ABB Product Brochure, 2011.
- [33] *ACS 5000 Medium Voltage Drive*, ABB Product Brochure, 2005.

- [34] *ALSPA Drive Range-Drive solutions for all applications*, ALSTOM Product Brochure, 2001.
- [35] *AXPERT-HIVERT Medium Voltage Drive*, Amtech Electronics Product Brochure, 2008.
- [36] *AMPGARD SC 9000 Medium Voltage Adjustable Frequency Drive*, Eaton Product Brochure, 2010.
- [37] GE Energy Power Conversion Technology Ltd., “Voltage balancing system and method for multilevel converters,” European Patent EP2784926 A2, Oct. 1, 2014.
- [38] G. Gateau, T. A. Meynard, and H. Foch, “Stacked multicell converter (SMC): properties and design,” in *Proc. Power Electron. Spec. Conf. (PESC)*, pp. 1583-1588, 2001.
- [39] *MV 6 Series-The Compact, General Purpose Medium Voltage Drive*, GE Power Conversion Produce Brochure, 2013.
- [40] *MV 7000 Reliable, High Performance Medium Voltage Drive*, GE Power Conversion Produce Brochure, 2013.
- [41] *HIVECTOL-HV Brochure*, Hitachi Ltd., 2012.
- [42] *INGEDRIVE MV 700 Brochure*, Ingeteam. 2015.
- [43] *High-Performance Medium Voltage Variable Frequency Drives*, Nidec ASI Product Brochure, 2013.
- [44] *PowerFlex 7000 MV Drive Brochure*, Rockwell Automation Canada Inc., 2002.
- [45] *Clean and Compact MV Drive-Fan, Pump, Compressor, Conveyor Applications*, Schneider Electric Altivar 1200 Product Brochure, 2013.
- [46] *The Reliable Medium-Voltage Drive with IGCTs*, Siemens Product Brochure, 2009.
- [47] *Low and Medium Voltage Drive Specifications*, TMEIC Product Brochure, 2011.
- [48] *FSDrive-MXIS Brochure*, Yaskawa Electric Corp., 2014.

- [49] J. Kang, E. Yamamoto, M. Ikeda, and E. Watanabe, "Medium-voltage matrix converter design using cascaded single-phase power cell modules," *IEEE Trans. Ind. Electron.*, vol. 58, no. 11, pp. 5007-5013, Nov. 2011.
- [50] D. Banerjee, and V. T. Ranganathan, "Load-commutated SCR current-source-inverter-fed induction motor drive with sinusoidal motor voltage and current," *IEEE Trans. Power Electron.*, vol. 24, no. 4, pp. 1048-1061, Apr. 2009.
- [51] S. D. Sudhoff, E. L. Zivi, and T. D. Collins, "Start up performance of load-commutated inverter fed synchronous machine drives," *IEEE Trans. Energy Convers.*, vol. 10, no. 2, pp. 268-274, Jun. 1995.
- [52] R. Emery, and J. Eugene, "Harmonic losses in LCI-fed synchronous motors," *IEEE Trans. Ind. Appl.*, vol. 38, no. 4, pp. 948-954, Jul./Aug. 2002.
- [53] R. Bhatia, H. Krattiger, *et al.*, "Adjustable speed drive using a single 135000HP synchronous motor," *IEEE Trans. Energy Convers.*, vol. 14, no. 3, pp. 571-576, Sept. 1999.
- [54] A. N. Alcaso, and A. J. M. Cardoso, "Asymmetrical operation of a twelve-pulse LCI drive system with power converters faults," in *Proc. IEEE*, vol. 82, no. 8, pp. 1266-1286, Aug. 1994.
- [55] A. N. Alcaso, and A. J. M. Cardoso, "Remedial operating strategies for a twelve-pulse LCI drive system," in *Proc. IEEE Int. Conf. Ind. Technol.*, pp. 619-624, 2003.
- [56] J. Rodriguez, J. Pontt, *et al.*, "Technical evaluation and practical experience of high power grinding mill drives in mining applications," *IEEE Trans. Ind. Appl.*, vol. 42, no. 3, pp. 866-874, May/Jun. 2005.
- [57] J. C. Wiseman, and B. Wu, "Active damping control of a high-power PWM current-source rectifier for line-current THD reduction," *IEEE Trans. Ind. Electron.*, vol. 52, no. 3, pp. 758-764, Jun. 2005.
- [58] Y. Xiao, B. Wu, N. R. Zargari, and R. Sotudeh, "Design of line/motor side capacitors for PWM CSR-CSI drives to achieve optimal power factor in high power fan/pump applications," in *Proc. IEEE APEC 2007*, pp. 333-337.

- [59] H. R. Karshenas, H. A. Kojori, and S. B. Dewan, "Generalized techniques of selective harmonic elimination and current control in current source inverters/converters," *IEEE Trans. Power Electron.*, vol. 10, no. 5, pp. 566-573, Sept. 1995.
- [60] J. I. Guzman, J. R. Espinoza, L. A. Moran, and G. Joos, "Selective harmonic elimination in multimodule three-phase current-source converters," *IEEE Trans. Power Electron.*, vol. 25, no. 1, pp. 44-53, Jan. 2010.
- [61] J. R. Espinoza, G. Joos, J. I. Guzman, L. A. Moran, and R. P. Burgos, "Selective harmonic elimination and current/voltage control in current/voltage-source topologies: a unified approach," *IEEE Trans. Ind. Electron.*, vol. 48, no. 1, pp. 71-81, Feb. 2001.
- [62] Y. W. Li, B. Wu, D. Xu, and N. R. Zaragri, "Space vector sequence investigation and synchronization methods for active front-end rectifier in high-power current-source drives," *IEEE Trans. Ind. Electron.*, vol. 55, no. 3, pp. 1022-1034, Mar. 2008.
- [63] M. F. Naguib, and L. A. C. Lopes, "Minimize low-order harmonics in low-switching-frequency space-vector-modulated current source converters with minimum harmonic tracking technique," *IEEE Trans. Power Electron.*, vol. 24, no. 4, pp. 881-893 Apr. 2009.
- [64] L. A. C. Lopes, and M. F. Naguib, "Space vector modulation for low switching frequency current source converters with reduced low-order noncharacteristic harmonics," *IEEE Trans. Power Electron.*, vol. 24, no. 4, pp. 903-910, Apr. 2009.
- [65] J. Dai, Y. Lang, B. Wu, D. Xu, and N. R. Zargari, "A multi-sampling SVM scheme for current source converter with superior harmonic performance," in *Proc. IEEE APEC 2009*, pp. 132-138.
- [66] B. Wu, and F. Dewinter, "Voltage stress on induction motor in medium voltage (2300V to 6900V) PWM GTO CSI drives," *IEEE Trans. Ind. Appl.*, vol. 37, no. 2, pp. 213-220, Nov. 1997.

- [67] B. Wu, S. Rizzo, N. R. Zargari, *et al.*, “Integrated dc link choke and method for suppressing common-mode voltage in a motor drive,” U.S. Patent 6617814 B1, Sept. 9, 2003.
- [68] A. Testa, M. F. Akram, *et al.*, “Interharmonics: theory and modeling,” *IEEE Trans. Power Del.*, vol. 22, no. 4, pp. 2335-2348, Oct. 2007.
- [69] E. W. Gunther, “Interharmonics in power systems,” in *Proc. Power Engineering Society Summer Meeting*, 2001, pp. 813-817.
- [70] R. Yacamini, “Power system harmonics. Part 4: interharmonics,” *Power Engineering Journal*, pp. 185-193, Aug. 1996.
- [71] H. C. Lin, “Sources, effects, and modelling of interharmonics,” *Mathematical Problems in Engineering*, 2014.
- [72] V. Kus, Z. Peroutka, and P. Drabek, “Non-characteristic harmonics and interharmonics of power electronic converters,” in *Proc. Inter. Conf. Electricity Distr. (18th CIRED)*, vol. 6, Jun. 2005.
- [73] G. W. Chang, S. K. Chen, H. J. Su, and P. K. Wang, “Accurate assessment of harmonic and interharmonic currents generated by VSI-fed drives under unbalanced supply voltages,” *IEEE Trans. Power Del.*, vol. 26, no. 2, pp. 1083-1091, Apr. 2011.
- [74] C.B. Mayer, “Torsional Vibration Problems and Analyses of Cement Industry Drives,” *IEEE Trans. Ind. Appl.*, vol. IA-17, no.1, pp.81-89, Feb. 1981.
- [75] G. Ellis and R.D. Lorenz, “Resonant Load Control Methods for Industrial Servo Drives,” in *Conf. Rec. IEEE-IAS Annu. Meeting, Rome, Italy*, 2000, pp.1438-1445.
- [76] D.J. Sheppard, “Torsional Vibration Resulting from Adjustable-Frequency AC Drives,” *IEEE Trans. Ind. Appl.*, vol.24, no.5, pp.812-817, Oct. 1988.
- [77] M.A. Valenzuela, J.M. Bentley, and R.D. Lorenz, “Evaluation of Torsional Oscillations in Paper Machine Sections,” *IEEE Trans. Ind. Appl.*, vol.41, no.2, pp.493-501, Apr. 2005.
- [78] E. F. Fuchs and M. A. S. Masoum, *Power Quality in Power Systems and Electrical Machines*, Elsevier Inc., 2008, pp. 120-123.

- [79] F. Liu, B. Wu, N. R. Zargari, and M. Pande, "An active damping method using inductor-current feedback control for high-power PWM current-source rectifier," *IEEE Trans. Power Electron.*, vol. 26, pp. 2580-2587, Sep. 2011.
- [80] M. H. Bierhoff, and F. W. Fuchs, "Active damping for three-phase PWM rectifiers with high-order line-side filters," *IEEE Trans. Ind. Electron.*, vol. 56, pp. 371-379, Feb. 2009.
- [81] Y. Sato and T. Kataoka, "A current-type PWM rectifier with active damping function," *IEEE Trans. Ind. Appl.*, vol. 32, pp. 533-541, May. 1996.
- [82] Z. Wang, B. Wu, D. Xu, and N. R. Zargari, "Dynamic capacitor voltage control of high power current source converter fed PMSM drives for LC resonance suppression," in *Proc. IEEE ISIE*, 2010, pp. 792-797.
- [83] S. A. S. Grogan, D. G. Holms, and B. P. McGrath, "High performance voltage regulation of current source inverters," *IEEE Trans. Power Electron.*, vol. 26, pp. 2439-2448, Sep. 2011.
- [84] J. Dannehl, F. W. Fuchs, S. Hansen, and P. Bach, "Investigation of active damping approaches for PI-based current control of grid-connected pulse width modulation converters with LCL filters," *IEEE Trans. Ind. Appl.*, vol. 46, pp. 1509-1517, Jul. 2010.
- [85] Y. W. Li, "Control and resonance damping of voltage-source and current-source converters with LC filters," *IEEE Trans. Ind. Electron.*, vol. 56, pp. 1511-1521, May 2009.
- [86] Z. Bai, H. Ma, *et al.*, "Resonance damping and harmonic suppression for grid-connected current-source converter," *IEEE Trans. Ind. Electron.*, vol. 61, no. 7, pp. 3146-3154, Jul. 2014.
- [87] X. Wang, Y. W. Li, F. Blaabjerg, and P. C. Loh, "Virtual-impedance-based control for voltage-source and current-source converters," *IEEE Trans. Power Electron.*, in press, 2015.
- [88] J. R. Wells, B. M. Nee, P. L. Chapman, and P. T. Krein, "Selective harmonic control: a general problem formulation and selected solutions," *IEEE Trans. Power Electron.*, vol. 20, pp. 1337-1345, Nov. 2005.

- [89] J. Napoles, J. I. Leon, R. Portillo, L. G. Franquelo, and M. A. Aguirre, "Selective harmonic mitigation technique for high-power converters," *IEEE Trans. Ind. Electron.*, vol. 57, pp. 2315-2312, Jul. 2010.
- [90] C. Namuduri. and P.C. Sen, "Optimal pulsewidth modulation for current source inverters," *IEEE Trans. Ind. Appl.*, vol. 22, pp. 1052-1068, Nov. 1986.
- [91] R. Carbone, "Analyzing voltage background distortion effects on PWM adjustable-speed drives," *IEEE Trans. Power Electron.*, vol. 19, pp. 765-774, May 2004.
- [92] E. J. Delaney and R. E. Morrison, "The calculation of harmonic and interharmonic distortion in current source converter systems," in *Proc. IEEE ICHPS V*, Atlanta, 1992, pp. 251-255.
- [93] H. Zhou, Y. W. Li, *et al.*, "Selective harmonic compensation (SHC) PWM for grid-interfacing high-power converters," *IEEE Trans. Power Electron.*, vol. 29, pp. 1118-1127, Mar. 2014.
- [94] F.D. Rosa, R. Langella, A. Sollazzo, and A. Testa, "On the interharmonic components generated by adjustable speed drives," *IEEE Trans. Power Del.*, vol. 20, pp. 2535-2543, Oct. 2005.
- [95] M.B. Rifai, T.H. Ortmeier, and W.J. McQuillan, "Evaluation of current interharmonics from ac drives," *IEEE Trans. Power Del.*, vol.15, pp.1094-1098, Jul. 2000.
- [96] D. Basic, "Input current interharmonics of variable-speed drives due to motor current imbalance," *IEEE Trans. Power Del.*, vol.25, pp. 2797-2806, Oct. 2010.
- [97] G.W. Chang, and S.K. Chen, "An analytical approach for characterizing harmonic and interharmonic currents generated by VSI-fed adjustable speed drives," *IEEE Trans. Power Del.*, vol. 20, pp. 2585-2593, Oct. 2005.
- [98] R. Carbone, A. Testa, D. Menniti, R.E. Morrison and E.J. Delaney, "Harmonic and interharmonic distortion in current source type inverter drives," *IEEE Trans. Power Del.*, vol. 10, pp. 1576-1583, Jul. 1995.

- [99] S. Schramm, C. Sihler, J.S. Manguelle, and P. Rotondo, "Damping torsional interharmonic effects of large drives," *IEEE Trans. Power Electron.*, vol. 25, pp. 1090-1098, Apr. 2010.
- [100] L. Hu and R. Yacamini, "Harmonic transfer through converters and HVDC links," *IEEE Trans. Power Electron.*, vol. 7, pp. 514-525, Jul. 1992.
- [101] D. Zhang, W. Xu, and Y. Liu, "On the phase sequence characteristics of interharmonics," *IEEE Trans. Power Del.*, vol. 20, pp. 2563-2569, Oct. 2005.
- [102] R. Carbone, F. D. Rosa, R. Langella, and A. Testa, "A new approach to model AC/DC/AC conversion systems," in *Proc. Power Engineering Society Summer Meeting*, 2011, pp. 271-276.
- [103] L. Hu, and R. E. Morrison, "The use of modulation theory to calculate the harmonic distortion in HVDC systems operating on an unbalanced supply," *IEEE Trans. Power Systems*, vol. 12, no. 2, pp. 973-980, May 1997.
- [104] L. Hu, and L. Ran, "Direct method for calculation of AC side harmonics and interharmonics in an HVDC system," in *IEE Proc. Gener. Transm. Distrib.*, 2000, pp. 329-335.
- [105] L. Hu, and R. Yacamini, "Calculation of harmonics and interharmonics in HVDC schemes with low DC side impedance," in *IEE Proc. Gener. Transm. Distrib.*, 1993, pp. 469-476.
- [106] B. Sivaneasan, E. Gunawan, and P. L. So, "Modeling and performance analysis of automatic meter-reading systems using PLC under impulsive noise interference," *IEEE Trans. Power Del.*, vol. 25, no. 3, pp. 1465-1475, Jul. 2010.
- [107] S. Mak and D. Radford, "Design considerations for implementation of large scale automatic meter reading systems," *IEEE Trans. Power Del.*, vol. 10, no. 1, pp. 97-103, Jan. 1995.
- [108] T. M. O'Sullivan, C. M. Bingham, and N. Schofield, "High-performance control of dual-inertia servo-drive systems using low-cost integrated SAW torque transducers," *IEEE Trans. Ind. Electron.*, vol. 53, no. 4, pp. 1226-1237, Aug. 2006.

- [109] J. S. Manguelle, J. M. N. Yome, and G. Ekemb, "Pulsating torques in PWM multi-megawatt drives for torsional analysis of large shafts," *IEEE Trans. Ind. Appl.*, vol. 46, no. 1, pp. 130-138, Jan./Feb. 2010.
- [110] J. S. Manguelle, C. Sihler, and S. Schramm, "A general approach of damping torsional resonance modes in multimegawatt applications," *IEEE Trans. Ind. Appl.*, vol. 47, no. 3, pp. 1390-1399, May/Jun. 2011.
- [111] K. Szabat, and T. O. Kowalska, "Vibration suppression in a two-mass drive system using PI speed controller and additional feedbacks-comparative study," *IEEE Trans. Ind. Electron.*, vol. 54, no. 2, pp. 1193-2006, Apr. 2007.
- [112] V. G. Agelidis, A. Balouktisis, I. Balouktsis, and C. Cossar, "Multiple sets of solutions for harmonic elimination PWM bipolar waveforms: analysis and experimental verification," *IEEE Trans. Power Electron.*, vol. 21, no. 2, pp. 415-421, Mar. 2006.
- [113] J. N. Chiasson, L. M. Tolbert, and *et al.*, "A complete solution to the harmonic elimination problem," *IEEE Trans. Power Electron.*, vol. 19, no. 2, pp. 491-499, Mar. 2004.
- [114] H. Zhou, Y.W. Li, N.R. Zargari, Z.Y. Cheng, "Input resonance investigation and LC filter design for PWM current source rectifiers," in *Proc. IEEE ECCE*, Atlanta, 2010, pp. 2079-2086.
- [115] R. Ni, Y. W. Li, Y. Zhang, N. R. Zargari, and G. Cheng, "Virtual impedance based selective harmonic compensation (VI-SHC) PWM for current-source rectifiers," *IEEE Trans. Power Electron.*, vol. 29, no. 7, pp. 3346-3356, Jul. 2014.
- [116] D. G. Holmes, and T. A. Lipo, *Pulse Width Modulation for Power Converters Principles and Practice*. New York, NY, USA: IEEE, 2003, pp. 409-411.